

CHAPTER 3

Generalizations of the Voronoi Diagram

Since the early 1970s the ordinary Voronoi diagram has been extended or generalized in many directions, and those generalized Voronoi diagrams facilitate many practical applications in various fields. In this chapter we show the definitions of those generalized Voronoi diagrams together with their major geometric properties. First, to give a perspective of this section, we fix a general framework for possible generalizations and make general comments. (If the reader is interested in only a specific generalized Voronoi diagram, he or she may skip this introduction and go directly to the section on that Voronoi diagram.)

We notice from the definition of the ordinary Voronoi diagram (Definition V1) that an abstract idea for defining a Voronoi diagram is that every point in a space is assigned to at least one of the generators according to a certain assignment rule, and that the resulting sets of points associated with the generators are collectively exhaustive and mutually exclusive except for boundaries. To formalize this abstract idea, we consider a non-empty space S and a set, $A = \{A_1, \dots, A_n\}$, of n distinct subsets of S ($2 \leq n < \infty$) satisfying $A_i \cap A_j = \emptyset, i \neq j$, which we shall call a *generator set*. In the ordinary Voronoi diagram the space S is the Euclidean space, and the generator set A is a set of points $P = \{p_1, \dots, p_n\}$ ($A = P, A_i = p_i$). In general the space S may be the Euclidean space or a non-Euclidean space, and an element A_i in A may be a point, a set of points, a line, an area, a polyhedron, etc.

Given a space S and a set A , we consider an assignment of a point p in S to at least one element of A according to a certain rule. If we assign p to A_i , we put 1 for (p, A_i) ; if we do not assign p to A_i , we put 0 for (p, A_i) , $p \in S, A_i \in A$. Then this assignment can be regarded as a mapping from $S \times A$ to $\{1, 0\}$. Mathematically, we consider a mapping, δ_A , from $S \times A$ to $\{0, 1\}$ such that

$$\delta_A(p, A_i) = \begin{cases} 1 & \text{if } p \text{ is assigned to } A_i \text{ in } A, \\ 0 & \text{otherwise.} \end{cases} \quad (3.0.1)$$

We call the mapping δ_A an *assignment rule*. In the ordinary Voronoi diagram, for example, the assignment rule δ_A is given by

$$\delta_A(p, A_i) = \begin{cases} 1, & \text{if } \|x - x_i\| \leq \|x - x_j\|, \quad j \neq i, j \in I_n, \\ 0, & \text{otherwise,} \end{cases} \quad (3.0.2)$$

where x and x_i are the location vectors of p and p_i in \mathbb{R}^m , respectively.

Under an assignment rule δ_A , we consider the closure (see Section 1.3.1) of the set of points assigned to A_i , i.e.

$$V(A_i) = \text{Closure}[(p \mid \delta_A(p, A_i) = 1, \quad p \in S)]. \quad (3.0.3)$$

In terms of $V(p_i)$ we define

$$e(A_i, A_j) = V(A_i) \cap V(A_j), \quad i \neq j, \quad (3.0.4)$$

and

$$\mathcal{V}(A, \delta_A, S) = [V(A_1), \dots, V(A_n)]. \quad (3.0.5)$$

The mapping δ_A of equation (3.0.1) allows many assignment rules. Among them, we are concerned with a family of assignment rules that satisfy the following four conditions.

(i) Every point p in S is assigned to at least one element of A , i.e.

$$\sum_{i=1}^n \delta_A(p, A_i) \geq 1, \quad p \in S. \quad (3.0.6)$$

This condition guarantees that $V(A_1), \dots, V(A_n)$ are collectively exhaustive, i.e.

$$\bigcup_{i=1}^n V(A_i) = S. \quad (3.0.7)$$

Condition (i) implies that there exists at least one non-empty set $V(A_i)$ in \mathcal{V} , but if the whole space consists of only one $V(A_i)$, i.e. $\mathcal{V}(A, \delta_A, S) = V(A_i) = S$, such a \mathcal{V} does not constitute a tessellation. Thus δ_A is supposed to satisfy

(ii) There exists at least two non-empty sets, $V(A_i)$ and $V(A_j)$, in $\mathcal{V}(A, \delta_A, S)$.

Under Conditions (i) and (ii), it may happen that a non-empty set $V(A_i)$ may be degenerate, i.e. the Lebesgue measure of $V(A_i)$ may be zero (for example, the area of $V(p_i) \in \mathbb{R}^2$ is zero, i.e. $V(A_i)$ is given by a point or a line (Figure 3.0.1(a)); the volume of $V(A_i) \in \mathbb{R}^3$ is zero, i.e. $V(A_i)$ is given by a point, a line and a surface). It is arguable whether or not such a $V(A_i)$ constitutes a tessellation as a special case. In this text we mainly consider non-degenerate $V(A_i)$. To be explicit, δ_A is supposed to satisfy

(iii) For all $i \in I_n$, if $V(A_i)$ is non-empty and connected, the measure of $V(A_i)$ is positive; if $V(A_i)$ is non-empty and disconnected, the measure of every disconnected subset of $V(A_i)$ is positive.

In some cases, however, we relax this condition, and suppose that δ_A satisfies (iii').

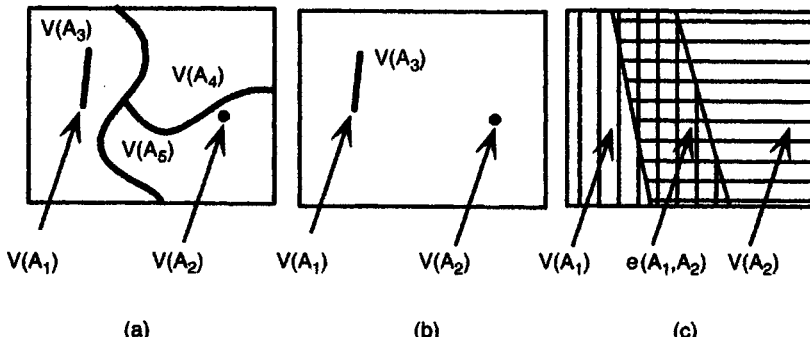


Figure 3.0.1 (a) Sets $V(A_i, A_j)$ that do not satisfy condition (iii); (b) a set $e(A_i, A_j)$ that does not satisfy condition (iv); (c) $e(A_i, A_j)$ that has a positive measure.

(iii') There exist at least two regions, $V(A_i)$ and $V(A_j)$, that satisfy condition (iii) (observe that panel (a) in Figure 3.0.1 satisfies condition (iii'), but panel (b) does not).

Generally $e(A_i, A_j)$ may be empty or not; if it is not empty, its measure may positive or zero (an actual example will be shown in Section 3.7). If the measure of $e(A_i, A_j)$ is positive (as in Figure 3.0.1(c)), then $V(A_i)$ and $V(A_j)$ share an overlapped region and \mathcal{V} does not form a tessellation. To exclude such an $e(A_i, A_j)$, we suppose

(iv) If $e(A_i, A_j)$ is not empty, $e(A_i, A_j)$ coincides with the intersection of the boundary of $V(A_i)$ and that of $V(A_j)$, i.e.

$$e(A_i, A_j) = \partial V(A_i) \cap \partial V(A_j) \quad \text{for } \partial V(A_i) \cap \partial V(A_j) \neq \emptyset, i \neq j. \quad (3.0.8)$$

From equations (3.0.4) and (3.0.8), the equation

$$[V(A_i) \cap V(A_j)] \setminus [\partial V(A_i) \cap \partial V(A_j)] = \emptyset, \quad i \neq j. \quad (3.0.9)$$

holds. This implies that $V(A_i)$ and $V(A_j)$ are exclusive except for boundaries. Therefore, under the assignment rule δ_A satisfying conditions (i), (ii), (iii) and (iv), the sets in $\mathcal{V}(A, \delta_A, S)$ are collectively exhaustive and mutually exclusive except for boundaries, that is, $\mathcal{V}(A, \delta_A, S)$ forms a tessellation of S . We designate this tessellation the *generalized Voronoi diagram* generated by the generator set A with the assignment rule δ_A in S , and $V(A_i)$ the *generalized Voronoi region* associated with A_i . We call the assignment rule δ_A that generates a generalized Voronoi diagram the *Voronoi generation assignment rule*, or briefly the *V-assignment rule*. As we remarked above, condition (iii) may be too strict in some cases. In those cases, we consider a weaker assignment rule than the above, i.e. δ_A is supposed to satisfy conditions (i), (ii), (iii') and (iv). When distinction is necessary, we call the resulting diagram obtained under these assumptions the *generalized weak Voronoi diagram*.

In the literature, the generalized Voronoi diagram sometimes is used to refer to more specific Voronoi diagrams than the above generalized Voronoi diagram. For example, the generalized Voronoi diagrams referred to by Drysdale and Lee (1978), Miles and Maillardet (1982) and Ó'Dúnlaing *et al.* (1986) are what we call the higher-order Voronoi diagram, the line Voronoi diagram and the area Voronoi diagram, respectively, in what follows. The generalized Voronoi diagram used in this text is much wider than their generalized Voronoi diagrams. In spirit, our generalization is similar to Leven and Sharir (1987), Klein (1988), Lavender *et al.* (1992), Melkemi and Chassery (1992), and Hamann and Tsai (1996).

The definition of the generalized Voronoi diagram by equation (3.0.3) is a generalization of Definition V2 of the ordinary Voronoi diagram. In Section 2.1 we defined the ordinary Voronoi diagram with half planes (Definition V3) as an alternative to Definition V2. When we examine the properties of Voronoi diagrams, we often find this definition more convenient and more operational. Motivated by this advantage, we next consider a generalization of Definition V3.

In the ordinary Voronoi diagram, the half plane $H(p_i, p_j)$ is alternatively called the *dominance region* of p_i over p_j (recall equation (2.1.6)). To emphasize this notion, we may write $\text{Dom}(p_i, p_j)$ for $H(p_i, p_j)$. We notice that the dominance region $\text{Dom}(p_i, p_j)$ is the same as $V(p_i)$ of $\mathcal{V}(P)$ generated by $P = \{p_i, p_j\}$ (two generator points). Keeping this property in mind, let us extend $\text{Dom}(p_i, p_j)$ to $\text{Dom}(A_i, A_j)$ for A in S .

For a pair $\{A_i, A_j\} \subset A = \{A_1, \dots, A_n\}$ ($2 \leq n < \infty$), we consider an assignment rule, $\delta_{\{A_i, A_j\}}$, given by

$$\delta_{\{A_i, A_j\}}(p, A_i) = \begin{cases} 1 & \text{if } p \text{ is assigned to } A_i \text{ in } \{A_i, A_j\}, \\ 0 & \text{otherwise} \end{cases} \quad (3.0.10)$$

(note that $\delta_{\{A_i, A_j\}}$ is a special case of δ_A , i.e. $A = \{A_i, A_j\}$). If $\delta_{\{A_i, A_j\}}$ satisfies conditions (i), (ii), (iii) and (iv), we can obtain the generalized Voronoi diagram $\mathcal{V}(\{A_i, A_j\}, \delta_{\{A_i, A_j\}}, S) = \{V(A_i), V(A_j)\}$. We call $V(A_i)$ the *dominance region* of A_i over A_j , and denote it by $\text{Dom}(A_i, A_j)$. Let

$$b(A_i, A_j) = \text{Dom}(A_i, A_j) \cap \text{Dom}(A_j, A_i). \quad (3.0.11)$$

We call this set the *bisector* between A_i and A_j . The sets $\text{Dom}(A_i, A_j)$ and $\text{Dom}(A_j, A_i)$ are collectively exhaustive and mutually exclusive except for the common boundary $b(A_i, A_j)$.

In terms of $\text{Dom}(A_i, A_j)$ we define

$$V(A_i) = \bigcap_{j \in I_n \setminus \{i\}} \text{Dom}(A_i, A_j), \quad (3.0.12)$$

and

$$\mathcal{V}(A, \text{Dom}, S) = \{V(A_1), \dots, V(A_n)\}. \quad (3.0.13)$$

In general, the resulting set $\mathcal{V}(A, \text{Dom}, S)$ may not coincide with $\mathcal{V}(A, \delta_A, S)$ of equation (3.0.5) under conditions (i), (ii), (iii), and (iv), because

$$\delta_A(p, A_i) = \prod_{j=1}^n \delta_{[A_i, A_j]}(p, A_i) \quad (3.0.14)$$

may not hold. For example, if δ_A is given by the assignment rule in which a point p is assigned to the k th nearest point ($3 \leq k \leq n$), then $\delta_{[A_i, A_j]}$ becomes meaningless, because there is no k th point in two generator points. When $\delta_{[A_i, A_j]}$ satisfies conditions (i), (ii), (iii), (iv) and equation (3.0.14) holds, we say that $\text{Dom}(A_i, A_j)$ and $b(A_i, A_j)$ are *well-behaving*.

In the above we defined the bisector $b(A_i, A_j)$ in terms of $\text{Dom}(A_i, A_j)$. Conversely, we may define $\text{Dom}(A_i, A_j)$ in terms of a bisector. Klein (1988, 1989) proposed this method in \mathbb{R}^2 (a similar method was also proposed by Hamann and Tsai, 1996). Let $b(A_i, A_j)$ be a simple (i.e. not self-intersecting) and continuous curve tending to infinity at both ends (or mathematically, $b(A_i, A_j)$ is homeomorphic to the open interval $(0,1)$). Klein (1989) calls $b(A_i, A_j)$ a *bisecting curve*. The bisecting curve $b(A_i, A_j)$ bisects \mathbb{R}^2 into two open unbounded domains, $D(A_i, A_j)$ and $D(A_j, A_i)$, each of which has $b(A_i, A_j)$ as its complete boundary. For convenience, $b(A_i, A_j)$ is to be assigned to one of $D(A_i, A_j)$ and $D(A_j, A_i)$. To this end, a total order is introduced in A , that is, for any pair $\{A_i, A_j\}$ in A , either $A_i < A_j$ or $A_j < A_i$ holds, but not both. Let

$$\text{Dom}^*(A_i, A_j) = \begin{cases} D(A_i, A_j) \cup b(A_i, A_j) & \text{if } A_i < A_j, \\ D(A_i, A_j) & \text{if } A_j < A_i. \end{cases} \quad (3.0.15)$$

In terms of $\text{Dom}^*(A_i, A_j)$, $V^*(A_i)$ is defined as

$$V^*(A_i) = \bigcap_{j \in I_n \setminus \{i\}} \text{Dom}^*(A_i, A_j). \quad (3.0.16)$$

Klein (1988) calls $\bigcup_{i=1}^n \partial V^*(A_i)$ an *abstract Voronoi diagram*. It should be noted that the abstract Voronoi diagram does not always result in a tessellation. The conditions that produce a tessellation are examined in depth by Klein (1989) and Mehlhorn *et al.* (1991). The reader who is interested in this derivation should consult those papers. Amato and Ramos (1996) specify the abstract Voronoi diagram by assuming that bisecting curves are simple curves consisting of a constant number of algebraic pieces of bounded degree, and call it an *algebraic planar Voronoi diagram*.

To construct a generalized Voronoi diagram in practice, we have to specify the assignment rule δ_A in terms of algebraic relations such as equation (3.0.2) or, more broadly, logical relations. In the literature, V-assignment rules are often specified in terms of a distance relation or a set of distance relations. One of the simplest and most frequently adopted V-assignment rules is that a point p is assigned to the closest generator(s), i.e.

$$\delta_A(p, A_i) = \begin{cases} 1 & \text{if } d(p, A_i) \leq d(p, A_j) \text{ for any } j \in I_n \setminus \{i\}, \\ 0 & \text{otherwise,} \end{cases} \quad (3.0.17)$$

where $d(p, A_i)$ is a ‘distance’ from a point p to an element A_i in A . Aurenhammer (1991) calls this rule the *nearest-neighbour rule*. The assignment rule of equation (3.0.2) is a special case of the assignment rule of

equation (3.0.17). When a generator is a point (i.e. $A_i = p_i$), the distance $d(p, p_i)$ usually implies a distance metric. The *distance metric* or *metric* for points in S is defined as a mapping, $d(p_i, p_j)$, of $S \times S$ into non-negative reals satisfying the following four axioms: for points $p_i, p_j, p_k \in P$, Axiom (i) $d(p_i, p_i) = 0$; Axiom (ii) $d(p_i, p_j) \leq d(p_i, p_k) + d(p_k, p_j)$; Axiom (iii) $d(p_i, p_j) = d(p_j, p_i)$; Axiom (iv) if $p_i \neq p_j$, then $d(p_i, p_j) > 0$. In the ordinary Voronoi diagram, the distance $d(p, A_i) = d(p, p_i)$ is given by the Euclidean distance, $d(p, p_i) = \|x - x_i\|$. Obviously the Euclidean distance is a distance metric. In general, however, the 'distance' $d(p, p_i)$ in the assignment rule of equation (3.0.17) for $A = P$ is not necessarily a distance metric. The distance metric $d(p_i, p_j)$ is defined for any point p_i in S and any point p_j in S , but when we define the assignment rule of equation (3.0.17) for $A = P$, it is sufficient to define $d(p, p_i)$ for any point p in S and any point p_i in P (not S). More generally, $d(p, A_i)$ in equation (3.0.17) is defined as a mapping of $S \times A$ (not $S \times S$) into \mathbb{R} . If the assignment rule δ_A of equation (3.0.17) with this mapping is a V-assignment rule, we call the mapping $d(p, A_i)$ a *Voronoi generation distance* or a *V-distance* (or just a *distance*) for short. The assignment rule of equation (3.0.17) with a V-distance produces a generalized Voronoi diagram, and we write it symbolically as $\mathcal{V}(A, d, S)$. The ordinary Voronoi diagram is written as $\mathcal{V}(P, \|x - x_i\|, \mathbb{R}^m)$.

An example of a non-metric V-distance is given by

$$d(p_i, p_j) = \|x - x_i\| - w, \quad w \neq 0. \quad (3.0.18)$$

This distance does not satisfy $d(p_i, p_i) = -w \neq 0$, i.e. Axiom (i) is not satisfied. We notice, however, that the set $\text{Dom}(p_i, p_j) = \{x \mid \|x - x_i\| - w \leq \|x - x_j\|\}$ produces exactly the same dominance region defined with the Euclidean distance; consequently, the distance given by equation (3.0.18) is a V-distance. This example shows that a V-distance allows many more forms than a distance metric.

We should note, however, that some of these are trivial. To show which generalizations are trivial, let F be a strictly increasing function of a V-distance, i.e. $F(d(p, A_i)) \leq F(d(p, A_j))$ if and only if $d(p, A_i) \leq d(p, A_j)$. It follows from this relation that $\text{Dom}(A_i, A_j)$ defined with $F(d(p, A_i))$ is the same as $\text{Dom}(A_i, A_j)$ defined with $d(p, A_i)$, and hence $\mathcal{V}(A, F(d), \mathbb{R}^m) = \mathcal{V}(A, d, \mathbb{R}^m)$. In this case we say that the distance $F(d(p, A_i))$ is *transformable* to the distance $d(p, A_i)$, and that the Voronoi diagram with $F(d(p, A_i))$ is a *trivial generalization* of the Voronoi diagram with $d(p, A_i)$.

In applications, we often use the exponential distance $d(p, p_i) = \exp(\|x - x_i\|)$, the logarithmic distance $d(p, p_i) = \log(\|x - x_i\|)$ and the power distance $d(p, p_i) = \|x - x_i\|^a$ ($a > 0$). Apparently, these distances are transformable to the Euclidean distance. Thus, Voronoi diagrams with these distances are trivial generalizations of the ordinary Voronoi diagram.

In the following sections we show several generalized Voronoi diagrams defined with V-distances that are not transformable to the Euclidean distance. Stated a little more specifically, we show $\mathcal{V}(P, d, \mathbb{R}^m)$, where $d(p, p_i)$ is the weighted distance (Section 3.1), the shortest-path distance, the visibility-

shortest-path distance (Section 3.4), the Minkowski metric, the Karlsruhe metric, the convex distance, the boat-on-a-river distance, and the Hausdorff distance (Section 3.7).

In the above generalized Voronoi diagrams, the generator set A is restricted to a set of points and the space S is restricted to the Cartesian space. Recalling the definition of equation (3.0.1), we can of course relax these restrictions. Regarding the generalizations with respect to a generator set A , we shall show $\mathcal{V}(A, d, \mathbb{R}^m)$, where the set A is a set of sets of points (Sections 3.2 and 3.3), a set of lines (Section 3.5), a set of areas (Section 3.6), and a set of moving points (Section 3.9). Regarding generalized Voronoi diagrams with respect to a space S , we show $\mathcal{V}(P, \text{the length of the shortest path on } S, S)$, where S is a sphere, a cylinder, a cone, a polyhedral surface (Section 3.7), and a network (Section 3.8).

As is noticed from the notation $\mathcal{V}(A, \delta_A, S)$, we can generalize the ordinary Voronoi diagram with respect to a generator set A , an assignment rule δ_A and a space S . This implies that the number of generalizations is potentially as many as the product of the numbers of generalizations of each factor. In the following sections, however, to avoid complicated exposition, we mainly deal with a single factor keeping the other factors the same as those of the ordinary Voronoi diagram. The reader may attempt to formulate a new generalized Voronoi diagram by combining those generalized Voronoi diagrams. We also note that the reader who wishes to understand generalized Voronoi diagrams from a more computational view point should consult Edelsbrunner and Seidel (1986), Klein (1989) and Mehlhorn *et al.* (1991); for an axiomatic approach, consult Stifter (1991).

3.1 WEIGHTED VORONOI DIAGRAMS

In the ordinary Voronoi diagram we implicitly assume that generator points are identical (except for their locations) or that each generator point has the same weight. In some practical applications, however, this assumption may not be appropriate. Rather, it is more appropriate to assume that generator points have different weights reflecting the variable property of the generator points; for example, the population size of a settlement, the number of functions in a shopping centre, the amount of emissions from a polluter, the size of an atom in a crystal structure, and so forth. In this section we show the family of generalized Voronoi diagrams that take these different weights into account in terms of the 'weighted distance'.

We consider a set of distinct points, $P = \{p_1, \dots, p_n\} \subset \mathbb{R}^m$ ($2 \leq n < \infty$) ($A = P, S = \mathbb{R}^m$) and assign a weight to each p_i which relates to some variable property of the phenomenon, such as those mentioned above. We represent this weight by a set of parameters $W_i = \{w_{i1}, \dots, w_{in_w}\}$ (if $n_w = 1$, we write w_i for W_i). With this weight we define a distance, $d_w(p, p_i)$, from p to p_i , called a *weighted distance*, which will be specified in the following

subsections. The dominance region of p_i over p_j with the weighted distance is written as

$$\text{Dom}(p_i, p_j) = \{p \mid d_w(p, p_i) \leq d_w(p, p_j)\}, \quad j \neq i. \quad (3.1.1)$$

Let

$$V(p_i) = \bigcap_{j \in I_n \setminus \{i\}} \text{Dom}(p_i, p_j), \quad (3.1.2)$$

and $\mathcal{V}(P, d_w, \mathbb{R}^m) = \mathcal{V}_w = \{V(p_1), \dots, V(p_n)\}$. If the dominance region given by equation (3.1.1) is well-behaving, \mathcal{V}_w gives a generalized Voronoi diagram. We call \mathcal{V}_w the *weighted Voronoi diagram* generated by P with the weight $\{W_1, \dots, W_n\}$, and the set $V(p_i)$ the *weighted Voronoi region* associated with p_i .

Since the weighted distance allows many functional forms, many weighted Voronoi diagrams are possible. In the following subsections we show four types of weighted Voronoi diagrams that often appear in the related literature. We mainly deal with \mathbb{R}^2 , but conceptually the extension to \mathbb{R}^m is straightforward.

3.1.1 The multiplicatively weighted Voronoi diagram

The first type of the weighted Voronoi diagram is characterized by the weighted distance given by

$$d_{mw}(p, p_i) = \frac{1}{w_i} \|x - x_i\|, \quad w_i > 0. \quad (3.1.3)$$

We call this distance the *multiplicatively weighted distance* or the *MW-distance* for short. After a few steps of calculation, we obtain the bisector as

$$b(p_i, p_j) = \left\{ x \mid \left\| x - \frac{w_i^2}{w_i^2 - w_j^2} x_j + \frac{w_j^2}{w_i^2 - w_j^2} x_i \right\| = \frac{w_i w_j}{w_i^2 - w_j^2} \|x_j - x_i\| \right\}, \quad (3.1.4)$$

$w_i \neq w_j, i \neq j.$

This bisector is the locus of a point p satisfying that the distance from p to the fixed point, $w_i^2 x_j / (w_i^2 - w_j^2) - w_j^2 x_i / (w_i^2 - w_j^2)$, is constant. Obviously, this locus is a circle in \mathbb{R}^2 . This circle passes through the interior and exterior division points (denoted by p_{ij1} and p_{ij2}) of $\overline{p_i p_j}$ with ratio w_i/w_j , and its diameter is given by $\overline{p_{ij1} p_{ij2}}$ (Figure 3.1.1). In classic geometry this circle is known as the *Apollonius circle*. Figure 3.1.1 shows the Apollonius circles representing the bisector defined with the MW-distance for several ratios $\alpha = w_i/w_j$ (where $w_i/w_j \geq 1$ is assumed without loss of generality). In the special case of $\alpha = 1$ ($w_i = w_j$), the bisector becomes a straight line, or a circle with an infinite radius.

In equation (3.1.3) we use $1/w_i$, but mathematically w_i is also acceptable. In equation (3.1.3) we adopt the former, because, as can be seen from Figure 3.1.1, the dominance region of p_i over p_j becomes larger as the weight w_i (or α) increases.

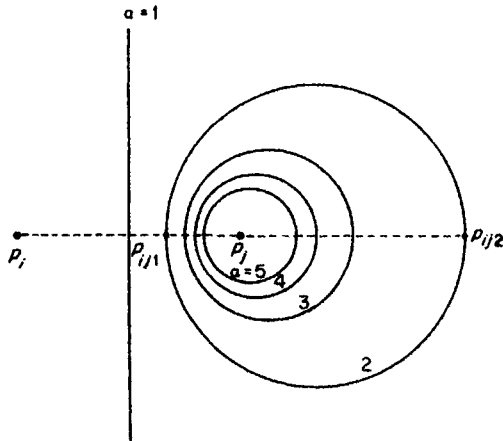


Figure 3.1.1 The bisectors with a multiplicatively weighted distance for several ratios $\alpha = w_i/w_j = 1, 2, 3, 4, 5$, or multiplicatively weighted Voronoi diagrams for $n = 2$.

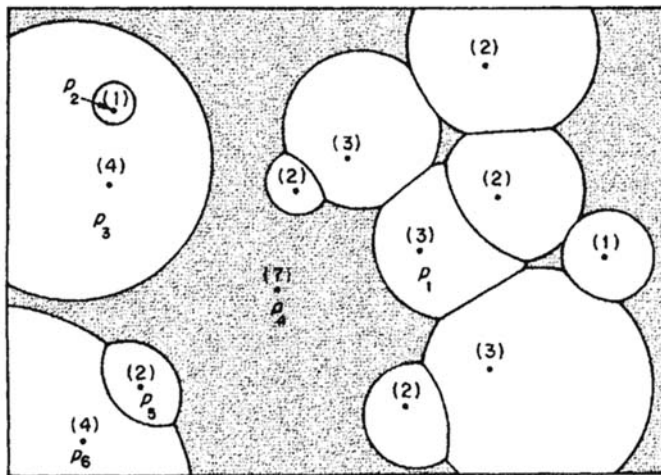


Figure 3.1.2 A multiplicatively weighted Voronoi diagram in \mathbb{R}^2 (the numbers in parentheses represent weights associated with the generators).

Since the Apollonius circle divides \mathbb{R}^2 into two disjoint regions, the bisector with the MW-distance is well-behaving. Thus the set $\mathcal{V}(P, d_{\text{mw}}, \mathbb{R}^2) = \mathcal{V}_{\text{mw}} = \{V(p_1), \dots, V(p_n)\}$ gives a generalized Voronoi diagram, where $V(p_i)$ is given by equation (3.1.2) with equation (3.1.3). We call \mathcal{V}_{mw} the *multiplicatively weighted Voronoi diagram* generated by P with the MW-distance or the *MW-Voronoi diagram* of P with $d_{\text{mw}}(p, p_i)$ (Aurenhammer and Edelsbrunner, 1984; Aurenhammer, 1988a). Ash and Bolker (1986) call \mathcal{V}_{mw} the *circular*

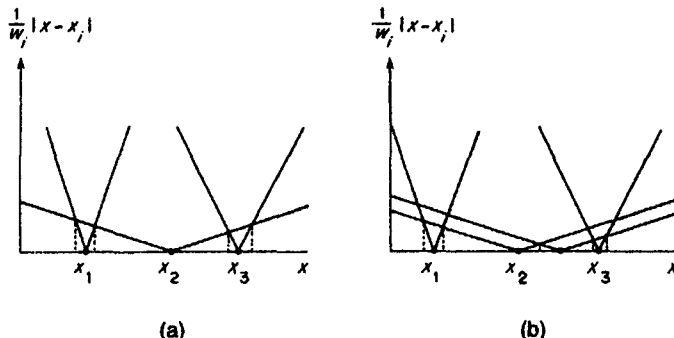


Figure 3.1.3 MW-Voronoi diagrams in \mathbb{R}^2 .

Dirichlet tessellation, and in crystallography, \mathcal{V}_{mw} is sometimes referred to as the *Apollonius model*. We call the set $V(p_i)$ the *multiplicatively weighted Voronoi region* associated with p_i , or briefly the *MW-Voronoi region* of p_i . Figures 3.1.1 and 3.1.2 show planar MW-Voronoi diagrams. The MW-Voronoi diagram reduces to the ordinary Voronoi diagram when w_i is the same constant for all $i \in I_n$. Thus the MW-Voronoi diagram includes the ordinary Voronoi diagram.

To observe the geometric properties of V_{MW} , let us inspect Figure 3.1.2, where the numbers in the parentheses represent weights associated with the generators. First, $V(p_1)$ is not convex. Second, $V(p_2)$ is contained in $V(p_3)$ or $V(p_4)$, has a hole. Third, $V(p_4)$ indicated by the shaded area is not connected. Fourth, the weights of the MW-Voronoi regions adjacent to a convex MW-Voronoi region, say $V(p_5)$, are not smaller than the weight of the convex MW-Voronoi region ($w_5 < w_4, w_6$). We can understand this convexity property from the dominance region in Figure 3.1.1 and the fact that $V(p_i)$ is the intersection of the dominance regions. Fifth, from the same figure and the same equation, we notice that $V(p_i)$ is not empty because the weights are finite. To sum up, we have the following property.

Property MW1 An MW-Voronoi region is a non-empty set; it need not be convex, or connected; and it may have a hole(s). An MW-Voronoi region $V(p_i)$ is convex if and only if the weights of adjacent MW-Voronoi regions are not smaller than w_i .

To observe another geometric property, we depict a one-dimensional MW-Voronoi diagram in Figure 3.1.3 where the value of $|x - x_i|/w_i$ is shown on the vertical axis. Obviously, the slope of $|x - x_i|/w_i$ becomes flatter as the weight w_i increases. From Figure 3.1.3(a) we readily notice that the generator whose weight is the largest eventually dominates the places far from the locations of the generators; consequently, the MW-Voronoi region of the largest weight is infinite. When two or more generators have the same largest

weight as in Figure 3.1.3(b), however, the rightmost and leftmost Voronoi regions are infinite. Generalizing these properties in \mathbb{R}^2 , we obtain the following property.

Property MW2 Let $w_{\max} = \max_j \{w_j, j \in I_n\}$ and P_{\max} be the subset of P given by $P_{\max} = \{p_j \mid w_j = w_{\max}\}$. An MW-Voronoi region $V(p_i)$ is unbounded if and only if $p_i \in P_{\max}$ and p_i is on the boundary of $\text{CH}(P_{\max})$.

If the generator with the maximum weight is unique, we have only one unbounded MW-Voronoi region. An example is shown by the shaded MW-Voronoi region in Figure 3.1.2.

We observe in Figure 3.1.1 that the bisector $b(p_i, p_j)$ is either a circle or a straight line. In Figure 3.1.2 we find that the Voronoi edge shared by $V(p_4)$ and $V(p_6)$ is disconnected. From these findings we notice the following property with respect to edges.

Property MW3 Two MW-Voronoi regions may share disconnected edges. An edge is a circular arc if and only if the weights of the MW-Voronoi regions sharing the edge are different; an edge is a straight line if and only if the weights of the MW-Voronoi regions sharing the edge are the same.

3.1.2 The additively weighted Voronoi diagram

The second type of the weighted Voronoi diagram is characterized by the weighted distance

$$d_{aw}(p, p_i) = \|x - x_i\| - w_i. \quad (3.1.5)$$

We call this distance the *additively weighted distance* or briefly the *AW-distance*. The dominance region of p_i over p_j with the AW-distance is written as

$$\text{Dom}(p_i, p_j) = \{x \mid \|x - x_i\| - \|x - x_j\| \leq w_i - w_j\}, \quad i \neq j. \quad (3.1.6)$$

The shape of the dominance region varies according to the parameter values $\alpha = \|x_i - x_j\|$ and $\beta = w_i - w_j$ (where $w_i - w_j \geq 0$ is assumed without loss of generality). First, if $0 < \alpha < \beta$, then the generator p_i dominates the whole plane or the dominance region of p_j disappears, i.e. $\text{Dom}(p_i, p_j) = \mathbb{R}^2$ (which is not well-behaving). Such a case never happens for the dominance region defined with the MW-distance.

Second, if $\alpha = \beta$, then the dominance region is the whole plane except for the half line radiating from p_i in the direction from p_i to p_j (Figure 3.1.4, $\beta = 10$). This dominance region is also not well-behaving.

Third, if $\alpha > \beta$, then the boundary of the dominance region or the bisector is given by

$$b(p_i, p_j) = \{x \mid \|x - x_i\| - \|x - x_j\| = \beta\} \quad \text{if } \alpha > \beta, i \neq j. \quad (3.1.7)$$

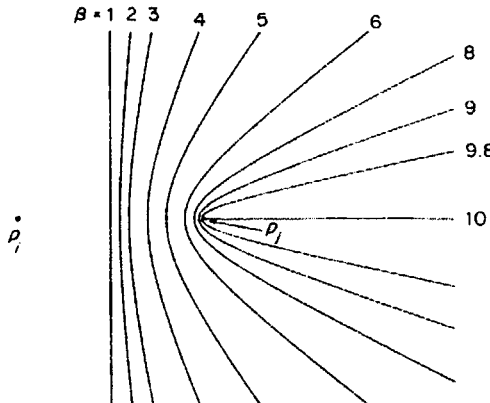


Figure 3.1.4 The bisectors with the additively weighted distance for parameter values $\alpha = \|x_i - x_j\| = 10$ and $\beta = w_i - w_j = 0, 1, 2, 3, 4, 5, 6, 8, 9, 9.8, 10$, or additively weighted Voronoi diagrams for $n = 2$.

This bisector is the locus of a point p satisfying that the difference between the distance from p to p_i and that from p to p_j is constant. This locus is known as a branch of the hyperbolic curve with foci p_i and p_j (Figure 3.1.4, $\beta = 1-9.8$). Note that if $\beta = 0$, the bisector becomes the straight line perpendicularly bisecting $\overline{p_i p_j}$ (Figure 3.1.4, $\beta = 0$). Figure 3.1.4 shows the bisectors for several parameter values.

In equation (3.1.5) we do not restrict the sign of w_i . Usually we assume a positive w_i because, as can be seen in Figure 3.1.4, the dominance region of p_i over p_j becomes larger as the weight w_i increases. Obviously, both $-w_i$ and $+w_i$ are acceptable in equation (3.1.5); in some applications (for example, in the market area analysis in Section 7.3), the latter form is used.

Since the bisector defined with the AD-distance is well-behaving for $\alpha > \beta$, we can obtain a generalized Voronoi diagram $\mathcal{V}(P, d_{aw}, \mathbb{R}^n) = \mathcal{V}_{aw} = \{V(p_1), \dots, V(p_n)\}$ for $\alpha > \beta$, where $V(p_i)$ is given by equations (3.1.1), (3.1.2) and (3.1.5). We call $V(p_i)$ the *additively weighted Voronoi region* associated with p_i , or briefly the *AW-Voronoi region* of p_i , and \mathcal{V}_{aw} the *additively weighted Voronoi diagram* generated by P with the AW-distance, or briefly the *AW-Voronoi diagram* of P with $d_{aw}(p, p_i)$ (Aurenhammer, 1988a). Ash and Bolker (1986) call \mathcal{V}_{aw} the *hyperbolic Dirichlet tessellation*. Figures 3.1.4 and 3.1.5 show planar AW-Voronoi diagrams.

The AW-Voronoi diagram reduces to the ordinary Voronoi diagram when w_i is the same constant for all $i \in I_n$ and so \mathcal{V}_{aw} includes the ordinary Voronoi diagram. Like the dual relationship between the ordinary Voronoi diagram and the ordinary Delaunay triangulation, we may define the (*additively weighted Delaunay diagram*) as the dual of the AW-Voronoi diagram, but note that a few modifications are necessary (Mirzaian, 1993). Having noticed this diagram, we might consider the possibility of the multiplicatively weighted

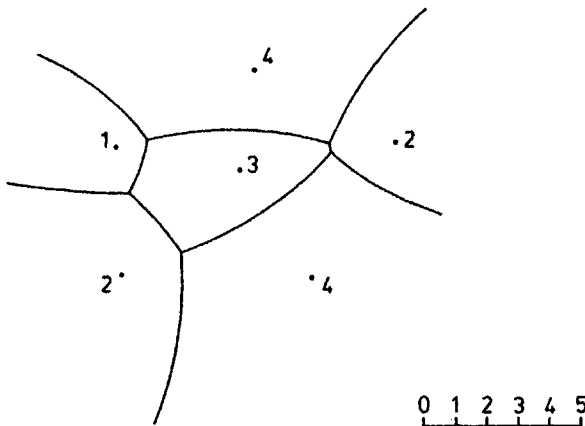


Figure 3.1.5 An additively weighted Voronoi diagram (the numbers indicate weights, w_i).

Delaunay diagram. Figure 3.1.2 shows that such a diagram is difficult to define because the line segments connecting generators whose AW-Voronoi regions share the common boundaries may cross.

The AW-Voronoi diagram is often discussed in conjunction with a special case of the (general) Voronoi growth model (see Section 7.2 for details), which is called the *Johnson-Mehl model* (Section 5.8). Suppose that a finite number of points or disks with zero radius are placed on a plane. Each disk grows with the same constant growth rate keeping its centre at the initial point but the growth of each disk starts at a different time. In the early stages disks do not overlap, but after a certain time a disk may touch another. The growth of a disk ceases whenever two or more disks impinge. Eventually, every disk is deformed into a certain shape in the region, which is an AW-Voronoi region. We might consider that in the above process, if the same constant growth rate is replaced with a different growth rate and starting at a different time is replaced with one starting at the same time, then the process eventually leads to the MW-Voronoi diagram. This is not true because the MW-distance may not be applicable due to obstacles made by grown disks. Considering this fact, Schaudt and Drysdale (1991) modify the growth process in that the distance between points is replaced by the shortest path distance. We may call the resulting tessellation the *shortest-path multiplicatively weighted Voronoi diagram* (see Section 3.4).

The properties of the AW-Voronoi diagram are different from those of the MW-Voronoi diagram. In particular, we first note the following property.

Property AW1 The set $V(p_i)$ is empty if and only if

$$\min_{j \neq i} \{ \|x - x_j\| - w_j, j \in I_n \} < -w_i. \quad (3.1.8)$$

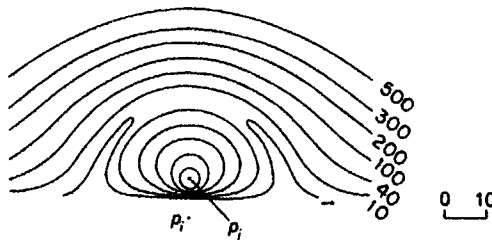


Figure 3.1.6 The bisectors with the generalized AW-distance given by $\phi(\|x - x_i\|) = (\|x - x_i\| - 3)^3 - w_i$, $\alpha = w_i - w_j = 1, 10, 40, 100, 200, 300, 500$, or additively weighted Voronoi diagrams with the generalized AW-distance for $n = 2$.

The set $V(p_i)$ is a half line or a line segment if and only if

$$\min_{j \neq i} \{\|x - x_j\| - w_j, j \in I_n\} = -w_i. \quad (3.1.9)$$

The set $V(p_i)$ has a positive area if and only if

$$\min_{j \neq i} \{\|x - x_j\| - w_j, j \in I_n\} > -w_i. \quad (3.1.10)$$

The properties of equations (3.1.8) and (3.1.9) contrast with those of the ordinary Voronoi diagram (Property V1) and the MW-Voronoi diagram (Property MW1). In those Voronoi diagrams a Voronoi region is neither empty nor degenerates into a line.

From equation (3.1.7) we understand the following property.

Property AW2 An edge of an AW-Voronoi region is either a hyperbolic arc or a straight line segment.

As a consequence of Property AW2, we notice the following property.

Property AW3 If at least one weight, w_i , is different from the others and relation (3.1.10) holds, then there exists at least one non-convex AW-Voronoi region. Every non-convex AW-Voronoi region is star-shaped with respect to its generator.

Besides these properties, Ash and Bolker (1986) show the properties related to the generator recognition problem (recall Problem P5) of the AW-Voronoi diagram (as well as the MW-Voronoi diagram).

We may generalize the AW-Voronoi diagram slightly by replacing equation (3.1.5) with

$$d_{g,aw}(p, p_i) = \phi(\|x - x_i\|) - w_i, \quad (3.1.11)$$

where ϕ is usually a strictly increasing function (Ash and Bolker, 1986; Hanjoul *et al.*, 1989). We call this distance the *generalized AW-distance*. The generalized AW-distance is general in the sense that it includes not only the

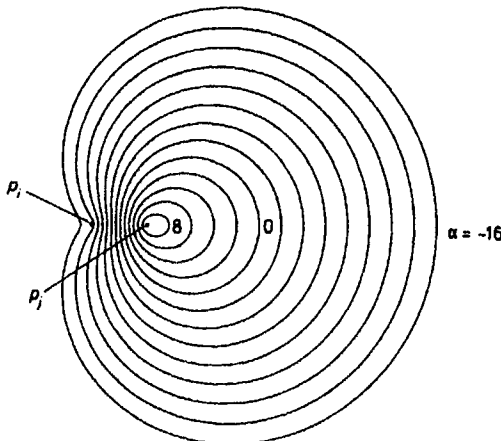


Figure 3.1.7 The bisectors with the compoundly weighted distance for several parameter values, $w_{i1}/w_{j1} = 1.5$, $\alpha = w_{i1}(w_{i2} - w_{j2}) = -16, \dots, -2, 0, 2, \dots, 8$ or compoundly weighted Voronoi diagrams for $n = 2$.

AW-Euclidean distance but also the MW-distance (the former is obtained by setting $\phi(t) = t$ and the latter is obtained by setting $\phi(t) = \log t$). Figure 3.1.6 shows planar AW-Voronoi diagrams with generalized AW-distances for $n = 2$.

3.1.3 Compoundsly weighted Voronoi diagram

The third type of weighted Voronoi diagram is obtained by compounding the MW-distance and the AW-distance, i.e.

$$d_{cw}(p, p_i) = \frac{1}{w_{i1}} \|x - x_i\| - w_{i2}, \quad w_{i1} > 0, \quad (3.1.12)$$

which we call the *compoundsly weighted distance* or simply the *CW-distance*. The CW-distance becomes the AW-distance if $w_{i1} = 1, i \in I_n$; it becomes the MW-distance if $w_{i2} = 0, i \in I_n$. The bisector with the CW-distance is given by the fourth-order polynomial function, and its shape is fairly complex, as is shown in Figure 3.1.7.

Although the shape of the bisector is fairly complex, it is easy to see that the bisector is well-behaving for $\|x_i - x_j\| > w_{i2}/w_{i1} - w_{j2}/w_{j1}$ (recall $\alpha > \beta$ in Section 3.1.2). Thus we can obtain a generalized Voronoi diagram, $\mathcal{V}(P, d_{cw}, \mathbb{R}^m) = \mathcal{V}_{cw} = \{V(p_i), \dots, V(p_n)\}$, where $V(p_i)$ is given by equations (3.1.1), (3.1.2) and (3.1.12). We call this generalized Voronoi diagram the *compoundsly weighted Voronoi diagram* generated by P , or the *CW-Voronoi diagram* of P . We call the set $V(p_i)$ the *compoundsly weighted Voronoi region* associated with p_i , or briefly the *CW-Voronoi region* of p_i . Figure 3.1.8 shows planar CW-Voronoi diagrams for different parameter values. The CW-Voronoi diagram reduces to the ordinary Voronoi diagram when

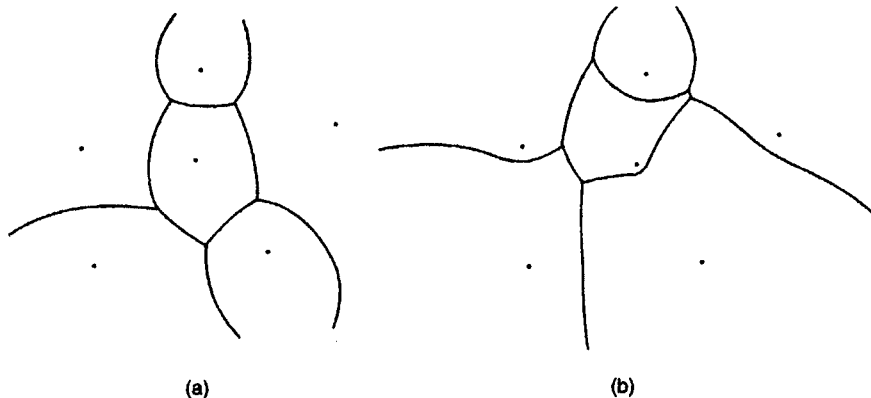


Figure 3.1.8 Compoundly weighted Voronoi diagrams in \mathbb{R}^2 .

$w_{i1} = 1, w_{i2} = 0, i \in I_n$. Thus, the CW-Voronoi diagram can be regarded as a generalization of the ordinary Voronoi diagram.

Since the CW-Voronoi diagram becomes the MW-Voronoi diagram if $w_{i1} = 0$ for $i \in I_n$ and it becomes the AW-Voronoi diagram if $w_{i2} = 1$ for $i \in I_n$, the CW-Voronoi diagram shows the properties of the AW-Voronoi diagram and the MW-Voronoi diagram for these specific cases. In other cases its proper properties appear. We show one example.

Property CW1 An edge of a CW-Voronoi region is part of the fourth-order polynomial curve (a proper property), a hyperbolic arc (Property AW2), a circular arc (Property MW3) or a straight line (Properties AW2 and MW3).

3.1.4 The power diagram

The fourth type of the weighted Voronoi diagram is characterized by the weighted distance

$$d_{pw}(p, p_i; w_i) = \|x - x_i\|^2 - w_i, \quad (3.1.13)$$

which we call the *additively weighted power distance* or, following Aurenhammer (1988a), the *power distance*. For simplicity, we usually employ the latter term, but the power distance should be distinguished from the ordinary power distance, $\|x - x_i\|^2$. Recalling the MW-distance, we might consider the multiplicatively weighted power distance $\|x - x_i\|^2/w_j$ (where $w_j > 0$). This distance, however, is transformable to the MW-distance, and hence it is a trivial extension.

The bisector with the MW-distance is, after a few steps of calculation, written as

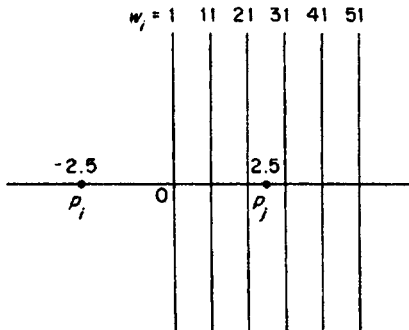


Figure 3.1.9 The bisectors with the additively weighted power distance for several parameter values, $x^T = (-2.5, 0.0)$, $x^T = (2.5, 0.0)$, $w_j = 1, w_i = 1, 11, 21, 31, 41$, or a power diagram for $n = 2$.

$$b(p_i, p_j) = \{x \mid (x_j - x_i)^T x = \frac{1}{2}(\|x_j\|^2 - \|x_i\|^2 + w_i - w_j)\}, \quad j \neq i. \quad (3.1.14)$$

We notice from this equation that the bisector is the straight line perpendicular to $\overline{p_i p_j}$ passing through the point x_{ij}^* given by

$$x_{ij}^* = \frac{\|x_j\|^2 - \|x_i\|^2 + w_i - w_j}{2\|x_j - x_i\|^2} (x_j - x_i). \quad (3.1.15)$$

As w_i increases, the dominance region becomes larger. Because of this property, we usually use a positive weight for w_i . Mathematically, however, we may replace $-w_i$ with $+w_i$ in equation (3.1.13). Figure 3.1.9 shows $\text{Dom}(p_i, p_j)$ for several parameter values. As is seen in this figure, the generator p_i may not be in $\text{Dom}(p_i, p_j)$, for example, $w_i = 31, 41, 51$.

Since the line of equation (3.1.15) splits \mathbb{R}^2 into two disjoint half planes, the bisector of equation (3.1.14) is well-behaving. Thus, equation (3.1.2) with (3.1.1) and (3.1.13) gives a generalized Voronoi diagram $\mathcal{V}(P, d_{pw}, \mathbb{R}^m) = \mathcal{V}_{pw} = \{V(p_1), \dots, V(p_n)\}$. We call this generalized Voronoi diagram the *additively weighted power diagram* generated by P or simply the *power diagram* of P (Aurenhammer, 1988), and call the set $V(p_i)$ the *power Voronoi polygon* associated with p_i . As we shall show in Section 3.6, the power diagram can be regarded as a Voronoi diagram of circles or a Voronoi diagram with Laguerre geometry (called the Laguerre Voronoi diagram). Also, as we shall discuss in the next subsection, the power diagram can be regarded as a sectional Voronoi diagram. The power diagrams in \mathbb{R}^3 and \mathbb{R}^4 are investigated by Chan *et al.* (1995) and Amato and Ramos (1996), respectively.

We find in Figure 3.1.10 that some power polygons are unbounded. Imai *et al.* (1985) derive the conditions for a bounded or an unbounded region as follows.

Property PW1 (i) The set $V(p_i)$ defined by equations (3.1.1), (3.1.2) and (3.1.13) is non-empty and unbounded if p_i is a vertex of $\text{CH}(P)$.

(ii) The set $V(p_i)$ is either unbounded or empty if p_i is on the boundary of $\text{CH}(P)$ except the vertices (at least three generators are on a boundary line segment of $\text{CH}(P)$).

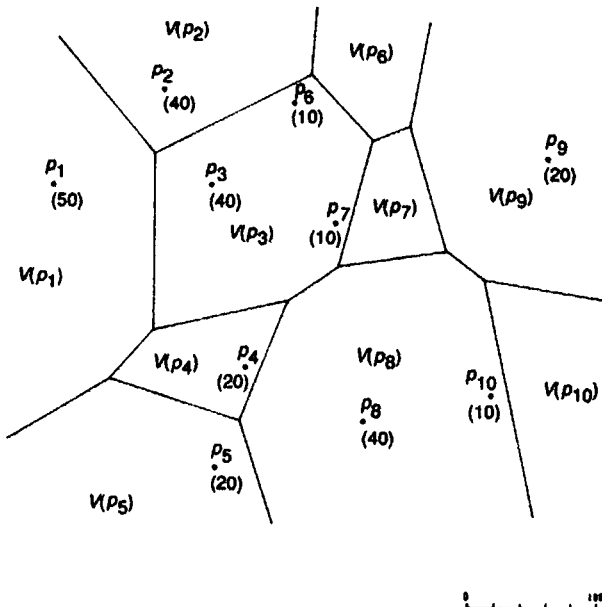


Figure 3.1.10 A(n) (additively weighted) power diagram.

(iii) The set $V(p_i)$ is either bounded or empty if p_i is an interior point of $\text{CH}(P)$.

The proof is provided by Imai *et al.* (1985, Lemma 3).

From the fact that the dominance region is a half plane and that $V(p_i)$ is the intersection of half planes, we note the following property.

Property PW2 If the set $V(p_i)$ is not empty, it is a convex polygon.

In Figure 3.1.9, we observe that the dominance region $\text{Dom}(p_i, p_j)$ with the parameter values $w_i = 31, 41, 51$ includes not only p_i but also p_j . From this property, we notice the following property.

Property PW3 The generator of $V(p_i)$ may not be in $V(p_i)$.

Similar to how we obtained the Delaunay triangulation as the dual of the ordinary Voronoi diagram, we can define a Delaunay diagram of the power diagram by connecting two generator points by a line segment if and only if their regions are adjacent. We refer to it as the *Delaunay power diagram*.

The Delaunay power diagram may be defined in the context of a more general tessellation. For a set $P = \{(x_1, y_1), \dots, (x_n, y_n)\}$ of points in \mathbb{R}^2 , we construct a set $P^* = \{(x_1, y_1, a_1), \dots, (x_n, y_n, a_n)\}$ of points in \mathbb{R}^3 with a set $A = \{a_1, \dots, a_n\}$ in such a way that every lower facet of $\text{CH}(P^*)$ (see the

proof of Property D7) is a triangle (a simplex). The orthographic projection of the lower facets of $\text{CH}(P^*)$ onto the x - y plane produces a triangulation of the convex hull of P . We call this resulting triangulation the *regular triangulation* spanning P induced by A (Edelsbrunner and Shah, 1996; Masada *et al.*, 1996a). We can easily extend the definition of the regular triangulation in \mathbb{R}^2 to that in \mathbb{R}^m (Edelsbrunner, 1986; Schlottmann, 1993).

Suppose that a_i is given by $a_i = x_i^2 + y_i^2 - w_i$. Then we notice that the Delaunay power diagram is a regular triangulation. More strongly, we have the following property.

Property PW4 A triangulation, \mathcal{T} , spanning P is a regular triangulation if and only if there are weights w_1, \dots, w_n such that \mathcal{T} is the Delaunay power diagram for P with these weights.

Since the Delaunay power diagram is a generalization of the Delaunay triangulation, it shares many properties with the Delaunay triangulation, some of which are shown below (Aurenhammer, 1991).

Property PW5 An edge of the regular triangulation spanning P is perpendicular to the corresponding edge of the power diagram generated by P .

3.1.5 The sectional Voronoi diagram

In the literature the sectional Voronoi diagram to be shown here is usually not subsumed under the family of weighted Voronoi diagrams. We refer to it here, however, because it can be regarded as a weighted Voronoi diagram.

Let $\mathcal{V} = \{V(p_1), \dots, V(p_n)\}$ be the three-dimensional ordinary Voronoi diagram generated by P , and K be a plane in \mathbb{R}^3 . Let J_s be the set of indices of i that satisfy $V(p_i) \cap K \neq \emptyset$,

$$V_{\text{sec}}(p'_i) = V(p_i) \cap K \neq \emptyset, \quad (3.1.16)$$

and $\mathcal{V}_{\text{sec}} = \{V_{\text{sec}}(p'_1), \dots, V_{\text{sec}}(p'_n)\}$, where p'_i is the orthogonal projection of p_i onto the plane K . The set $V_{\text{sec}}(p_i)$ is the intersection of polyhedron $V(p_i)$ with the plane K . We call $V_{\text{sec}}(p'_i)$ a *sectional Voronoi polygon*. Obviously, the collection of resulting sectional Voronoi polygons covers the plane K and they are not overlapping, except at the boundaries. Thus the set \mathcal{V}_{sec} forms a tessellation. We call this tessellation the *sectional Voronoi diagram* obtained as the intersection of \mathcal{V} with the plane K (Ash and Bolker, 1986; Aurenhammer, 1988a; Imai *et al.*, 1985; Sibson, 1980a). An example is shown in Figure 3.1.11, where generators are placed at $(1, 0, 1)$, $(-1, 0, 0)$ and $(0, -1, 0)$ in \mathbb{R}^3 . The ordinary Voronoi diagram of those generator points are indicated by the heavy lines (to make visual perception easy, the intersection of \mathcal{V} with the rectangle parallelopipedon is shown). The intersection of \mathcal{V} with the x_1 - x_2 plane (the plane K) is shown by the diagram on the x_1 - x_2 plane. We might expect that the resulting diagram is an ordinary Voronoi diagram, but this expectation is false. Chiu *et al.* (1996) prove that a sectional

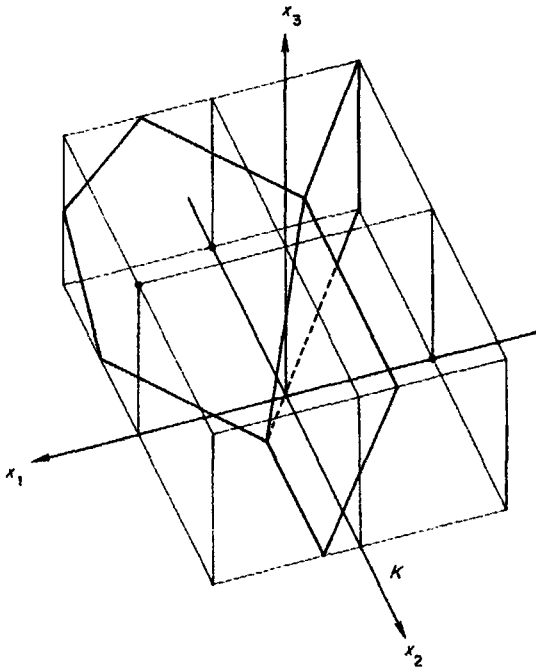


Figure 3.1.11 A sectional Voronoi diagram obtained from the three-dimensional ordinary Voronoi diagram with the x_1-x_2 plane, $n = 3$.

Voronoi diagram for points generated by the Poisson point process (see the sectional Poisson Voronoi diagrams in Section 5.7) is not the ordinary Voronoi diagram.

The sectional Voronoi diagram is related to the power diagram. To show this relation, suppose, for simplicity, that the plane K is the x_1-x_2 plane (we can place the plane K on the x_1-x_2 plane by rotating the plane K with P). Then $V_{\text{sec}}(p'_i)$ is written as

$$\begin{aligned} V_{\text{sec}}((x_i, x_n)) &= \left\{ (x_1, x_2) \mid \sqrt{(x_1 - x_{i1})^2 + (x_2 - x_{i2})^2 + x_{i3}^2} \right. \\ &\leq \sqrt{(x_1 - x_{j1})^2 + (x_2 - x_{j2})^2 + x_{j3}^2}, j \neq i, j \in I_n \}. \end{aligned} \quad (3.1.17)$$

If we write $\|x - x_i\|^2$ for $(x_1 - x_{i1})^2 + (x_2 - x_{i2})^2$, then equation (3.1.17) is written as

$$V_{\text{sec}}(x_i) = \{x \mid \|x - x_i\|^2 + x_{i3}^2 \leq \|x - x_i\|^2 + x_{j3}^2, j \neq i, j \in J_s\}. \quad (3.1.18)$$

Recalling the power distance of equation (3.1.13), we notice that this sectional Voronoi diagram is indeed the power diagram with the weight $\{-x_{i3}^2, j \in J_s\}$.

Extending the concept of the sectional Voronoi diagram in \mathbb{R}^3 , we can define a sectional Voronoi diagram of an m -dimensional ordinary Voronoi

diagram with a hyperplane in \mathbb{R}^m . Modifying it, we may consider a k -dimensional polytope Q defined by hyperplanes and a k -flat in \mathbb{R}^m , $k \leq m$, and define a Voronoi diagram by the collection of all non-empty intersections of the Voronoi polytopes with Q . Chan *et al.* (1995) call this diagram the *Voronoi diagram clipped to Q* or a *clipped Voronoi diagram*. Furthermore, we can define a *generalized sectional Voronoi diagram* by the intersection between a hyperplane in \mathbb{R}^m and a generalized Voronoi diagram in \mathbb{R}^m . A notable one is the *sectional multiplicatively weighted Voronoi diagram* defined by the intersection of a plane and the three-dimensional multiplicatively weighted Voronoi diagram (Moukarzel, 1995). Similarly we can define the *sectional additively weighted Voronoi diagram*, which is alternatively called the *sectional Johnson-Mehl Voronoi diagram* (Møller, 1992).

3.1.6 Applications

The family of weighted Voronoi diagrams is often adopted in market area analysis to determine the market areas of firms or stores, where the weights w_{i1} and w_{i2} in equation (3.1.12) correspond to a transportation cost and a mill price of goods or products, respectively. According to Shieh (1985), the earliest study dates back to Rau (1841). Launhardt (1882) and Fetter (1924) are also forerunners, followed by Tuominen (1949), Hyson and Hyson (1950), Gambini *et al.* (1967), Beckmann (1971), Boots (1980), Von Hohenbalken and West (1984), Aurenhammer (1987a), Hanjoul and Thisse (1987), Sakamoto and Takagi (1987), Hanjoul *et al.* (1989), O'Kelly and Miller (1989) and many others.

Gambini *et al.* (1967), Huff and Jenks (1968) and Huff (1973) studied national urban systems with the MW-Voronoi diagram. Huff and Lutz (1979) also used the same diagram to discuss a geographical delivery system for serving public interest in the Republic of Ireland. Illeris (1967) adopted the same diagram to determine functional regions of urban centres in Denmark; Hubbard (1970) and Wood (1974) carried out similar studies in Jamaica and Kenya, respectively. Cox and Agnew (1974) used the MW-Voronoi diagram to produce a partition of all Ireland into theoretical counties, which are compared with the actual counties (note that their map contains an error pointed by Weaire and Rivier, 1984). Archaeologists have used the MW-Voronoi diagram to define territories for various sites. Their work in this regard is reviewed by Hodder and Orton (1976, pp. 187–95). The most extensive of such studies is that of Hogg (1971) who used the MW-Voronoi diagram as a surrogate for territories of Neolithic hillforts south of the River Thames in England. Melachrinoudis and Smith (1995) uses the MW-Voronoi diagram to find the location that achieves the maximum distance to the nearest facility (imagine obnoxious facilities) where the facilities are characterized by their weights (Melachrinoudis and Cullinane, 1986). This problem is an extension of the largest empty circle problem in the ordinary Voronoi diagram discussed in Section 2.3. Billia *et al.* (1991) statistically analyze defects and disorder in two-dimensional cellular arrays in the

directional solidification of binary alloys using the MW-Voronoi diagram. Moukarzel (1993) examines the equilibrium state of foams represented by the MW-Voronoi diagram. Boots (1994) illustrates how the cross-product form of most spatial autocorrelation models, such as those of Geary and Moran, is equivalent to the form of the MW-Voronoi diagram and show a method of visualizing spatial autocorrelation in point data. Gerstein *et al.* (1995) models a cell structure of globular proteins in terms of the MW-Voronoi diagram. Billia *et al.* (1991) investigate the disorder of cellular arrays where the weight reflects the diameter of a cell. Siersma (1998) examines the Voronoi surface of the MW-Voronoi diagram (recall Section 2.1) in terms of the Morse theory. Inaba *et al.* (1994) apply the MW- and AW-Voronoi diagrams to a variance-based clustering.

The AW-Voronoi diagram is a special case of the Johnson–Mehl model (Johnson and Mehl, 1939; see Sections 5.8 and 7.2), which provides many diverse applications, such as crystal growth, cell structures of plants and foams made out of soap bubbles (Matzke and Nestler, 1946; Smith, 1954; Williams, 1968). Lesley (1976), Vaughan and Cousins (1977) and Wirasinghe and Ghoneim (1981) represented service areas of bus stops in terms of the AW-Voronoi diagram. Tao and Huang (1996) and Hai and Huang (1996) apply the AW-Voronoi diagram to warping, widely used in image distortion correction, special animation effects and human expression synthesis.

The sectional Voronoi diagram, which is regarded as the power diagram, may be utilized in stereology, which attempts to recover three-dimensional information from one- or two-dimensional samples. In the same fashion, van de Weygaert (1994) shows how to infer information on the actual three-dimensional galaxy distribution from a survey confined to two dimensions (i.e. slices), or one dimension (i.e. pencil beams). Moukarzel (1995) shows that equilibrium configurations of two-dimensional foams are well represented by the sectional multiplicatively weighted Voronoi diagram.

The power diagram is also used in modelling the crystal structure of organic compounds (Fischer and Koch, 1979), grain growth in a two-dimensional polycrystal (Telly *et al.*, 1992), metallic glass (Gellatly and Finney, 1982a), globular proteins (Gellatly and Finney, 1982b), and muscle fibres (Venema, 1991) (see also the applications in Sections 3.5.5 and 7.1). Aurenhammer (1987) refers to the power diagram in conjunction with the problem called the *illumination of balls* (Linhart, 1981): the union of n balls in a space can be illuminated by the vertices of the power diagram for the corresponding spheres. The power diagram is also applied to the grain boundary structure of polycrystalline materials (Ogawa *et al.*, 1996b).

3.2 HIGHER-ORDER VORONOI DIAGRAMS

In the ordinary Voronoi diagram, a generator is a point p_i , or a generator set is a set $P = \{p_1, \dots, p_n\}$ of points. In this section, which extends a point to a set of points, we consider the family of generalized Voronoi diagrams

generated by a set of all possible subsets consisting of k points out of P , i.e. $A^{(k)}(P) = \{\{p_{11}, \dots, p_{1k}\}, \dots, \{p_{l1}, \dots, p_{lk}\}\}$, where $p_{ij} \in P$ and $l = n!/(k!(n-k)!)$. We shall call this family the ‘higher-order’ Voronoi diagram. Here the ‘order’ means the number of points constituting a generator and ‘higher’ means more than one point. Note that ‘higher’ does not refer to the dimension of a space. In this section we deal with only \mathbb{R}^2 , but conceptually the extension from \mathbb{R}^2 to \mathbb{R}^m is straightforward.

The higher-order Voronoi diagram has been studied by many researchers, including Miles (1970a), Shamos and Hoey (1975), Shamos (1978), Bentley and Maurer (1979), Sibson (1980a), Dehne (1982), Lee (1982b), Miles and Maillardet (1982), Edelsbrunner (1986), Chazelle *et al.* (1986), Chazelle and Edelsbrunner (1987), Aurenhammer (1990b), Aurenhammer and Schwarzkopf (1991) and Agarwal *et al.* (1994). This section is based upon the results obtained by those researchers.

3.2.1 The order- k Voronoi diagram

Suppose, as is illustrated in Figure 3.2.1, that a set of distinct points (the filled circles) is placed in the Euclidean plane. We consider the Euclidean distances from a location, say the location indicated by the unfilled circle in the figure, to all points in the point set. As can be seen from the dashed lines in Figure 3.2.1, the first and the second nearest points from the location are p_1 and p_4 . In this case we assign the location to the set $\{p_1, p_4\}$. In general, if a set of the first and the second nearest points from a location is $\{p_i, p_j\}$, we assign the location to $\{p_i, p_j\}$. If the set is not only $\{p_i, p_j\}$ but also other sets of two points, we assign the location to those sets. Note that we are not

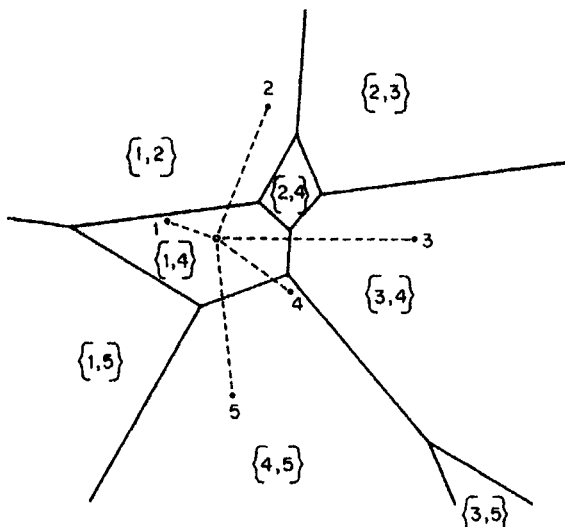


Figure 3.2.1 An order-2 Voronoi diagram ($n = 5$).

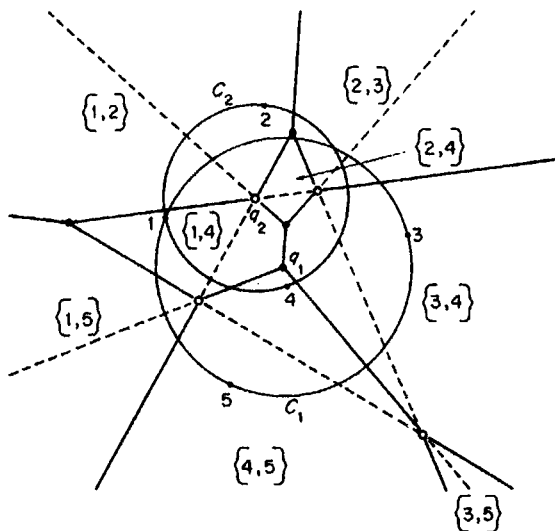


Figure 3.2.2 The ordinary Voronoi diagram (the dashed lines) and the order-2 Voronoi diagram (the solid lines) generated by the same set of generator points ($n = 5$; the locations of generator points are the same as those in Figure 3.2.1).

concerned with which point is the first nearest point in $\{p_i, p_j\}$; p_i may be the first or the second nearest point. Following this assignment rule, we assign all locations in the plane to at least one of the sets of two points. As a result, locations assigned to $\{p_i, p_j\}$ form a region, which we call the *order-2 Voronoi polygon* associated with $\{p_i, p_j\}$. A collection of the resulting order-2 Voronoi polygons is depicted in Figure 3.2.1, where the region with symbol $\{i, j\}$ indicates the order-2 Voronoi polygon associated with $\{p_i, p_j\}$ and i associated with a filled circle indicates the point p_i . This collection forms a tessellation, which we call the *order-2 Voronoi diagram* generated by the set of points.

Having understood the order-2 Voronoi diagram, the reader may be curious to know what the configurational relationship is between this diagram and the ordinary Voronoi diagram. Figure 3.2.2 shows this relationship. The dashed lines indicate the ordinary Voronoi diagram and the solid lines indicate the order-2 Voronoi diagram generated by the same generator set. We notice from this figure that the two Voronoi diagrams do not share edges but share some vertices (the unfilled circles). These vertices have an interesting property. To show it precisely, we first give the mathematical definition of the order-2 Voronoi diagram.

Let $P = \{p_1, \dots, p_n\}$ be a set of distinct points in \mathbb{R}^2 , where $2 \leq n < \infty$; $A^{(2)}(P) = \{P_1^{(2)}, \dots, P_i^{(2)}, \dots, P_l^{(2)}\}$, where $P_i^{(2)} = \{p_{i1}, p_{i2}\}$, $p_{i1}, p_{i2} \in P$, and $l = n!/(2!(n - 2)!)$ (the number of all possible subsets consisting of two points out of P); and $d(p, p_{ij})$ be the Euclidean distance from p to p_{ij} . The points p_{i1} and p_{i2} are the first and the second nearest points from p if and only if

the distances from p to p_{i1} and p_{i2} are both shorter than or equal to the distances from p to the other points (i.e. points in $P \setminus \{p_{i1}, p_{i2}\}$). Thus the set, $V(P_i^{(2)})$, of points assigned to $\{p_{i1}, p_{i2}\}$ is written as

$$\begin{aligned} V(P_i^{(2)}) &= \{p \mid d(p, p_{i1}) \leq d(p, p_j) \\ &\quad \text{and } d(p, p_{i2}) \leq d(p, p_j), \text{ for } p_j \in P \setminus P_i^{(2)}\}. \end{aligned} \quad (3.2.1)$$

The assignment rule in equation (3.2.1) is equivalent to the assignment rule that the longest distance among the distances from p to p_{i1} and p_{i2} is shorter than or equal to the shortest distance among the distances from p to the other points (i.e. points in $P \setminus \{p_{i1}, p_{i2}\}$). Thus $V(P_i^{(2)})$ is alternatively written as

$$\begin{aligned} V(P_i^{(2)}) &= \{p \mid \max_{p_h} \{d(p, p_h) \mid p_h \in P_i^{(2)}\} \\ &\leq \min_{p_j} \{d(p, p_j) \mid p_j \in P \setminus P_i^{(2)}\}\}. \end{aligned} \quad (3.2.2)$$

The extension of the order-2 Voronoi diagram to the order- k Voronoi diagram is straightforward. Let $A^{(k)}(P)$ be the set of all possible subsets consisting of k points out of P , i.e. $A^{(k)}(p) = \{P_1^{(k)}, \dots, P_i^{(k)}, \dots, P_l^{(k)}\}$, where $P_i^{(k)} = \{p_{i1}, \dots, p_{ik}\}$, $p_{ij} \in P$ and $l = n!/(k!(n - k)!)$. In these terms, we define

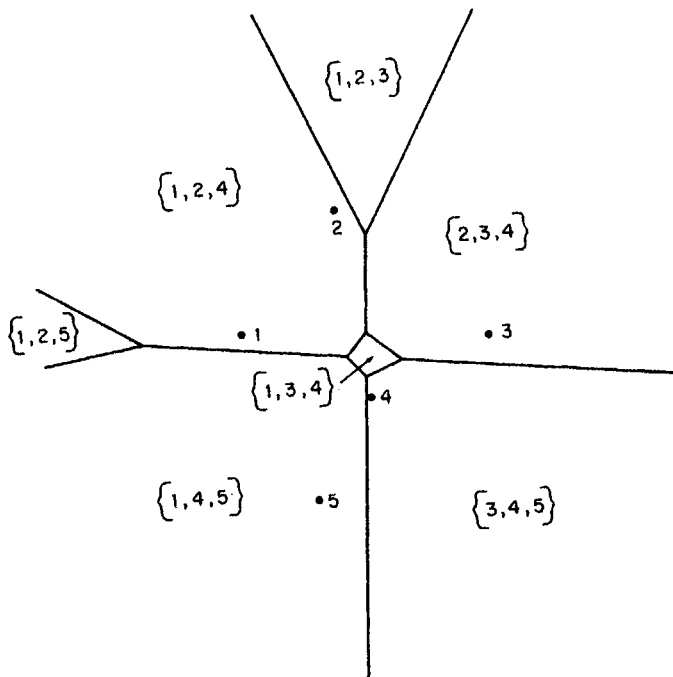
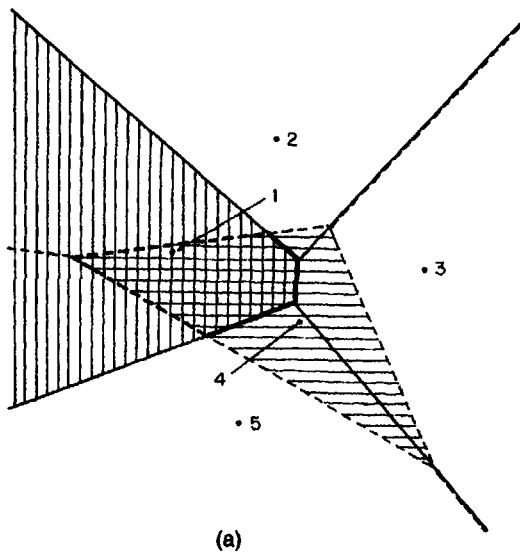
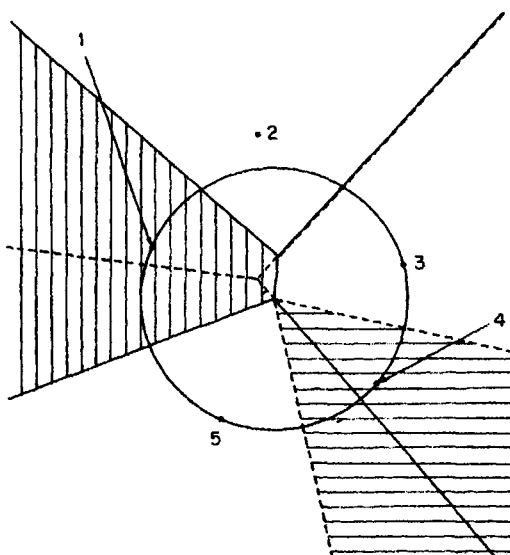


Figure 3.2.3 An order-3 Voronoi diagram ($n = 5$, the locations of points are the same as those in Figure 3.2.1).



(a)



(b)

Figure 3.2.4 An order-2 Voronoi polygon obtained from the intersection of two ordinary Voronoi polygons: (a) the intersection has a non-zero area; (b) the intersection is a point.

$$\begin{aligned} V(P_i^{(k)}) &= \{ p \mid \max_{p_h} \{ d(p, p_h) \mid p_h \in P_i^{(k)} \} \\ &\leq \min_{p_j} \{ d(p, p_j) \mid p_j \in P \setminus P_i^{(k)} \} \}. \end{aligned} \quad (3.2.3)$$

We call the set $V(P_i^{(k)})$ the *order- k Voronoi polygon* associated with $P_i^{(k)}$, and the set of order- k Voronoi polygons, $\mathcal{V}(A^{(k)}(P), d, \mathbb{R}^m) = \mathcal{V}^{(k)} = \{V(P_1^{(k)}), \dots, V(P_n^{(k)})\}$, the *order- k Voronoi diagram* generated by P . In the literature, $\mathcal{V}^{(k)}$ is sometimes called the *generalized Voronoi diagram*, the *k th order Voronoi diagram* and the *Voronoi diagram of order k* . Figure 3.2.3 shows an order-3 Voronoi diagram in which the region with the symbol $\{i, j, k\}$ indicates the order-3 Voronoi polygon of $\{p_i, p_j, p_k\}$.

In addition to the definitions of $V(P_i^{(2)})$ and $V(P_i^{(k)})$ by equations (3.2.1) and (3.2.3), we give one more definition. Since the set of points satisfying $d(p, p_{i1}) \leq d(p, p_i)$ and $d(p, p_{i2}) \leq d(p, p_i)$ is given by $H(p_{i1}, p_i) \cap H(p_{i2}, p_i)$, equation (3.2.1) is alternatively written as

$$V(P_i^{(2)}) = \bigcap_{p_j \in P \setminus \{p_{i1}, p_{i2}\}} [H(p_{i1}, p_i) \cap H(p_{i2}, p_i)], \quad (3.2.4)$$

where $H(p_{i1}, p_i)$ is the half plane used in defining the ordinary Voronoi diagram. Generalizing this definition for a general k , we obtain:

$$V(P_i^{(k)}) = \bigcap_{p_j \in P \setminus P_i^{(k)}} [H(p_{i1}, p_i) \cap \dots \cap H(p_{ik}, p_i)]. \quad (3.2.5)$$

This definition is useful in examining the properties of the order- k Voronoi diagram.

The order, k , varies from one to n . An order-1 Voronoi diagram is the ordinary Voronoi diagram; thus an order- k Voronoi diagram includes the ordinary Voronoi diagram. If $k = n$, then $A^{(n)}(P) = \{P\}$, and $\mathcal{V}^{(k)} = \{\mathbb{R}^2\}$. Since this diagram is too trivial, we exclude it from our discussion. If $k = n - 1$, an order- $(n-1)$ Voronoi diagram has a special name, which we shall discuss in the next subsection.

As we remarked in the introduction to this chapter, we may generalize the order- k Voronoi diagram with respect to a distance. Among many possible distances, the order- k Voronoi diagram with the additively weighted power distance (equation (3.1.13)) is notable. In the literature this Voronoi diagram is called the *order- k power diagram* (Aurenhammer, 1987). The reader who wishes to understand this Voronoi diagram in depth should consult Aurenhammer (1988a).

Having defined $\mathcal{V}^{(k)}$, we now wish to examine its geometric properties. From the definition of equation (3.2.4) we obtain:

$$V(P_i^{(2)}) = \left[\bigcap_{p_j \in P \setminus P_i^{(2)}} H(p_{i1}, p_j) \right] \cap \left[\bigcap_{p_j \in P \setminus P_i^{(2)}} H(p_{i2}, p_j) \right]. \quad (3.2.6)$$

Let $V(p_{i1}|P \setminus \{p_j\})$ denote the Voronoi polygon of p_{i1} in the ordinary Voronoi diagram generated by $P \setminus \{p_j\}$, i.e. $\mathcal{V}(P \setminus \{p_j\})$. Then, equation (3.2.6) is written as

$$V(P_i^{(2)}) = V(p_{i1} | P \setminus \{p_{i2}\}) \cap V(p_{i2} | P \setminus \{p_{i1}\}). \quad (3.2.7)$$

Figure 3.2.4(a) illustrates equation (3.2.7). The solid lines show $V(P \setminus \{p_4\})$ and the vertically hatched region indicates $V(p_1 | P \setminus \{p_4\})$. The vertically hatched region consists of the region in which the first nearest point is p_1 and the region in which the first and second nearest points are p_4 and p_1 . The dashed lines show $V(P \setminus \{p_1\})$ and the horizontally hatched region indicates $V(p_4 | P \setminus \{p_1\})$. The horizontally hatched region consists of the region in which the first nearest point is p_4 and the region in which the first and second nearest points are p_1 and p_4 . Thus the intersection of the vertically and horizontally hatched regions is the region in which the first and the second nearest points are p_1 and p_4 , respectively, or they are p_4 and p_1 , respectively. Thus the intersection gives $V(\{p_1, p_4\})$. In panel (a), the intersection is non-empty, but in some cases it may be empty. In a very special case, the intersection may be a point. In fact, panel (b) shows this example. This special case occurs when points in P are cocircular.

We can generalize equation (3.2.7) for a general k (Miles and Maillardet, 1982, Lemma on p. 102). From equation (3.2.5), we obtain the following property.

Property OK1

$$V(P_i^{(k)}) = \bigcap_{h=1}^k V(p_{ih} | [P \setminus P_i^{(k)}] \cup \{p_{ih}\}). \quad (3.2.8)$$

From this property we can derive a few important properties. First, as we mentioned above, the set $V(P_i^{(k)})$ may be empty. If $V(P_i^{(k)})$ is not empty, it is a point or an area. If it is a point, $V(P_i^{(k)})$ does not constitute a tessellation. If $V(P_i^{(k)})$ is an area, it is a polygon and, moreover, it is convex, because $V(p_{ih} | [P \setminus P_i^{(k)}] \cup \{p_{ih}\})$ is, from Property V1, a convex polygon and the intersection of convex polygons is a convex polygon. To sum up, we obtain the following property.

Property OK2 The set $V(P_i^{(k)})$ given by equation (3.2.3) may be empty, a point or an area. Under the non-cocircularity assumption, a non-empty $V(P_i^{(k)})$ is a convex polygon.

In observing Figure 3.2.2 we notice that every order-2 Voronoi polygon is split by one Voronoi edge of the ordinary Voronoi polygon. We can intuitively understand this property from the fact that the first nearest point from a point in $V(\{p_i, p_j\})$ is p_i or p_j , i.e. $V(\{p_i, p_j\})$ consists of part of $V(p_i)$ and part of $V(p_j)$ which share one Voronoi edge. From this property and Property D7, the number, $n_f^{(2)}$, of non-empty order-2 Voronoi polygons is equal to the number of Voronoi edges in the ordinary Voronoi diagram, i.e. $n_f^{(2)} = n_e = 3n - 3 - n_u$. Generalizing this equation for k , Lee (1982b, Theorem 2 and Corollary 3) proves the following property.

Property OK3 If P satisfies the non-cocircularity assumption, the number, $n_f^{(k)}$, of non-empty Voronoi polygons in $\mathcal{V}^{(k)}$ is given by

$$n_f^{(k)} = (2k - 1)n - (k^2 - 1) - \sum_{i=1}^k n_u^{(i-1)}, \quad (3.2.9)$$

where $n_u^{(i-1)}$ is the number of unbounded order- $(i-1)$ Voronoi polygons ($n_u^{(0)} = 0$). Consequently, $n_f(k)$ is $O(k(n - k))$.

When we use equation (3.2.9), we have to count $n_u^{(i-1)}$. To this end, let us obtain the necessary and sufficient condition for an order- $(i-1)$ Voronoi polygon to be unbounded. Let P_1 and P_2 be two disjoint sets of points in the plane. We say that a line L separates P_1 and P_2 if the points in P_1 and the points in P_2 lie in mutually opposite open half planes defined by L . In these terms the necessary and sufficient condition is written as follows.

Property OK4 The order- k Voronoi polygon $V(P_i^{(k)})$ is unbounded if and only if either (i) there is a line that separates $P_i^{(k)}$ (the filled circles in Figure 3.2.5(a), (b)) and $P \setminus P_i^{(k)}$ (the unfilled circles in Figure 3.2.5(a), (b)) or (ii) there are two consecutive points $p_j, p_l (\in P \setminus P_i^{(k)})$ on $\partial\text{CH}(P \setminus P_i^{(k)})$ such that the points in $P_i^{(k)} \setminus \overline{p_j p_l}$ are in the open half plane defined by the line passing through p_j and p_l opposite to $\text{CH}(P \setminus P_i^{(k)})$ (Figure 3.2.5(c)).

Proof First, suppose that either (i) or (ii) holds. If (i) holds, we transform the coordinate system in such a way that the separating line L is vertical and $\text{CH}(P \setminus P_i^{(k)})$ is to the left of L (Figure 3.2.5(a)). If (ii) holds, we transform the coordinate system in such a way that $\overline{p_j p_l}$ is vertical, the midpoint of $\overline{p_j p_l}$ lies on the x -axis, and $\text{CH}(P \setminus P_i^{(k)})$ is to the left of $\overline{p_j p_l}$ (Figure 3.2.5(c)). In both cases the point at infinity on the x -axis in the positive x direction belongs to the region $V(p_{ih} \mid [P \setminus P_i^{(k)}] \cup \{p_{ih}\})$ for any $p_{ih} \in P_i^{(k)}$. Hence we see from Property OK1 that if either (i) or (ii) holds, the Voronoi polygon $V(P_i^{(k)})$ is unbounded.

Next, suppose that $V(P_i^{(k)})$ is unbounded. Then, there exists at least one ray X such that the point at infinity on X belongs to $V(P_i^{(k)})$. We transform the coordinate system in such a way that X lies on the x -axis facing toward

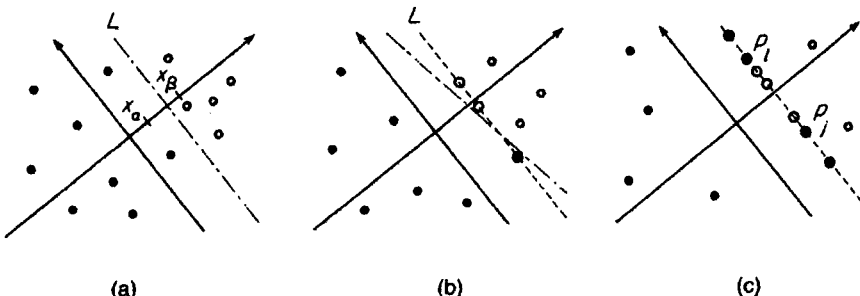


Figure 3.2.5 Illustration of the proof of Property OK4.

the positive x direction. Let x_α be the maximum value of the x coordinates of the points in $P \setminus P_i^{(k)}$, and x_β be the minimum value of the x coordinates of the points in $P_i^{(k)}$ (Figure 3.2.5(a), (b)). Then we get $x_\alpha \leq x_\beta$; this is because if $x_\alpha > x_\beta$, then for the point p_{ih} with the x coordinate x_β , the polygon $V(p_{ih} | [P \setminus P_i^{(k)}] \cup \{p_{ih}\})$ does not contain the point at infinity on the x -axis in the positive x direction.

Case 1. Suppose that $x_\alpha < x_\beta$ (Figure 3.2.5(a)). Then the vertical line defined by $x = (x_\alpha + x_\beta)/2$ separates $P_i^{(k)}$ and $P \setminus P_i^{(k)}$; hence (i) holds.

Case 2. Suppose that $x_\alpha = x_\beta$ (Figure 3.2.5(b), (c)). Let P_α be the set of points in $P \setminus P_i^{(k)}$ whose x coordinates are equal to x_β (the large filled circles in Figure 3.2.5(b), (c)), and let P_β be the set of points in $P_i^{(k)}$ whose x coordinates are equal to x_β ($= x_\alpha$) (the large unfilled circles in Figure 3.2.5(c)).

Case 2.1. Suppose that P_α contains exactly one point: $P_\alpha = \{p_j\}$. Then either all the points in P_β are above p_j or all the points in P_β are below p_j , because if $p_{ih} \in P_i^{(k)}$ is above p_j and $p_{il} \in P_i^{(k)}$ is below p_j , the regions $V(p_{ih} | [P \setminus P_i^{(k)}] \cup \{p_{ih}\})$ and $V(p_{il} | [P \setminus P_i^{(k)}] \cup \{p_{il}\})$ have no point in common. If the points in P_β are above p_j , we rotate the coordinate axes counter-clockwise slightly (the dash-dot line in Figure 3.2.5(b)), and get the situation where $x_\alpha < x_\beta$ and the point at infinity on the new x -axis in the positive x direction still belongs to $V(P_i^{(k)})$; thus we get (i). If the points in P_β are below p_j , we rotate the coordinate axes clockwise and get (i) similarly.

Case 2.2. Suppose that P_α contains two or more points. Then for any $p_j \in P_\alpha$ either all the points in P_β are above p_j or all the points in P_β are below p_j , because otherwise $V(P_i^{(k)})$ becomes empty, as we saw in Case 2.1. If all the points in P_β are above the highest point in P_α or below the lowest, we reduce the situation to Case 2.1 by slightly rotating the coordinate axes counter-clockwise or clockwise, respectively, as we did in Case 2.1. Hence, the only remaining case is that there are two points p_j and p_l in P_α such that $\overline{p_j p_l}$ contains no other points in P_α and $\overline{p_j p_l}$ contains all the points in P_β , which implies (ii). Thus, in all cases either (i) or (ii) holds. \square

In inspecting Figure 3.2.1 we notice that $V(\{p_1, p_5\})$ contains no points of P ; $V(\{p_1, p_2\})$ contains one point of P ; $V(\{p_4, p_5\})$ contains two points of P . In general, we notice the following property.

Property OKS A non-empty order- k Voronoi polygon contains 0, 1, . . . , or k points of P .

In an ordinary Voronoi diagram, every Voronoi vertex has the empty circle (Property V7). To find the corresponding property in an order- k Voronoi diagram, let us first examine a vertex, say q_1 , shared by $V(\{p_1, p_4\})$, $V(\{p_3, p_4\})$ and $V(\{p_4, p_5\})$ in Figure 3.2.2. We notice that p_1, p_3 and p_5 are equally distant from the vertex q_1 , and hence we can draw the circle C_1 centred at q_1 which passes through p_1, p_3 and p_5 . This circle contains p_4 . From this inspection and recalling Property V7, we might expect that for every vertex in an order-2 Voronoi diagram, there exists a circle which passes through three points of P .

and contains exactly one point of P in its interior. This expectation is, however, false. A counterexample is given by the circle C_2 centred at the vertex q_2 shared by $V(\{p_1, p_2\})$, $V(\{p_2, p_4\})$ and $V(\{p_1, p_4\})$ (Figure 3.2.2). The circle C_2 does not contain any point of P in its interior. If we draw circles at all vertices in Figure 3.2.2, we can see that the circles centred at the unfilled circles (which are called ‘old vertices’ in Lee, 1982b) have no points of P in their interiors, and the circles centred at the large filled circles (which are called ‘new vertices’) have exactly one point of P in their interiors. This result can be proved theoretically and is generalized by Lee (1982b, Lemma 6) as follows.

Property OK6 Under the non-cocircularity assumption, for every vertex q_i of an order- k Voronoi polygon, there exists a unique circle centred at q_i which passes through three points of P and contains $k-2$ or $k-1$ points of P in its interior.

The condition for $k-2$ or $k-1$ is explicitly stated in Lee (1982b, Lemma 6).

Applying almost the same derivation used for Property D11, we obtain the following property.

Property OK7 Let $n_v^{(k)}$, $n_e^{(k)}$, $n_f^{(k)}$ and $n_u^{(k)}$ be the number of vertices, edges, order- k Voronoi polygons and unbounded order- k Voronoi polygons, respectively. Then under the non-cocircularity assumption, the following equations hold:

$$n_v^{(k)} = 2(n_t^{(k)} - 1) - n_u^{(k)}, \quad (3.2.10)$$

$$n_e^{(k)} = 3(n_t^{(k)} - 1) - n_u^{(k)}. \quad (3.2.11)$$

These equations with $k = 1$ are, of course, the same as equations (2.4.13) and (2.4.14) in Property D11. The proof is shown by Lee (1982b, Lemma 11).

In addition to these properties, the statistical properties of the order- k Voronoi diagram are investigated in spatial statistics. We show these properties in Chapter 5. Regarding the properties of the order- k power diagram, see Aurenhammer (1988a).

We may define an order- k Voronoi diagram with the additively weighted distance (Section 3.1.2). We call a set of regions $V(P_i^{(k)})$ defined by equation (3.2.5) with the distance between x and x_i given by $\|x - x_i\| - w_i$ the *additively weighted order- k Voronoi diagram* generated by P (Rosenberger, 1991). The additively weighted order- k Voronoi diagram has the following property.

Property OK8 For the additively weighted order- k Voronoi diagram generated by P , let D_i be a disk centred at $p_i \in P$ with radius $|w_i|$, and assume that no disk is contained in another and $1 \leq k < n$. Then the relations

$$n_v^{(k)} \leq (4k - 2)(n - k) - \min\{k, n - k\} - 1, \quad (3.2.12)$$

$$n_e^{(k)} \leq (6k - 2)(n - k) - \min\{k, n - k\} - 1 \quad (3.2.13)$$

hold.

The proof is shown by Rosenberger (1991, Theorem 5).

We may also define an order- k Voronoi diagram by extending a generator set of points to a generator set of points, lines and polygons (Roos, 1989; regarding Voronoi diagrams for a set of lines and a set of polygons, see Sections 3.5 and 3.6, respectively).

3.2.2 The ordered order- k Voronoi diagram

The order- k Voronoi diagram has a closely related tessellation which we call the ‘ordered’ order- k Voronoi diagram. In the order- k Voronoi diagram, points in a generator set are not ordered (recall that in $V^{(k)}$ we were not concerned with which point was the first nearest point in a generator set), whereas in the ordered order- k Voronoi diagram, they are ordered. To show this contrast, let us begin our discussion with the same example used in Figure 3.2.1.

Suppose that a set of distinctive points (the filled circles in Figure 3.2.6) is placed in the Euclidean plane. We consider the Euclidean distances from a location, say the location indicated by the unfilled circle in Figure 3.2.6, to all points in the point set. The dashed lines in Figure 3.2.6 show that the first nearest point from the location is p_1 and the second nearest point from the location is p_4 . In this case we assign this location to the ordered pair (p_1, p_4) (note that $(p_1, p_4) \neq (p_4, p_1)$). In general, if an ordered pair of the first and the second nearest points from a location is (p_i, p_j) , we assign the location to (p_i, p_j) . If the ordered pairs are not only (p_i, p_j) but also other ordered pairs, then we assign the location to those ordered pairs. In this manner we

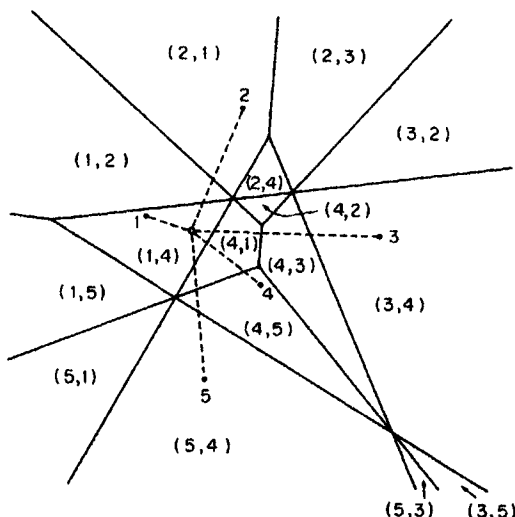


Figure 3.2.6 An ordered order-2 Voronoi diagram ($n = 5$; the locations of the generator points are the same as those in Figure 3.2.1).

assign all locations in the plane to at least one ordered pair. As a result, locations assigned to each pair form a region, which we call the *ordered order-2 Voronoi polygon* associated with (p_i, p_j) . The collection of ordered order-2 Voronoi polygons is shown in Figure 3.2.6 in which the region with the symbol (i, j) indicates the ordered order-2 Voronoi polygon associated with (p_i, p_j) . This collection forms a tessellation, which we call the *ordered order-2 Voronoi diagram* generated by the set of points.

To observe the geometric properties of an ordered order- k Voronoi diagram, it is instructive to compare this diagram with the ordinary Voronoi diagram, \mathcal{V} , generated by the same set of generator points. In Figure 3.2.7 the dashed lines show \mathcal{V} , and the solid lines show the ordered order-2 Voronoi diagram. In this figure, consider a Voronoi polygon, for example $V(p_4)$ in \mathcal{V} . Since the first nearest point of P from a location in $V(p_4)$ is p_4 , the ordered order-2 Voronoi polygons associated with $(p_4, p_j), j = 1, 2, 3, 5$, are included in $V(p_4)$, and these polygons constitute $V(p_4)$. Thus the Voronoi edges in \mathcal{V} are the edges of the order-2 Voronoi diagram. To deepen this analysis, let us restate the above verbal definition in mathematical terms.

Let $A^{(2)}(P)$ be the set of all ordered pairs of points obtained from $P = \{p_1, \dots, p_n\}$, i.e. $A^{(2)}(P) = \{P_1^{(2)}, \dots, P_i^{(2)}, \dots, P_l^{(2)}\}$, where $P_i^{(2)} = (p_{i1}, p_{i2})$, $p_{i1}, p_{i2} \in P$, and $l = n(n - 1)$. For a set $P_i^{(2)}$ in $A^{(k)}(P)$, we define

$$V(P_i^{(2)}) = \{p \mid d(p, p_{i1}) \leq d(p, p_{i2}) \leq d(p, p_j), p_j \in P \setminus \{p_{i1}, p_{i2}\}\}. \quad (3.2.14)$$

We call the set $V(P_i^{(2)})$ the *ordered order-2 Voronoi polygon* associated with $P_i^{(2)}$.

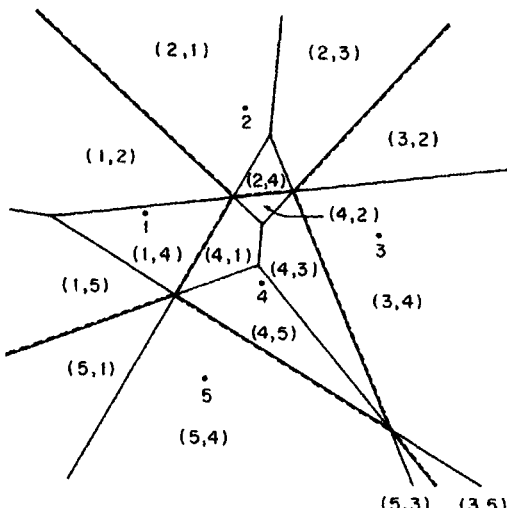


Figure 3.2.7 The ordered order-2 Voronoi diagram (the solid lines) and the ordinary Voronoi diagram (the broken lines) generated by the same set of points ($n = 5$; the locations of the generator points are the same as those in Figure 3.2.1).

The extension to a general k is immediate. Let $A^{(k)}(P)$ be the set of all ordered k -tuples of points obtained from P , i.e. $A^{(k)}(P) = \{P_1^{(k)}, \dots, P_i^{(k)}, \dots, P_l^{(k)}\}$, where $P_i^{(k)} = (p_{i1}, \dots, p_{ik})$, $p_{ij} \in P$, $j \in I_k$, and $l = n(n-1) \dots (n-k+1)$. For a set $P_i^{(k)}$ in $A^{(k)}(P)$, we define

$$V(P_i^{(k)}) = \{p \mid d(p, p_{i1}) \leq d(p, p_{i2}) \leq \dots \leq d(p, p_{ik}) \leq d(p, p_j), \\ p_j \in P \setminus \{p_{i1}, \dots, p_{ik}\}\}. \quad (3.2.15)$$

We call the set $V(P_i^{(k)})$ the *ordered order- k Voronoi polygon* associated with $P_i^{(k)}$ and $\mathcal{V}(A^{(k)}(P), d, \mathbb{R}^m) = \mathcal{V}^{(k)} = \{V(P_1^{(k)}), \dots, V(P_l^{(k)})\}$ the *ordered order- k Voronoi diagram* generated by P . Figure 3.2.8 shows an ordered order-3 Voronoi diagram.

To analyse the geometric properties of the ordered order- k Voronoi diagram, the following alternative definition is more useful. The set of points satisfying $d(p, p_{i1}) < d(p, p_{i2}) < d(p, p_j)$ is given by $H(p_{i1}, p_{i2}) \cap H(p_{i2}, p_j)$. Thus, equation (3.2.14) is written as

$$V(P_i^{(2)}) = \bigcap_{p_j \in P \setminus \{p_{i1}, p_{i2}\}} H(p_{i1}, p_{i2}) \cap H(p_{i2}, p_j). \quad (3.2.16)$$

Similarly, for a general k , equation (3.2.15) is written as

$$V(P_i^{(k)}) = \bigcap_{p_j \in P \setminus \{p_{i1}, \dots, p_{ik}\}} H(p_{i1}, p_{i2}) \cap \dots \cap H(p_{ik-1}, p_{ik}) \cap H(p_{ik}, p_j). \quad (3.2.17)$$

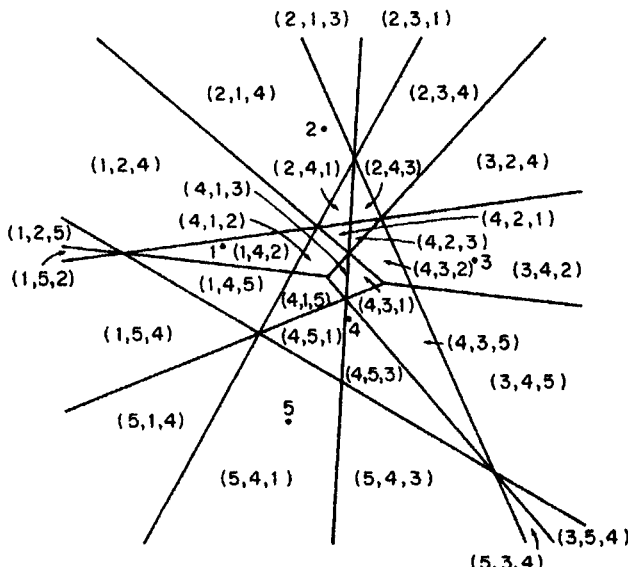


Figure 3.2.8 An ordered order-3 Voronoi diagram ($n = 3$; the locations of generator points are the same as those in Figure 3.2.1).

Having defined the ordered order- k Voronoi diagram $\mathcal{V}^{(k)}$ mathematically, we are now ready to examine its geometric properties. From equation (3.2.16) we can write $V(P_i^{(2)})$ as

$$\begin{aligned} V(P_i^{(2)}) &= \bigcap_{p_j \in P \setminus \{p_n, p_n\}} H(p_n, p_n) \cap H(p_n, p_j) \cap H(p_n, p_j) \\ &= \left[\bigcap_{p_j \in P \setminus \{p_n\}} H(p_n, p_j) \right] \cap \left[\bigcap_{p_j \in P \setminus \{p_n, p_n\}} H(p_n, p_j) \right] \\ &= V(p_n) \cap V(p_n | P \setminus \{p_n\}). \end{aligned} \quad (3.2.18)$$

Let us confirm this equation with $V((p_1, p_4))$ in Figure 3.2.7. Since the first nearest point in $V((p_1, p_4))$ is p_1 , $V((p_1, p_4))$ is included in $V(p_1)$. The second nearest point in $V((p_1, p_4))$ becomes the first nearest point if p_1 is deleted from P . Thus $V((p_1, p_4))$ is given by $V(p_1) \cap V(p_4 | P \setminus \{p_1\})$. Generalizing equation (3.2.18), we obtain the following equation.

Property OOK1 An ordered order- k Voronoi polygon is written in terms of ordinary Voronoi polygons as

$$V(P_i^{(k)}) = \bigcap_{h=1}^k V(p_{ih} | P \setminus \{p_{i1}, \dots, p_{ih-1}\}), \quad (3.2.19)$$

where $\{p_{i1}, \dots, p_{ih-1}\} = \emptyset$ for $h = 1$.

In Figure 3.2.7 we observe that $V(p_4)$ consists of $V((p_4, p_2))$, $V((p_4, p_1))$, $V((p_4, p_5))$ and $V((p_4, p_3))$. We can generalize this property for a general k as follows.

Property OOK2 Let $A^{(k-1)}(P \setminus \{p_{i1}\})$ be all possible ordered $(k-1)$ -tuples obtained from $P \setminus \{p_{i1}\}$. Then

$$V(p_{i1}) = \bigcup_{(p_{i2}, \dots, p_{ik}) \in A^{k-1}(P \setminus \{p_{i1}\})} V((p_{i1}, p_{i2}, \dots, p_{ik})). \quad (3.2.20)$$

This property implies that the ordered order- k Voronoi diagram $\mathcal{V}^{(k)}$ generated by $A^{(k)}(P)$ is a refinement of the ordinary Voronoi diagram generated by P . Figure 3.2.6 shows the refinement of $\mathcal{V}(P)$ by $\mathcal{V}^{(2)}(A^{(2)}(P))$.

An ordered order- k Voronoi diagram also refines the order- k Voronoi diagram. The region in which the first and the second nearest points are $\{p_i, p_j\}$ consists of the region in which the first and second nearest points are p_i and p_j , respectively, and the region in which the first and the second nearest points are p_j and p_i , respectively (observe this relation in Figure 3.2.9). Thus $V(\{p_i, p_j\}) = V((p_i, p_j)) \cup V((p_j, p_i))$. More generally, we have the following property.

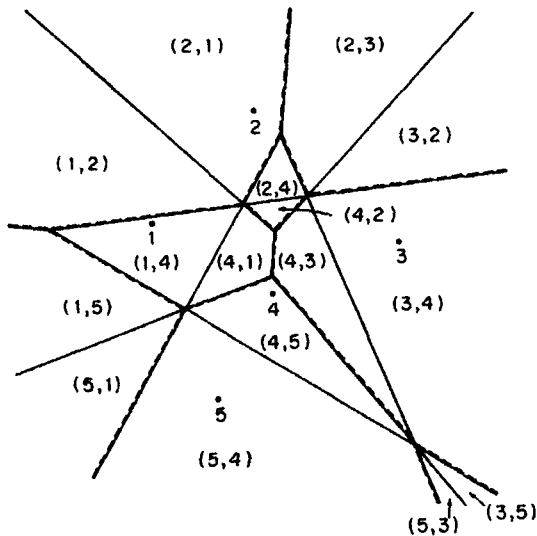


Figure 3.2.9 The order-2 Voronoi diagram (the dashed lines) and the ordered order-2 Voronoi diagram (the solid lines) generated by the same set of points; the ordered order-2 Voronoi diagram is a refinement of the order-2 Voronoi diagram.

Property OOK3

$$V(P_i^{(k)}) = \bigcup_{P_j^{(k)} \in A^{(k)}(P_i^{(k)})} V(P_j^{(k)}), \quad (3.2.21)$$

where $A^{(k)}(P_i^{(k)})$ is the set of all possible k -tuples made of p_{i1}, \dots, p_{ik} .

Equation (3.2.21) says that $\mathcal{V}^{(k)}$ generated by P is a refinement of $\mathcal{V}^{(k)}$ generated by P . An example is shown in Figure 3.2.9.

From Property OOK1, we obtain the next property.

Property OOK4 The set $V(P_i^{(k)})$ given by equation (3.2.15) may be empty. If $V(P_i^{(k)})$ is not empty, it is a point or an area. Under the non-cocircularity assumption, a non-empty $V(P_i^{(k)})$ is a convex polygon.

In Property OK4 we saw the necessary and sufficient condition for an order- k Voronoi polygon to be unbounded. A similar condition is obtained for an ordered order- k Voronoi polygon. To avoid unnecessary complication, we next state the condition that is valid only when no two lines passing through two points in P are parallel to each other.

Property OOK5 Suppose that no two lines passing through two points in P are mutually parallel. Let $P_i^{(k)} = (p_{i1}, p_{i2}, \dots, p_{ik})$ be an ordered k -tuple of elements of P . Then the ordered order- k Voronoi polygon $V(P_i^{(k)})$ is

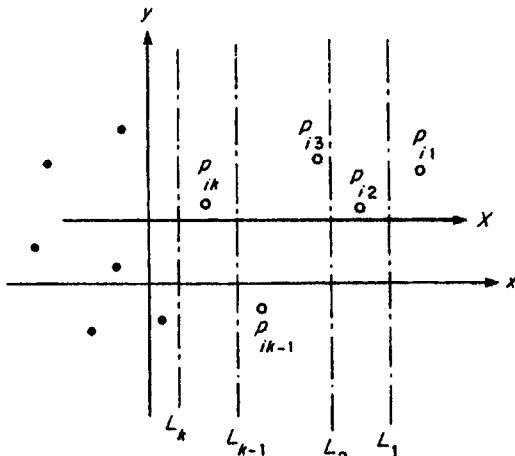


Figure 3.2.10 Illustration of the proof of Property OOK5.

unbounded if and only if there are k mutually parallel lines L_1, L_2, \dots, L_k such that L_h separates $\{p_{i1}, p_{i2}, \dots, p_{ih}\}$ and $P \setminus \{p_{i1}, p_{i2}, \dots, p_{ih}\}$ for $h = 1, 2, \dots, k$ (Figure 3.2.10).

Proof First, suppose that there exist k mutually parallel lines L_1, \dots, L_k specified in Property OOK5 (Figure 3.2.10). We transform the coordinate system in such a way that L_1, \dots, L_k are vertical and p_{i1} is the rightmost point in P . Then the point at infinity in the positive x direction is contained in the region $V(p_{i1} | P \setminus \{p_{i1}, \dots, p_{ih-1}\})$ for any k . Hence it follows from Property OOK1 that $V(P_i^{(k)})$ contains the point at infinity in the positive x direction; that is, $V(P_i^{(k)})$ is unbounded.

Next, suppose that $V(P_i^{(k)})$ is unbounded. Then there exists a ray X such that the point at infinity on X belongs to $V(P_i^{(k)})$. Since no two lines passing through two points in P are mutually parallel, the perpendicular bisectors of two points in P are not parallel to each other. In particular, no two edges on the boundary of $V(P_i^{(k)})$ are parallel, and hence we can choose the ray X in such a way that X is not perpendicular to any line passing through two points in P .

Now we transform the coordinate system in such a way that X is parallel to the x -axis (Figure 3.2.10). Let x_{ih} be the x coordinate of p_{ih} for $h = 1, 2, \dots, k$. Property OOK1 implies that x_{ih} is greater than the x coordinate of any point in $P \setminus \{p_{i1}, \dots, p_{ih-1}\}$ and consequently we get $x_{i1} > x_{i2} > \dots > x_{ik}$ and all the points in $P \setminus P_i^{(k)}$ have smaller x coordinates than p_{ik} . Let L_h be the vertical line defined by $x = (x_{ih} + x_{ih+1})/2$ for $h = 1, \dots, k$, where x_{ik+1} is the x coordinate of the rightmost point in $P \setminus P_i^{(k)}$. Then L_1, \dots, L_k are mutually parallel (actually they are vertical) and L_{ih} separates $\{p_{i1}, \dots, p_{ih}\}$ and $P \setminus \{p_{i1}, \dots, p_{ih}\}$. \square

Corresponding to Property D7 and Property OK7, the following equations hold for the numbers of vertices, edges and polygons.

Property OOK6 Let $n_v^{(2)}$, $n_e^{(2)}$, $n_f^{(2)}$ and $n_u^{(2)}$ be the number of vertices, edges, ordered order-2 Voronoi polygons and unbounded ordered order-2 Voronoi polygons, respectively, in the ordered order-2 Voronoi diagram generated by P ; $n_v^{(2)}$, $n_e^{(2)}$, $n_f^{(2)}$ and $n_u^{(2)}$ be those in the order-2 Voronoi diagram generated by P ; and n_v , n_e , n_f and n_u be those in the ordinary Voronoi diagram generated by P which satisfies the non-cocircularity assumption. Then

$$n_v^{(2)} = n_v^{(2)}, \quad (3.2.22)$$

$$n_e^{(2)} = n_e^{(2)} + n_e, \quad (3.2.23)$$

$$n_f^{(2)} = 2n_f^{(2)} = 2n_e = 6n - 6 - 2n_u. \quad (3.2.24)$$

Equation (3.2.22) may be understood visually from Figure 3.2.9 in which vertices of $\mathcal{V}^{(2)}$ are coincident with vertices of $\mathcal{V}^{(2)}$. Also equation (3.2.23) is understandable from Figures 3.2.6 and 3.2.8 in which the edges of $\mathcal{V}^{(2)}$ consist of the edges of \mathcal{V} and $\mathcal{V}^{(2)}$. The first equation in equation (3.2.24) is obtained from the fact that $V(\{p_{i1}, p_{i2}\})$ consists of $V((p_{i1}, p_{i2}))$ and $V((p_{i2}, p_{i1}))$ (Figure 3.2.9). The second equation is obtained from $n_f^{(2)} = n_e$ (see the equation obtained below Property OK2), and the third equation is obtained from equation (3.2.9). Substituting equations (3.2.9), (3.2.10) and (3.2.11) into the above equations, we can write $n_v^{(2)}$, $n_e^{(2)}$ and $n_f^{(2)}$ in different terms, some of which are shown in Shamos (1978).

Last, it is worth noting an interesting property found by Sibson (1980a), called the *local coordinates property*, and extended by Piper (1993).

Property OOK7 The equation

$$\mathbf{x}_i = \frac{\sum_{j \in I_n \setminus \{i\}} |V((p_i, p_j))| \mathbf{x}_j}{\sum_{j \in I_n \setminus \{i\}} |V((p_i, p_j))|} \quad (3.2.25)$$

holds if the denominator is greater than zero and less than infinity, i.e. if p_i is the interior of the convex hull of $P \setminus \{p_i\}$.

This equation says that the location of the point p_i is the centroid of the locations of points of $p_j \in P \setminus \{p_i\}$ weighted with the area $|V((p_i, p_j))|$ of the ordered order-2 Voronoi polygon associated with (p_i, p_j) . Sibson (1980a) proves this property in a little more general context. Since the proof requires a few pages, it is omitted here (see the proof on pp. 153–154 in Sibson, 1980a). This property is useful for interpolation (Sibson, 1980b), which is discussed in Chapter 6.

3.2.3 Applications

A natural application is found in a facility location problem in which the  nearest facility is critical, for instance in the case of a single unit emergency depot when more than one unit is required or when the first nearest unit is in use (Keeney, 1972).

We can find other applications in multivariate density estimation (Loftsgaarden and Quesenberry, 1965), classification (Cover and Hart, 1967) and information retrieval systems (Fukunaga and Narendra, 1975; Chazelle, 1985). In the study of waves and crystals, the k th nearest-point Voronoi diagram gives an important concept called the Brillouin zone (Brillouin, 1953). As we shall see in Chapter 6, the ordered order- k Voronoi diagram can be used for spatial interpolation (Sibson, 1980a), which is applied in statistical estimation (Ripley, 1981, Chapter 4) as well as in cartography (isoline generation). The multiplicatively weighted order- k Voronoi diagram has been used for retail trade area analysis (Boots and South, 1997).

3.3 THE FARTHEST-POINT VORONOI DIAGRAM AND k TH NEAREST-POINT VORONOI DIAGRAM

The nearest generator point from a point in an ordinary Voronoi polygon is of course the generator point of the Voronoi polygon (Property V6). To emphasize this property, we alternatively call the ordinary Voronoi diagram the *nearest-point Voronoi diagram*. In opposition to the nearest point Voronoi diagram, we can consider the ‘farthest-point’ Voronoi diagram. More generally, we can consider the ‘ k th nearest-point’ Voronoi diagram. In this section we show these generalized Voronoi diagrams.

3.3.1 The farthest-point Voronoi diagram

The definition of the farthest-point Voronoi diagram is almost the same as that of the nearest-point Voronoi diagram (Definition V1) except that ‘closest’ is replaced with ‘farthest’.

Given a set of distinct points in the Euclidean plane, we assign all locations in that plane to the farthest member(s) of the point set. The result is a tessellation of the plane into a set of regions associated the members in the point set. We call this tessellation the *farthest-point Voronoi diagram* generated by the point set, and the regions constituting the Voronoi diagram *farthest-point Voronoi polygons*. Figure 3.3.1(a) shows a farthest-point Voronoi diagram.

To restate the above verbal definition mathematically, let $P = \{p_1, \dots, p_n\} \subset \mathbb{R}^2$ ($2 \leq n < \infty$), $p_i \neq p_j$ for $i \neq j$. Then the *farthest-point Voronoi polygon*, $V_{fp}(p_i)$, associated with p_i is written as

$$V_{fp}(p_i) = \{p \mid d(p, p_i) \geq d(p, p_j), p_j \in P \setminus \{p_i\}\}, \quad (3.3.1)$$

$$= \{p \mid d(p, p_i) \geq \max_{p_j} \{d(p, p_j), p_j \in P \setminus \{p_i\}\}\}. \quad (3.3.2)$$

Alternatively, in terms of the dominance region $\text{Dom}(p_i, p_j) = \{p \mid d(p, p_i) \geq d(p, p_j)\} = H(p_j, p_i)$, the set $V_{fp}(p_i)$ is written as

$$V_{fp}(p_i) = \bigcap_{p_j \in P \setminus \{p_i\}} H(p_j, p_i). \quad (3.3.3)$$

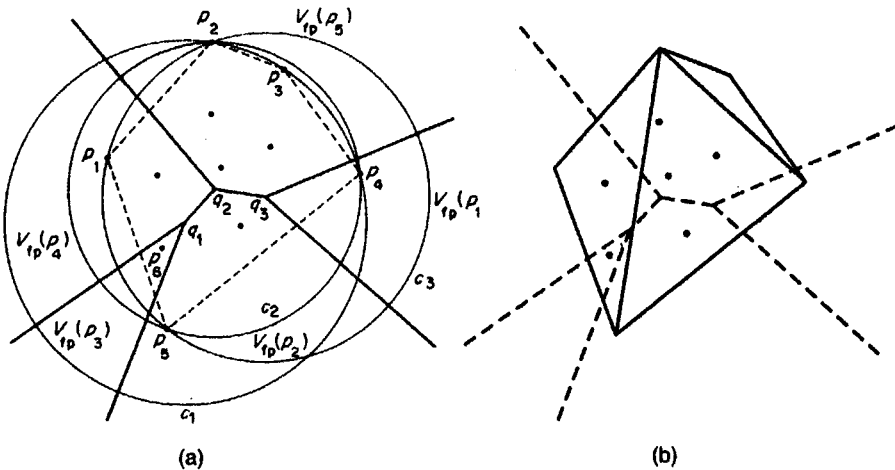


Figure 3.3.1 (a) A farthest-point Voronoi diagram and (b) its farthest-point Delaunay triangulation.

For brevity, we call the region $V_{fp}(p_i)$ the *FP-Voronoi polygon* of p_i . Since $\text{Dom}(p_i, p_j)$ is a half plane, it is well-behaving. Thus the set of FP-Voronoi polygons, $\mathcal{V}_{fp} = \{V_{fp}(p_1), \dots, V_{fp}(p_n)\}$, forms a tessellation of \mathbb{R}^2 . We call this tessellation the *farthest-point Voronoi diagram* generated by P , or briefly the *FP-Voronoi diagram* of P .

The FP-Voronoi diagram is, in fact, an order- k Voronoi diagram. If p_i is the farthest point from p , then the set $P \setminus \{p_i\}$ is the set of the first, the second, ..., the $(n-1)$ th nearest point from p_i . Thus the $V_{fp}(p_i)$ of \mathcal{V}_{fp} is the same as the order- $(n-1)$ Voronoi polygon associated with $P \setminus \{p_i\}$ of the order- $(n-1)$ Voronoi diagram generated by P . Following the notation of the order- k Voronoi diagram, we can write $V_{fp}(p_i)$ as $V(P_i^{(n-1)})$.

Since the FP-Voronoi diagram is the order- $(n-1)$ Voronoi diagram, the properties of the FP-Voronoi diagram are implicitly stated in the properties of the order- k Voronoi diagram. We, however, explicitly state some of them here adding slightly stronger properties.

From Properties OK2 and OK4, we obtain the following property.

Property FP1 The set $V_{fp}(p_i)$ given by equation (3.3.1) may be empty. If $V_{fp}(p_i)$ is not empty, the set $V_{fp}(p_i)$ is always an unbounded convex polygon.

Observe that there is no FP-Voronoi polygon associated with p_6 in Figure 3.3.1(a). Note too that the above property holds even if points in P are cocircular. The condition for a non-empty FP-Voronoi polygon is stated in Property FP2.

Property FP2 $V_{fp}(p_i)$ is not empty if and only if p_i is at a vertex of the convex hull of P . A non-empty FP-Voronoi polygon need not contain generator points.

Observe the broken lines in Figure 3.3.1(a). The proof is given by Seidel (1982, pp. 25–26).

In Section 2.3.1 we solved the closest pair problem (Problem P1) with the ordinary Voronoi diagram (Property V6). Similarly, we can solve the farthest-pair problem corresponding to the closest-pair problem with the FP-Voronoi diagram.

Problem FP1 (the reciprocal farthest-pair problem and the farthest-pair problem) For a given set P of distinct points in \mathbb{R}^2 , if p_j is the farthest point from p_i and in addition p_i is the farthest point from p_j , we say that the pair $\{p_i, p_j\}$ is a *reciprocal farthest pair*. If the distance between p_i and p_j is the farthest among the distances between all possible pairs of points in P , we say that the pair $\{p_i, p_j\}$ is the *farthest pair*. Given P , find the reciprocal farthest pairs and the farthest pair.

It follows from the definition of the FP-Voronoi diagram that:

Property FP3 $\{p_i, p_j\}$ is a reciprocal farthest pair if and only if $p_j \in V_{fp}(p_i)$ and $p_i \in V_{fp}(p_j)$.

Using this property and Property FP2, we can solve Problem FP1. Let us solve, for example, the reciprocal farthest-pair problem in Figure 3.3.1. We notice from Property FP2 that reciprocal farthest pairs are found at points on the boundary of the convex hull of P , i.e. $\{p_1, \dots, p_5\}$. First, consider p_1 . This point is included in $V_{fp}(p_4)$, and p_4 is included in $V_{fp}(p_1)$. Thus $\{p_1, p_4\}$ is a reciprocal farthest pair. Second, consider p_2 . This point is included in $V_{fp}(p_5)$, and p_5 is included in $V_{fp}(p_2)$. Thus $\{p_2, p_5\}$ is also a reciprocal farthest pair. Third, consider p_3 . This point is included in $V_{fp}(p_5)$, but p_5 is not included in $V_{fp}(p_3)$. Thus $\{p_3, p_5\}$ does not give a reciprocal farthest pair. Consequently the reciprocal farthest pairs are $\{p_1, p_4\}$ and $\{p_2, p_5\}$. The farthest pair is given by the reciprocal pair whose distance is the greatest among the obtained reciprocal farthest pairs. Hence $\{p_2, p_5\}$ is the farthest pair. Note that the farthest pair gives the diameter of P . The *diameter* of P is defined by the greatest distance among the distances between any two points in P . Thus the diameter is given by the farthest pair. In the example of Figure 3.3.1, $\overline{p_2 p_5}$ is the diameter. This method, however, is not the most efficient when we want to obtain only the diameter of P (Preparata and Shamos, 1985; Clarkson and Shor, 1989). Also note that to obtain the farthest pair, we should solve the point location problem (Section 2.3, Problem V3).

In Section 2.3 we considered the largest empty circle problem (Problem P4). Its counterpart problem is written as follows.

Problem FP2 (the smallest enclosing circle problem) Given a set of distinct points P , find the smallest circle, called the *smallest enclosing circle*, which contains all points of P in its interior or on it.

This problem is alternatively called the *minimum (radius) spanning circle* or the *short minimum spanning circle* (Bass and Schubert, 1967; Nair and Chandrasekaran, 1971; Hearn and Vijay, 1982; Melville, 1985; and Datta, 1996). We can solve this problem with the aid of the following property.

Property FP4 For every vertex q_i of FP-Voronoi polygons of the FP-Voronoi diagram generated by P , there exists the unique circle C_i centred at q_i which passes through three or more points of P , and in addition, which encloses all other points of P .

The smallest enclosing circle is determined either by the diameter of P or by three points of P . First, we examine if the circle whose diameter is given by the diameter of P encloses all points of P . If so, that circle is the smallest enclosing circle. If not, we draw the circles $\{C_i\}$ defined in Property FP4. Then the smallest enclosing circle is given by the smallest circle among $\{C_i\}$. In the example of Figure 3.3.1, since the circle with diameter $\overline{p_4p_5}$ does not include p_4 , we draw circles C_1 , C_2 and C_3 , and notice that C_2 is the smallest enclosing circle. Note that an alternative simple algorithm is proposed by Skyum (1991).

In conjunction with Property FP4, it may be worth recalling the definition of the Delaunay triangulation with the inversion transformation (Property D7 in Chapter 2). We defined there ‘near-side’ and ‘far-side’ triangles and defined a Delaunay triangulation with near-side triangles. In the same manner, we can define a triangulation with far-side triangles. As we showed in Section 2.4 (in the derivation from equation (2.4.6) to equation (2.4.9)), the circumcircle of the triangle mapped from a near-sided triangle through the inversion transformation does not contain any points of P in its interior. In the same manner, we can show that the circumcircle of the triangle mapped from a far-side triangle through the inversion transformation contains all points of P in its interior or on the boundary. This circumcircle indeed corresponds to the circle referred to in Property FP4.

From Properties OK7 and FP1 (non-empty FP-Voronoi polygons are all unbounded), we obtain the following property.

Property FP5 Let $n_v^{(n-1)}$, $n_e^{(n-1)}$ and $n_f^{(n-1)}$ be the numbers of vertices, edges and FP-Voronoi polygons in \mathcal{V}_{fp} . Then

$$n_v^{(n-1)} = n_f^{(n-1)} - 2 \leq n - 2, \quad (3.3.4)$$

$$n_e^{(n-1)} = 2n_f^{(n-1)} - 3 \leq 2n - 3. \quad (3.3.5)$$

In the above we treated \mathcal{V}_{fp} in \mathbb{R}^2 , but \mathcal{V}_{fp} can be defined in \mathbb{R}^m , $m \geq 2$. For this diagram, we have the following property which corresponds to Property V14 in Chapter 2 (Seidel, 1991).

Property FP6 The maximum number, $n_{\max}(i, m)$, of i -dimensional Voronoi faces of an m -dimensional farthest-point Voronoi diagram is given by:

for $n \leq m + 1$,

$$n_{\max}(i, m) = \binom{n}{m+1-1}; \quad (3.3.6)$$

for $1 \leq m + 1 \leq n$,

$$n_{\max}(i, m) = \begin{cases} C(m-i, m+1) - n+m, & i=0, \\ C(m-i, m+1) - n+m+1, & i=1, \\ C(m-i, m+1), & 2 \leq i \leq m, \end{cases} \quad (3.3.7)$$

where $C(m-i, m+1)$ is given by equation (2.3.14).

The proof is shown in Section 4 in Seidel (1991). The FP-Voronoi diagram in \mathbb{R}^3 is used for finding the farthest point from a point in P , but Edelsbrunner and Sharir (1985) show an alternative method.

In a similar fashion to how we defined the Delaunay triangulation as the dual diagram of the ordinary Voronoi diagram, we can define the dual diagram of the FP-Voronoi diagram by joining generator points p_i and p_j whose FP-Voronoi polygons $V_{fp}(p_i)$ and $V_{fp}(p_j)$ share the common FP-Voronoi edge by the line segment $\overline{p_i p_j}$ (Figure 3.3.1(b)). We call the resulting dual diagram the *farthest-point Delaunay triangulation* (Eppstein, 1992). This diagram has the following property that contrasts to Property D17.

Property FP7 Consider triangulations of the convex hull $\text{CH}(P)$ of a finite set P of distinct points satisfying the non-cocircularity assumption. The triangulation that lexicographically minimizes the sequence of angles, sorted from sharpest to the least sharp, of its triangles is the farthest-point Delaunay triangulation spanning P .

We note the contrast between ‘lexicographically maximized’ in Property D16 and ‘lexicographically minimized’ in Property FP7 (see Property D16). The proof is shown by Eppstein (1992, Theorem 2).

3.3.2 The k th nearest-point Voronoi diagram

The definition of the k th nearest-point Voronoi diagram is similar to that of the order- k Voronoi diagram.

Given a set of distinct points in the Euclidean plane, $P = \{p_1, \dots, p_n\}$ ($2 \leq n < \infty$), we assign a location p in the plane to a point p_i in the point set P if p_i is the k th nearest point from p ; if the k th nearest points are not only p_i but also other points in P , we assign the location to those points. Following this assignment rule, we assign all locations in the plane to at least one point in P . As a result, we obtain a collection of regions associated with points in P , denoted by $\mathcal{V}^{[k]} = \{V^{[k]}(p_1), \dots, V^{[k]}(p_n)\}$, which forms a tessellation.

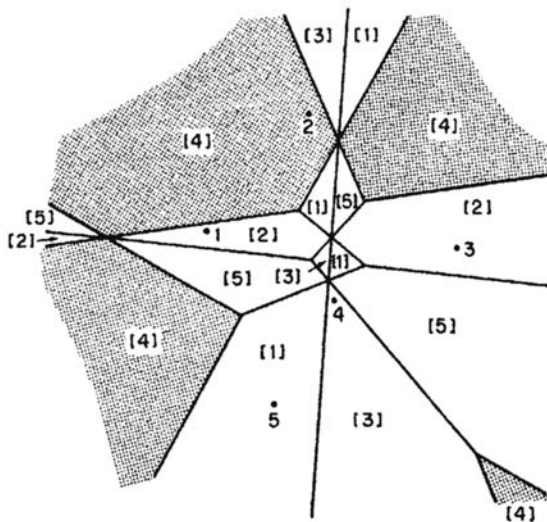


Figure 3.3.2 A third nearest-point Voronoi diagram ($[i]$ indicates $V^{[3]}(p_i)$).

We call the tessellation $\mathcal{V}^{[k]}$ the *kth nearest-point Voronoi diagram* generated by P , or briefly the *KNP-Voronoi diagram* of P , and the region $V^{[k]}(p_i)$ the *kth nearest-point Voronoi region* or the *KNP-Voronoi region* for short. An example is shown in Figure 3.3.2 where $k = 3$.

The definition of the KNP-Voronoi diagram with the dominance region $\text{Dom}(p_i, p_j)$ encounters a difficulty, because it is meaningless to consider the *kth nearest point* for only two points p_i and p_j . This difficulty is not so crucial because we usually define the KNP-Voronoi diagram through the ordered *order-k Voronoi diagram*. As a simple example, consider $V^{[2]}(p_1)$ in Figure 3.2.6. The region in which the second nearest point is p_1 is given by $V((p_2, p_1)), V((p_4, p_1))$ and $V(p_5, p_1))$, i.e. $V^{[2]}(p_1) = V((p_2, p_1)) \cup V((p_4, p_1)) \cup V((p_5, p_1))$. Generalizing this equation, we obtain the following property.

Property KNP1

$$V^{[k]}(p_i) = \bigcup_{(p_{j_1}, \dots, p_{j_{k-1}}) \in A^{(k-1)}(P \setminus \{p_i\})} V((p_{j_1}, \dots, p_{j_{k-1}}, p_i)), \quad (3.3.8)$$

where $A^{(k-1)}(P \setminus \{p_i\})$ is the set of all possible $(k-1)$ -tuples consisting of $k-1$ elements out of $P \setminus \{p_i\}$.

Since this property holds, it is an exercise to derive the properties of the KNP-Voronoi diagram from those of the ordered order- k Voronoi diagram. Here we mention only one distinctive property.

Property KNP2 For $k \geq 2$, a KNP-Voronoi region is not necessarily convex, and may be disconnected.

In fact, $V^{[3]}(p_4)$ in Figure 3.3.2 is disconnected (observe the shaded region).

Generalizing the nearest neighbour problem (Problem P2) in Chapter 2, we have the following problem.

Problem KNP1 (the k th nearest neighbour problem) Given a set of distinct points P , find the k th nearest neighbour point of p_i for all $p_i \in P$.

Once the KNP-Voronoi diagram is given, we immediately obtain the solution. If $p_j \in V^{[k]}(p_i)$, then the k th nearest point is p_j .

3.3.3 Applications

A natural application of the FP-Voronoi diagram is found in a facility location problem in which the k th nearest facility is critical, for instance in the case of a single unit emergency depot when more than one unit is required or when the first nearest unit is in use (Keeney, 1972). The FP-Voronoi diagram is also used for facility location problems of the min-max criteria (Okabe and Suzuki, 1997; Ohsawa and Imai, 1997), for determining the position of a specific object in an image (Ninomiya and Nakagawa, 1991), and finding the minimum radial separation centre which measures out-of-roundness (Le and Lee, 1991; Roy and Zhang, 1994).

An interesting application of the FP-Voronoi diagram is found in an industrial robot attaching a pin-grid array LSI (Large Scale Integrated circuit) to a board (Imai *et al.*, 1989). A print board has a set of holes centred at square grid points; pins of a LSI are fixed in the near neighbourhoods of square grid points (Figure 3.3.3). We wish to know the minimum radius of the holes which contain all the pins.

Problem FP3 (the pin-grid fitting problem) Let $P = \{p_{ij}, i \in I_n, j \in I_m\}$ be a configuration of points exactly placed on square grid points (Figure 3.3.3(b)), and $Q = \{q_{ij}, i \in I_n, j \in I_m\}$ be a configuration of points (Figure 3.3.3(c)) where p_{ij} and q_{ij} have a one-to-one correspondence. Fit P to Q by moving the configuration P through translation and rotation in such a way that the maximum distance between a point in P and its corresponding point in Q is minimized.

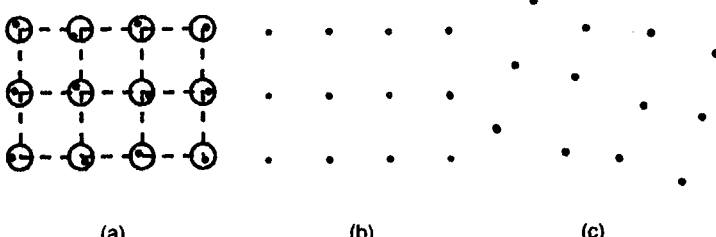


Figure 3.3.3 (a) Fitting holes (the big unfilled circles) of a print board to pins (the filled circles) of a LSI; (b) P ; (c) Q .

This problem can be solved using the FP-Voronoi diagram when the configuration P moves only through translation. To be explicit, let $p_{ij} = (x + a(i - 1), y + a(j - 1))$ and $q_{ij} = (u_{ij}, v_{ij})$. Then the Euclidean distance between p_{ij} and q_{ij} is given by

$$d(p_{ij}, q_{ij}) = \sqrt{(x + a(i - 1) - u_{ij})^2 + (y + a(j - 1) - v_{ij})^2}, \quad (3.3.9)$$

which is written alternatively as

$$d(p_{ij}, q_{ij}) = \sqrt{(x - (u_{ij} - a(i - 1)))^2 + (y - (v_{ij} - a(j - 1)))^2}. \quad (3.3.10)$$

Thus $d(p_{ij}, q_{ij})$ may be regarded as the distance between (x, y) and $(u_{ij} - a(i - 1), v_{ij} - a(j - 1))$. Let $o_{ij} = (u_{ij} - a(i - 1), v_{ij} - a(j - 1))$ and $O = \{o_{ij}, i \in I_{n_1}, j \in I_{n_2}\}$. Then the problem is re-stated as: find the point (x, y) from which the distance to the farthest point in O is the shortest. This problem is exactly the same as the smallest enclosing circle problem referred to above. When the configuration moves not only through translation but also rotation, we need a modification, which will be discussed in Section 3.9. In this connection it is worth noting a similar problem in which we find the minimum Hausdorff distance between two sets of points or line segments under translation. Huttenlocher *et al.* (1993) show how to solve this problem in terms of Voronoi surfaces.

We can find other applications of the KNP-Voronoi diagram in multivariate density estimation (Loftsgaarden and Quesenberry, 1965), classification (Cover and Hart, 1967) and information retrieval systems (Fukunaga and Narendra, 1975; Chazelle, 1985).

3.4 VORONOI DIAGRAMS WITH OBSTACLES

The ordinary Voronoi diagram is defined with the Euclidean distance. The assumption underlying the Euclidean distance is that we can take a straight path between any two points in a region. In some applications, however, this assumption is not acceptable. For example, consider a region in which there exist obstacles, such as rivers and lakes, that prevent traversal. If obstacles lie on the line between an origin and a destination, we cannot traverse straight; we have to make a detour around the obstacles. To deal with such obstacles in a Voronoi diagram, we develop two types of generalized Voronoi diagrams, called the 'shortest-path' Voronoi diagram and the 'visibility-shortest-path' Voronoi diagram. We also refer to a closely related diagram, called the 'constrained Delaunay triangulation'.

3.4.1 The shortest-path Voronoi diagram

We consider a generator set consisting of n distinct generator points, $P = \{p_1, \dots, p_n\}$, $p_i \in \mathbb{R}^2$, $i \in I_n$ ($2 \leq n < \infty$), and a set of n_0 closed regions,

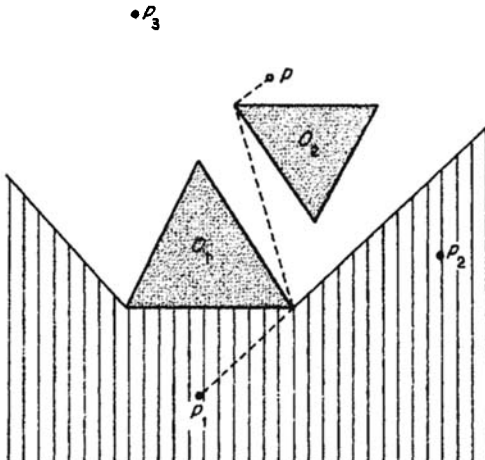


Figure 3.4.1 Generators (the filled circles), obstacles (the shaded areas), the visibility polygon with respect to p_1 (the hatched area) and the shortest path between p and p_1 (the dashed lines).

$O = \{O_1, \dots, O_{n_0}\}$, $(1 \leq n_0 < \infty)$. The set O represents a set of obstacles, which are neither transparent nor traversable. We assume that obstacles do not overlap each other; points of P are not allowed to locate in the obstacles; each obstacle is connected and has no holes. In addition, for analytical as well as computational convenience, we assume that O_i is a polygon (not necessarily convex; O_i may be connected line segments or a line segment; in general, O_i may be represented by a planar straight-line graph). Figure 3.4.1 shows an example of generator points (the filled circles) and obstacles (the shaded area) placed in the plane. The assumption of no holes can be easily relaxed. If a hole has no generator points, points in the hole are not assigned to any generator point. If there are some generator points in the hole, the Voronoi diagram in the hole can be treated as a Voronoi diagram in a simple polygon to be discussed in Section 3.4.3.

In the region $S = \mathbb{R}^2 \setminus O$, we define the distance between a point p and a point p_i in P by the length of the shortest path among all possible continuous paths connecting p and p_i , that do not intersect obstacles $O_i \setminus \partial O_i$, $i \in I_{n_0}$ (note that a path can pass through points on the boundary of O_i). We call this distance the *shortest-path distance* between p and p_i , and denote it by $d_{sp}(p, p_i)$. Alternatively, this distance is sometimes referred to as a *geodesic distance* in the computational geometry literature (Asano and Toussaint, 1987) or the *shortest obstacle-free path* (Mitchell, 1993). In practice, we obtain the shortest-path distance with the aid of a ‘visibility polygon’ and a ‘visibility graph’ (Sharir and Schorr, 1984).

A *visibility polygon*, denoted by $VIS(p_i)$, with respect to p_i is the set of points that are visible from p_i . Mathematically $VIS(p_i)$ is defined by

$$\text{VIS}(p_i) = \{p \mid \overline{p_i p} \cap [O_j \setminus \partial O_j] = \emptyset, \quad p \in \mathbb{R}^2, j \in I_{n_0}\}. \quad (3.4.1)$$

An example is shown in Figure 3.4.1, where the visibility polygon with respect to p_1 is indicated by the hatched area. If p is visible from p_i , there are no obstacles between p and p_i , and hence the shortest-path distance between p and p_i is given by the Euclidean distance, i.e. $d_{sp}(p, p_i) = \|x - x_i\|$ if $x \in \text{VIS}(p_i)$.

Computational methods for constructing a visibility polygon were developed by El Gindy and Avis (1981), Lee (1983), Lee and Chen (1985), Imai et al. (1985), Chazelle and Guibas (1985), Franklin et al. (1985) and others.

A 'visibility graph' is defined for a given geometric graph (Section 1.3). Let $G(Q, L)$ be a given geometric graph, where Q is a set of n_q nodes and L is a set of links (Figure 3.4.2(a)). We assume that links are not transparent. Let L_{vis} be the set of line segments $\overline{q_i q_j}$ satisfying that q_j is visible from q_i , i.e.

$$L_{\text{vis}} = \{\overline{q_i q_j} \mid q_j \in \text{VIS}(q_i), \quad i < j, \quad j \in I_{n_0}\} \quad (3.4.2)$$

(all lines in Figure 3.4.2(b) where $Q = \{q_1, \dots, q_6, p, p_1\}$). Note that line segments in L_{vis} may intersect. The *visibility graph* of $G(Q, L)$ is defined by the graph consisting of Q and L_{vis} , denoted by $G(Q, L_{\text{vis}})$. The computational methods for constructing the visibility graph were developed by Asano et al. (1986), Ghosh and Mount (1991), and Welzl (1985; for line obstacles).

With the aid of a visibility graph we can find the shortest path. As an example, let us obtain the shortest path between p and p_1 in Figure 3.4.1. We first consider the geometric graph $G(Q, L)$ in which Q is given by vertices of the obstacles O , p and p_i , and L is given by the edges of the obstacles O (Figure 3.4.2(a)). Second, we construct the visibility graph $G(Q, L_{\text{vis}})$ of the graph $G(Q, L)$ (Figure 3.4.2(b)). Third, we solve the shortest-path problem on this visibility graph (using, for example, the Dijkstra, 1959, method). Then, the shortest path between p and p_1 on $G(Q, L_{\text{vis}})$ gives the shortest path between p and p_1 in Figure 3.4.1. Note that Guibas et al. (1987) develop an

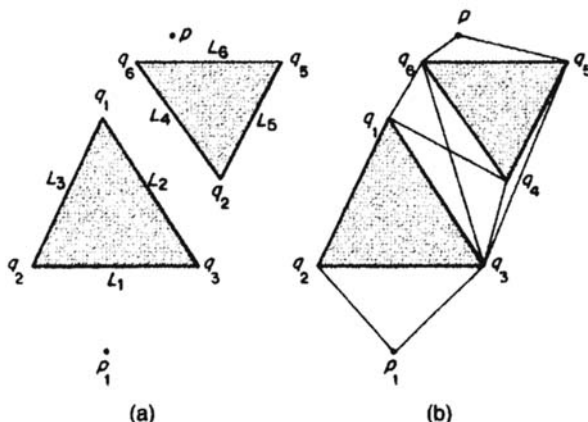


Figure 3.4.2 A shortest-path Voronoi diagram.

alternative efficient method for the shortest path in a simple polygon, Lee and Preparata (1984) for the shortest path in the presence of rectilinear barriers, Wu *et al.* (1987) for the rectilinear shortest path (the shortest path with the Manhattan metric) in the presence of rectilinear obstacles and Storer and Reif (1994) for the shortest path in the presence of polygonal obstacles. Also note that a new method, the 'continuous Dijkstra method' is developed by Mitchell *et al.* (1987) and Mitchell (1991, 1992, 1993, 1996) applying the analogy to wavefront propagation, and that Rajasekaran and Ramaswami (1995) develop a fast algorithm using a mesh-connected computer.

With the shortest path we define

$$V(p_i) = \{p \mid d_{sp}(p, p_i) \leq d_{sp}(p, p_j), j \neq i, j \in I_n\}. \quad (3.4.3)$$

We call this set the *shortest-path Voronoi region* associated with p_i , or briefly the *SP-Voronoi region* of p_i , and the set of SP-Voronoi regions, $\mathcal{V}(P, d_{sp}, \mathbb{R}^2) = \mathcal{V}_{sp} = \{V(p_1), \dots, V(p_n)\}$, the *shortest-path Voronoi diagram* generated by P with obstacles O , or the *SP-Voronoi diagram* of P with O for short. Alternatively \mathcal{V}_{sp} is called the *geodesic Voronoi diagram* (Asano and Asano, 1987; Aronov, 1989; Papadopoulou and Lee, 1995), or the *nearest-site geodesic Voronoi diagram* (Asano and Toussaint, 1987) (note that they define their diagrams for points in a simple polygon; see Section 3.3). Figure 3.4.3 shows \mathcal{V}_{sp} generated by p_1, p_2 and p_3 with the obstacles O_1 and O_2 in Figure 3.4.1. Tsin and Wang (1996) deal with a SP-Voronoi diagram with a set O of parallel line segments. Mitchell (1992) deals with a SP-Voronoi diagram with the Manhattan metric.

To observe the geometric properties of \mathcal{V}_{sp} , consider the bisector defined in terms of d_{sp} . Figure 3.4.4 shows $b(p_1, p_3)$ with O_1 and O_2 given by the triangles $\Delta q_1 q_2 q_3$ and $\Delta q_4 q_5 q_6$. If a point p is in the region given by $VIS(p_1) \cap VIS(p_3)$ (the hatched region), then the shortest-path distances $d(p, p_1)$ and

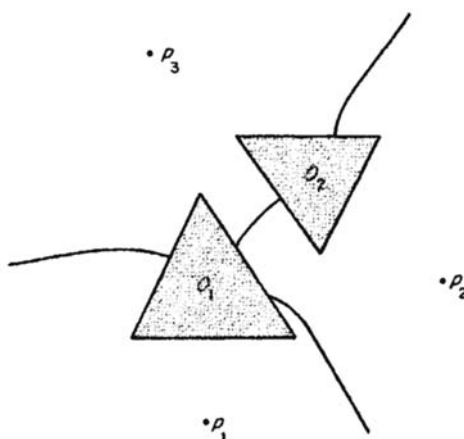


Figure 3.4.3 A geometric graph and its visibility graph.

$d(p, p_3)$ are given by the Euclidean distances. Thus the bisector between p_1 and p_3 in $\text{VIS}(p_1) \cap \text{VIS}(p_3)$ is given by

$$\begin{aligned} b(p_1, p_3) \cap [\text{VIS}(p_1) \cap \text{VIS}(p_3)] \\ = \{x \mid \|x - x_1\| = \|x - x_3\|\} \cap [\text{VIS}(p_1) \cap \text{VIS}(p_3)] \end{aligned} \quad (3.4.4)$$

(the half lines radiating from r_1 and r_7 in Figure 3.4.4). Second, in the region $\text{VIS}(q_2) \cap \text{VIS}(p_3)$ the shortest-path distance $d_{sp}(p, p_3)$ is given by the Euclidean distance, but the shortest-path distance $d_{sp}(p, p_1)$ is given by $\|x - u_2\| + \|u_2 - x_1\|$, where u_2 is the location vector of q_2 . This distance can be regarded as the additively weighted distance with the weight $-\|u_2 - x_1\|$ (equation (3.1.5)). The bisector in $\text{VIS}(q_2) \cap \text{VIS}(p_3)$ is hence given by

$$\begin{aligned} b(p_1, p_3) \cap [\text{VIS}(q_2) \cap \text{VIS}(p_3)] \\ = \{x \mid \|x - u_2\| + \|u_2 - x_1\| = \|x - x_3\|\} \cap [\text{VIS}(q_2) \cap \text{VIS}(p_3)], \end{aligned} \quad (3.4.5)$$

which is a hyperbolic arc (the curved line segment between r_1 and r_2 in Figure 3.4.4). Similarly, the bisector $b(p_1, p_3)$ in $\text{VIS}(q_3) \cap \text{VIS}(p_3)$, $\text{VIS}(q_3) \cap \text{VIS}(q_5)$ and $\text{VIS}(p_1) \cap \text{VIS}(q_5)$ is given by the hyperbolic arcs r_3 and r_4 ; r_5 and r_6 ; and r_6 and r_7 , respectively, in Figure 3.4.4. From this examination we notice that V_{sp} is closely related to the additively weighted Voronoi diagram.

Like the farthest-point Voronoi diagram shown in Section 3.3, we may define the *farthest-point SP-Voronoi diagram* by replacing $d(p, p_i)$ with $d_{sp}(p, p_i)$ in equation (3.3.1). Alternatively this diagram is called the *geodesic diagram*.

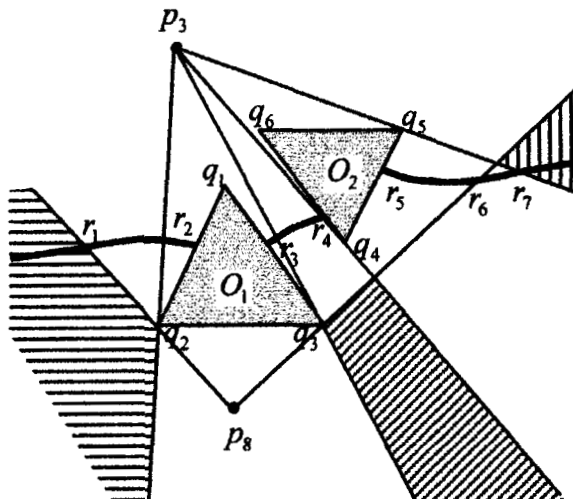


Figure 3.4.4 The bisector between p_1 and p_3 , where the distance is given by the shortest-path distance.

farthest-point Voronoi diagram (Asano and Toussaint, 1987), the *farthest-site Voronoi diagram with the geodesic distance* (Bhattacharya and Toussaint, 1985; Pollack *et al.*, 1989), and the *farthest-site geodesic Voronoi diagram* (Aronov *et al.*, 1993). Guha and Suzuki (1997) formulate the SP-Voronoi diagram with the shortest Manhattan metric avoiding rectangular obstacles.

3.4.2 The visibility-shortest-path Voronoi diagram

In the SP-Voronoi diagram we assumed that obstacles were polygons. Here we assume, for simplicity, that obstacles in O are all line segments that do not intersect each other at their interior points (possibly at their end points). In addition, we assume that the end points of the line segments in O are all generator points of P . Generator points in P are not necessarily end points of the line segments in O ; some points may be isolated. An example is shown in Figure 3.4.6, where generator points are indicated by the filled circles.

Given a set $P = \{p_1, \dots, p_n\}$ of generator points and a set $O = \{O_1, \dots, O_n\}$ of line obstacles, we define a distance by

$$d_{\text{vsp}}(p, p_i) = \begin{cases} \|x - x_i\|, & \text{if } p_i \in \text{VIS}(p), \\ \infty, & \text{otherwise} \end{cases} \quad (3.4.6)$$

This distance implies that if a point p is visible from p_i , the distance is given by the Euclidean distance; if it is not visible, the distance is infinite. We call this distance the *visibility-shortest-path distance* and abbreviate it to the *VSP-distance*, which is sometimes called the *bounded distance* (Aurenhammer, 1988a).

With the VSP-distance, we define the set $V(p_i)$ by equation (3.4.3), where $d_{\text{sp}}(p, p_i)$ is replaced by $d_{\text{vsp}}(p, p_i)$. We call the set $V(p_i)$ the *visibility-shortest-*

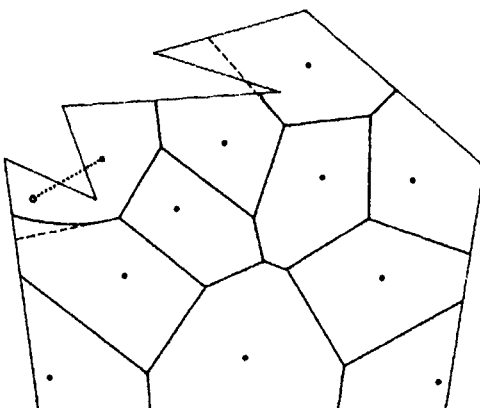


Figure 3.4.5 A Voronoi diagram in a simple polygon (a modification of the bounded Voronoi diagram (the dashed lines) with its SP-Voronoi diagram).

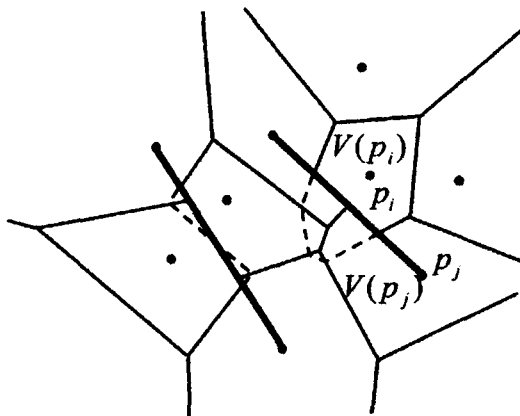


Figure 3.4.6 A visibility-shortest-path Voronoi diagram.

path Voronoi polygon associated with p_j , or briefly the *VSP-Voronoi polygon* of p_j ; the set of VSP-Voronoi polygons the *visibility-shortest-path Voronoi diagram*, \mathcal{V}_{vsp} , generated by P with obstacles O , or the *VSP-Voronoi diagram* of P with O for short. Alternatively, \mathcal{V}_{vsp} may be called the *bounded Voronoi diagram* (Wang and Schubert, 1987; Aurenhammer, 1988a; Djidjev and Lingas, 1991 (generated by vertices of a simple polygon); Klein and Lingas, 1992 (with the L_1 metric)), the *Voronoi diagram with barriers* (Lingas, 1989), or the *constrained Voronoi diagram* (Joe and Wang, 1993; Wang and Chin, 1995) (note that generators of those diagrams are slightly different from those of the VSP-Voronoi diagram defined above). An example of \mathcal{V}_{vsp} is illustrated in Figure 3.4.6 (the continuous lines).

As is seen in Figure 3.4.6, some edges of $\mathcal{V}_{\text{vsp}}(P)$ are the same as those of the corresponding ordinary Voronoi diagram $\mathcal{V}(P)$ and some are not (the broken lines and the continuous lines). A method for finding the difference between $\mathcal{V}_{\text{vsp}}(P)$ and $\mathcal{V}(P)$ is shown by Wang and Schubert (1987). This difference produces different properties, two of which are noted here.

Property VSP1 A VSP-Voronoi polygon may be non-convex (for example, the VSP-Voronoi polygon associated with p_j in Figure 3.4.6).

Property VSP2 Some edges of \mathcal{V}_{vsp} may not be part of a perpendicular line between generators (the boundary formed by an obstacle line); thus a point on an edge of \mathcal{V}_{vsp} may not be equally distant from two (or more) generators.

We note that \mathcal{V}_{vsp} has a special name when O is given by a line with a window and generators are placed on one side of the half plane produced by the line (Figure 3.4.7). This Voronoi diagram is called the *peeper's Voronoi diagram* (Aurenhammer, 1991). We may generalize the VSP-Voronoi diagram

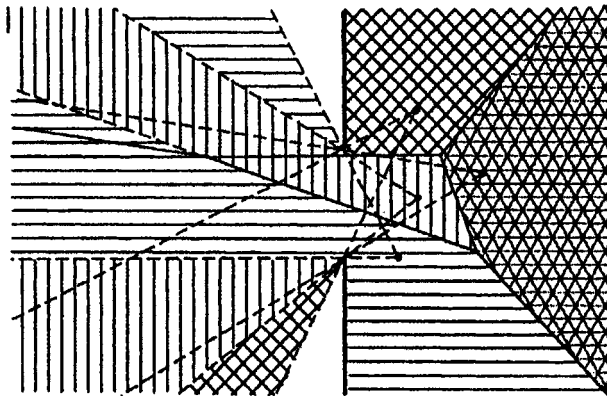


Figure 3.4.7 A peeper's Voronoi diagram.

by replacing the Euclidean distance in equation (3.4.6) with the weighted distance given by equation (3.1.3). We call the resulting diagram the *weighted visibility-shortest-path Voronoi diagram* (Wang and Tsin, 1990, call it the *constrained and weighted Voronoi diagram*).

3.4.3 The constrained Delaunay triangulation

In a similar fashion to how we obtained the Delaunay triangulation from the Voronoi diagram, we may obtain the dual diagram of \mathcal{V}_{vsp} by joining by line segments generators whose VSP-polygons share the common boundaries (note that VSP-polygons sharing obstacle boundaries are not considered as adjacent polygons). An example is shown in Figure 3.4.8(b). This dual diagram is closely related to a diagram, called the ‘constrained Delaunay triangulation’, which has been studied by many: Lee and Lin (1986), Chew (1989a,b), de Floriani and Puppo (1988), Agarwal *et al.* (1989a), Cline and Renka (1990), Jian-ming *et al.* (1990), Lu and Dai (1991), Dai (1991), Renka and Cline (1992), Baker (1992), de Floriani and Puppo (1992b), Sloan (1993), Wang (1993), Joe and Wang (1993), Loze and Saunders (1993), Fang and Piegl (1994), Guha (1994), Anglada (1997), and others. See also Section 6.3.

To be explicit, let $G(P_g, L_g)$ be a planar straight-line graph consisting of a set L_g of straight open line segments, and P_g be a set of end points of the line segments in L_g . Let Q be a set of points that are distinct from those in P_g , and $P = P_g \cup Q$. Note that Q may be empty.

Definition D4 (the constrained Delaunay triangulation) For a given planar straight-line graph $G(P_g, L_g)$ representing obstacles and a set Q of points, the *constrained Delaunay triangulation* is a triangulation spanning $P = P_g \cup Q$ satisfying the condition that the circumcircle of each triangle does not contain in its interior any other vertex which is visible from the vertices of the triangle.

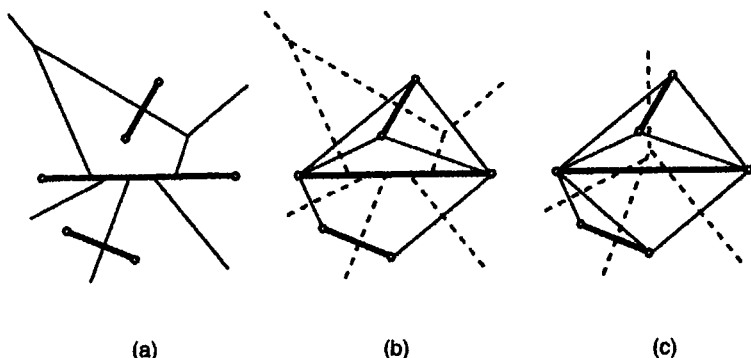


Figure 3.4.8 (a) A VSP-Voronoi diagram, (b) its dual and (c) the corresponding constrained Delaunay triangulation (the heavy lines indicate obstacles).

The constrained Delaunay triangulation is alternatively called the *generalized Delaunay triangulation* (Lee and Lin, 1986), the *obstacle triangulation* (Chew, 1986), and the *restricted Delaunay triangulation* (Sheng and Hirsch, 1992; Anglada, 1997). An example is shown in Figure 3.4.9 where the heavy lines indicate obstacles. Note that software for constructing a constrained Delaunay triangulation is provided by Renka (1996).

The constrained Delaunay triangulation is very useful for interpolation. Suppose that the heavy lines in Figure 3.4.9 are ridges of mountains, and the filled circles are points at which the height is known. In this case, we often want to obtain a triangulation spanning the filled circles whose edges coincide with the ridges. The constrained Delaunay triangulation can provide such a triangulation. Note that the constrained Delaunay triangulation is different from the ordinary Delaunay triangulation, but it is ‘as close as possible’ to the ordinary Delaunay triangulation (Chew, 1989a,b).

One might consider that the dual of the \mathcal{V}_{vsp} is the constrained Delaunay triangulation. This is not true, as is seen in Figure 3.4.8 where panel (b) shows the dual of \mathcal{V}_{vsp} , and panel (c) shows the corresponding constrained Delaunay triangulation. Although both are not completely the same, Joe and Wang (1993) prove that the dual of \mathcal{V}_{vsp} is a subgraph of the corresponding constrained Delaunay triangulation.

The constrained Delaunay triangulation is generally different from the ordinary Delaunay triangulation, but if we add a set S of points on L_g , then the constrained Delaunay triangulation spanning $P \cup S$ may coincide with the ordinary Delaunay triangulation spanning $P \cup S$ (Boissonnat *et al.*, 1988; Weatherill, 1990). We define such a special Delaunay triangulation as follows (Boissonnat *et al.*, 1988; Edelsbrunner and Tan, 1993).

For a given planar straight-line graph $G(P_g, L_g)$ representing obstacles and a set Q of points, we consider a set S of additional points and construct the ordinary Delaunay triangulation $\mathfrak{D}(P_g \cup Q \cup S)$ spanning $P_g \cup Q \cup S$. If all line segments in L_g are the union of the edges of $\mathfrak{D}(P_g \cup Q \cup S)$, we

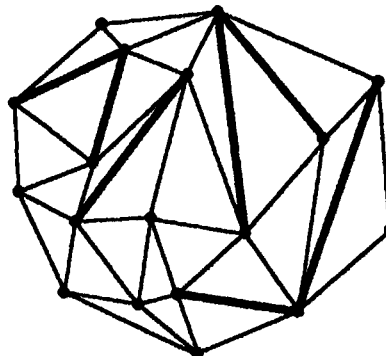


Figure 3.4.9 A constrained Delaunay triangulation (the heavy lines indicate obstacles). (Source: Lee and Lin, 1986, Figure 1.)

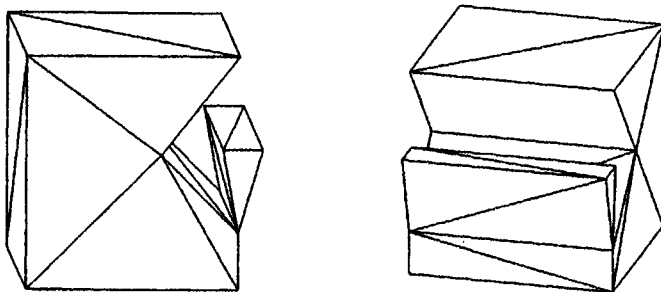


Figure 3.4.10 A domain Delaunay tetrahedrization. (Source: part of Figure 1 in Sapidis and Perucchio, 1991a).

call $\mathcal{D}(P_g \cup Q \cup S)$ the *conforming Delaunay triangulation* (Olooufa, 1991; Saalfeld, 1991; Sapidis and Perucchio, 1991a,b, 1992; Nackman and Srinivasan, 1994; see also Section 6.5.1). Ruppert (1995) calls a similar procedure a *Delaunay refinement*.

We readily notice that if we add many points on L_g , we can obtain the conforming Delaunay triangulation, but we wish to find a small set S . Edelsbrunner and Tan (1993) show an upper bound of such a set.

The constrained Delaunay triangulation can be extended to \mathbb{R}^3 , but its construction becomes harder, because the topology of faces forming a solid becomes complicated. To construct a topologically and geometrically valid Delaunay tetrahedrization, consider a solid S in \mathbb{R}^3 whose faces are given by F_1, \dots, F_k , which may be curved. We construct a triangulation $T(F_i)$ of F_i spanning points placed on F_i such that each edge of F_i corresponds to a unique boundary edge of $T(F_i)$. We call this triangulation the *domain triangulation* of F_i , and $\bigcup_{i=1}^k T(F_i)$ the *domain triangulation* of the boundary of S , denoted by $T(\partial S)$. We next construct a tetrahedrization of S spanning points placed on the surface of S such that its surface triangles are the domain

triangulation of the boundary of S . We call this tetrahedrization the *domain tetrahedrization* of S . Finally, if the domain tetrahedrization of S includes the Delaunay tetrahedra only, the domain tetrahedrization is called the *domain Delaunay tetrahedrization* of S . Sapidis and Perucchio (1991a,b, 1992) develop a computational method for constructing a domain Delaunay tetrahedrization. An example is shown in Figure 3.4.10. Hazlewood (1993) shows a method for approximating constrained tetrahedrization.

De Floriani *et al.* (1996) propose a triangulation using constrained Delaunay triangulations in a hierarchical manner. Let \mathcal{D} be a Delaunay triangulation consisting of triangles $\{T_1^{(0)}, \dots, T_n^{(0)}\}$. For each triangle $T_i^{(0)}$, we construct a constrained Delaunay triangulation of $T_i^{(0)}$ spanning points in $T_i^{(1)}$, i.e. $T_i^{(0)} = T_{i1}^{(1)} \cup \dots \cup T_{in_i}^{(1)}$. Note that this construction is achieved under the condition that adjacent subdivisions are matching. Applying the same procedure successively, we obtain a hierarchical set of Delaunay triangulations. We call this set the *hierarchical Delaunay triangulation*.

3.4.4 SP- and VSP-Voronoi diagrams in a simple polygon

We assumed in Section 2.1 that the boundary Voronoi polygons of a bounded Voronoi diagram, \mathcal{V}_{BS} (equation (2.1.4)), are star-shaped with respect to their generator points in terms of the Euclidean distance. This assumption is made because in many applications the shortest path that traverses outside of S is unrealistic (the dotted line in Figure 3.4.5). If we relax the star-shaped assumption with the Euclidean distance, we should consider the shortest path that is embedded in S (Franklin *et al.*, 1985; Asano and Asano, 1987; Seoung and Asano, 1987; Aronov, 1989). Recalling the SP-Voronoi diagram, the reader may notice that the bounded Voronoi diagram \mathcal{V}_{BS} can be regarded as an SP-Voronoi diagram with the obstacle given by $\mathbb{R}^2 \setminus S$. Figure 3.4.5 shows a modification of the bounded Voronoi diagram (the dashed lines) with its SP-Voronoi diagram. Note that every Voronoi polygon in this modified bounded Voronoi diagram is star-shaped with respect to its generator point in terms of the SP-distance (Aronov, 1989).

We may also consider the VSP-Voronoi diagram in a simple polygon. This diagram is treated by Klein and Lingas (1993) (generator points are vertices of a simple polygon) as an extension of Agarwal *et al.* (1989a). Klein and Lingas (1992, 1993) formulate a VSP-Voronoi diagram in a simple polygon with the Manhattan metric (also see Section 3.7).

3.4.5 Applications

Since an actual space often contains obstacles, Voronoi diagrams with obstacles are useful for relaxing the problems formulated in an ideal space (no obstacles) in the preceding sections. For example, imagine the sea in which there exist islands with ports. The nearest search problem in Chapter 2 in this context is written as: find the nearest port from a given point in the sea avoiding islands. This problem can be solved using the SP-Voronoi diagram.

The constrained Delaunay triangulation can be applied to the triangulation of geological surfaces. Since such surfaces often have faults, the triangulation is restricted by the discontinuity, which can be treated by the constrained Delaunay triangulation (Fowler and Little, 1979; Cline and Renka, 1990). The constrained Delaunay triangulation can also be applied to surface triangulation (Baker, 1992; Zhou *et al.*, 1992; Voigtmann *et al.*, 1994; Park and Kim, 1995), triangulation in a multiply connected region (Weatherill, 1988; Taniguchi *et al.*, 1992; Zhou *et al.*, 1993), cartographic generalization (Ware *et al.*, 1995), robot routing path planning (Chew, 1989a,b; Xie, 1990; Takizawa *et al.*, 1996; Hama and Etoh, 1997), patrol robot planning (Yamamoto *et al.*, 1995), object reconstruction (Boissannat, 1988; Bruzzone *et al.*, 1991), stereo data interpolation (Faugeras *et al.*, 1990; Bruzzone *et al.*, 1992; Takizawa *et al.*, 1996; Lechat *et al.*, 1997), image warping (Ruprecht and Müller, 1995) and multichip module layout (Lu and Dai, 1991; Dai, 1991).

The farthest-point SP Voronoi diagram is utilized to find the *geodesic centre* of points in a simple polygon or that of vertices of a simple polygon (i.e. the centre of points in terms of the SP-distance), and the *geodesic diameter* of a polygon (i.e. the diameter of a polygon in terms of the SP-distance) (Suri, 1989; Pollack *et al.*, 1989). It is shown by Asano and Toussaint (1987) that the geodesic centre of the vertices of a polygon is either the geodesic centre of the polygon or a vertex of the farthest-point SP-Voronoi diagram generated by the vertices of the polygon.

3.5 VORONOI DIAGRAMS FOR LINES

In the preceding four sections, a generator is a point or a set of points. In this section, extending a generator from a point to a line, we consider a generalized Voronoi diagram generated by a set of lines. In theory we can consider a general line, but in practice we deal with points (as a special case of lines), straight lines, chains of straight line segments, circular arcs, chains of circular arcs and full circles. Curved lines may not be exactly represented by those lines, but this restriction is not crucial in practice because we can approximate a curved line by a chain of small straight line segments. In computational geometry a generalized Voronoi diagram for lines has been intensively studied since the late 1970s by Drysdale and Lee (1978), Drysdale (1979), Kirkpatrick (1979), Lee and Drysdale (1981), Imai *et al.* (1985), Kokubo (1985), Sharir (1985), Fortune (1986), Yap (1987), Clarkson and Shor (1989), Goodrich *et al.* (1993), Burnikel *et al.* (1994), Rajasekaran and Ramaswami (1994, 1995), and Deng and Zhu (1996), among others. In this section we mainly follow their results.

We consider a generator set $L = \{L_1, \dots, L_n\} \subset \mathbb{R}^2$ ($1 \leq n < \infty$), where L_i is a point, a line segment (which may be curved) or a geometric element consisting of line segments that are connected. We assume that elements in L do not intersect each other. Under this assumption, we define the distance

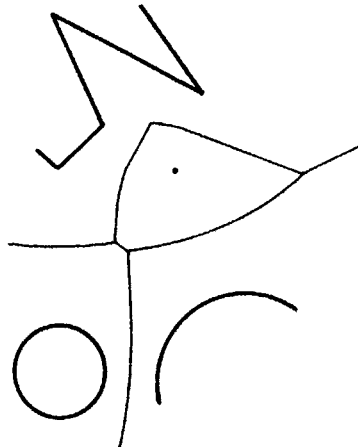


Figure 3.5.1 The line Voronoi diagram generated by the set of a point, a chain of straight line segments, a circular arc and a full circle.

from $p (=x)$ to L_i by the shortest Euclidean distance between p and a point $p_i (=x_i)$ on L_i , i.e.

$$d_s(p, L_i) = \min_{x_i} \{ \|x - x_i\| \mid x_i \in L_i \}. \quad (3.5.1)$$

With this distance, we define

$$V(L_i) = \{ p \mid d_s(p, L_i) \leq d_s(p, L_j), j \neq i, j \in I_n \}. \quad (3.5.2)$$

Alternatively, let

$$\text{Dom}(L_i, L_j) = \{ p \mid d_s(p, L_i) \leq d_s(p, L_j) \}, j \neq i, \quad (3.5.3)$$

Then the set $V(L_i)$ is written as

$$V(L_i) = \bigcap_{j \in I_n \setminus \{i\}} \text{Dom}(L_i, L_j). \quad (3.5.4)$$

Since the dominance region $\text{Dom}(L_i, L_j)$ is well-behaving, the resulting set $\mathcal{V}(L, d_s, \mathbb{R}^2) = \mathcal{V}(L) = \{V(L_1), \dots, V(L_n)\}$ gives a generalized Voronoi diagram. We call this generalized Voronoi diagram the *line Voronoi diagram* generated by L , and the set $V(L_i)$ the *line Voronoi region* associated with L_i . If L_i degenerates into a point for all i , the line Voronoi diagram reduces to the ordinary Voronoi diagram. Figure 3.5.1 shows the line Voronoi diagram generated by the set consisting of a point, a chain of straight lines, a circular arc and a full circle.

The line Voronoi diagram can be defined in the three-dimensional space. Chew *et al.* (1995) examine the combinatorial complexity of the line Voronoi diagram in \mathbb{R}^3 with a polyhedral convex distance (see Section 3.6.2). More generally, Dwyer (1997) examines the Voronoi diagram of random lines and flats in \mathbb{R}^m , $m \geq 3$.

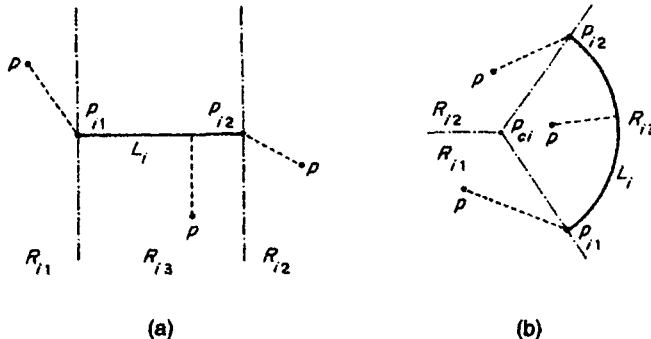


Figure 3.5.2 (a) The distance from a point to a straight line segment; (b) the distance from a point to a circular arc.

3.5.1 Voronoi diagrams for a set of points and straight line segments

In the above definition we consider a general line, but in this subsection we assume that a generator L_i is a point, a straight line segment, or a chain of straight line segments. We also assume that a straight line segment L_i contains both end points. Under these assumptions the shortest distance of equations (3.5.1) is explicitly written as

$$d_s(p, L_i) = \begin{cases} \|x - x_{i1}\| & \text{if } p \in R_{i1}, \\ \|x - x_{i2}\| & \text{if } p \in R_{i2}, \\ \left\| (x - x_{i1}) - \frac{(x - x_{i1})^T(x_{i2} - x_{i1})}{\|x_{i2} - x_{i1}\|}(x_{i2} - x_{i1}) \right\| & \text{if } p \in R_{i3} = \mathbb{R}^2 \setminus [R_{i1} \cup R_{i2}], \end{cases} \quad (3.5.5)$$

where x_{i1} and x_{i2} are the end points of L_i , and $R_{i1} = \{x \mid (x_{i2} - x_{i1})^T(x - x_{i1}) < 0\}$, $R_{i2} = \{x \mid (x_{i1} - x_{i2})^T(x - x_{i2}) < 0\}$ (see Figure 3.5.2(a)).

The bisectors between L_i and L_j with this distance are depicted in Figure 3.5.3, where L_i and L_j are: (a) a point and a point; (b) a point and a straight line segment; and (c) a straight line segment and a straight line segment. In any case, the bisector splits \mathbb{R}^2 into two disjoint regions, and so the dominance region is well-behaving. Thus the set $\mathcal{V}(L, d_s, \mathbb{R}^2)$ with the distance of equation (3.5.5) gives a line Voronoi diagram.

Figure 3.5.4 illustrates the line Voronoi diagram generated by the set L consisting of points, straight line segments and chains of straight line segments (the heavy lines). When we construct this Voronoi diagram, we add a modification to the generator set L to gain analytical and computational tractability. To be explicit, suppose that the first l elements in L are points, i.e. $L_1 = p_1, \dots, L_l = p_l$, and the rest of the elements are straight line segments. As we assumed in the above, a straight line segment or a chain of straight line segments L_i includes both end points, but now we decompose

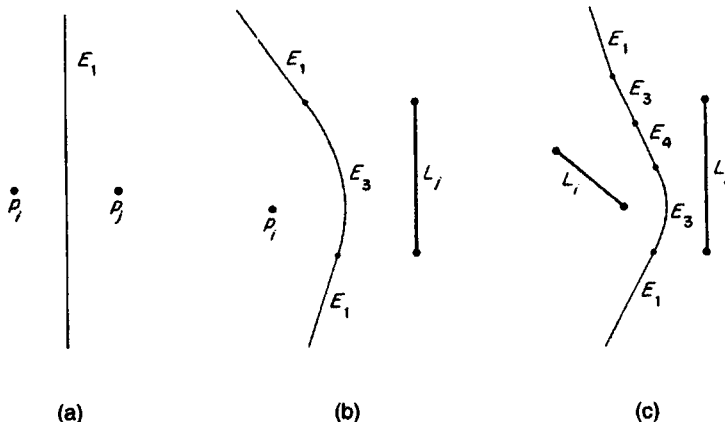


Figure 3.5.3 The bisectors between L_i and L_j , where L_i and L_j are (a) a point and a point; (b) a point and a straight line segment; (c) a straight line segment and a straight line segment.

this line segment into the end points, intermediate points and straight line segments without end points. The set of the points is denoted by $\{p_{ij}, j \in I_{n_i+1}\}$ and the set of the lines is denoted by $\{L_{ij}^o, j \in I_{n_i}\}$ ($n_i = 1$ for a straight line segment). As a result, the generator set L is decomposed into

$$L^{(d)} = \{p_i, i \in I_i\} \cup \left[\bigcup_{i=l+1}^n \{p_{ij}, j \in I_{n_i+1}\} \right] \cup \left[\bigcup_{i=l+1}^n \{L_{ij}^o, j \in I_{n_i}\} \right]. \quad (3.5.6)$$

We call this set the *decomposed generator set* of L . If we decompose the generator set of L in Figure 3.5.4, we obtain the decomposed generator set depicted by the filled circles and the heavy lines in Figure 3.5.5 (where a line segment with small gaps at both ends symbolically indicates a line segment without end points). Since L_i^o does not include end points, the distance of equation (3.5.1) is alternatively defined by

$$d_s(p, L_i^o) = \inf_{x_i} \{\|x - x_i\| \mid x_i \in L_i^o\}, \quad (3.5.7)$$

where ‘inf’ is an infimum operator (Section 1.3). Using this decomposed generator set with this distance, we generate the line Voronoi diagram $\mathcal{V}(L^{(d)})$, which is indicated by the light solid lines and the broken lines in Figure 3.5.5 (Reddy and Turkiiyah, 1995, call $\mathcal{V}(L^{(d)})$ the generalized Voronoi diagram of a *mixed dimensional set*.) Obviously, the edges of $\mathcal{V}(L)$ are included in $\mathcal{V}(L^{(d)})$. We can hence obtain $\mathcal{V}(L)$ from $\mathcal{V}(L^{(d)})$ by deleting the unnecessary edges indicated by the broken lines in Figure 3.5.5.

Like the ordinary Delaunay triangulation defined as the dual of the ordinary Voronoi diagram, we may consider the dual of $\mathcal{V}(L^{(d)})$ for separated line segments (Figure 3.5.6; Dehne *et al.*, 1991, Figure 13). Reddy and Turkiiyah (1995) call this dual diagram the *generalized Delaunay triangulation*. It should be noted, however, that the vertices of the generalized

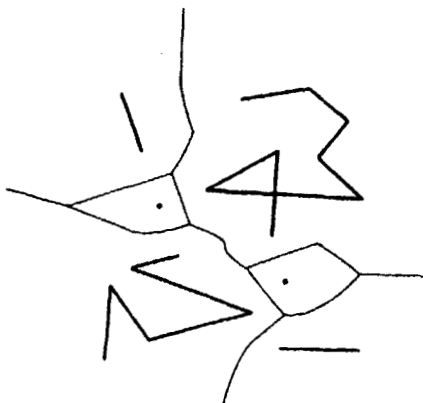


Figure 3.5.4 A line Voronoi diagram generated by the set consisting of points, two straight lines and two chains of straight line segments.

Delaunay triangulation do not have a specific geometric meaning; a Delaunay edge merely indicates the existence of a non-redundant edge.

As is noticed from Figures 3.5.4 and 3.5.5, the line Voronoi diagram $\mathcal{V}(L^{(d)})$ of the decomposed set $L^{(d)}$ is a refinement of the line Voronoi diagram $\mathcal{V}(L)$ of L . This refinement is fundamental in the sense that every edge in $\mathcal{V}(L^{(d)})$ is part of a unique conic curve. For this reason, we examine the geometric properties of $\mathcal{V}(L)$ through $\mathcal{V}(L^{(d)})$.

From equation (3.5.4) with Figure 3.5.3, we notice the following property.

Property L1 No line Voronoi region in $\mathcal{V}(L^{(d)})$ is empty. A line Voronoi region of a point to which three or more lines are incident is a point.

Substituting equation (3.5.5) into equation (3.5.3), we obtain the following property.

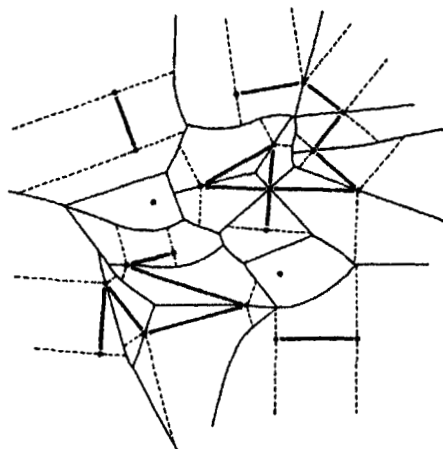


Figure 3.5.5 The line Voronoi diagram generated by the decomposed generator set obtained from the generator set in Figure 3.5.4.

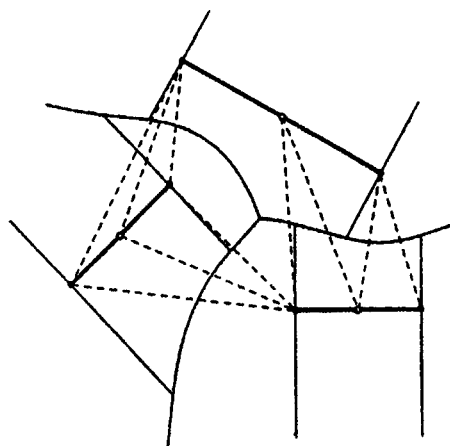


Figure 3.5.6 The dual of a line Voronoi diagram, called the generalized Delaunay triangulation (the broken lines).

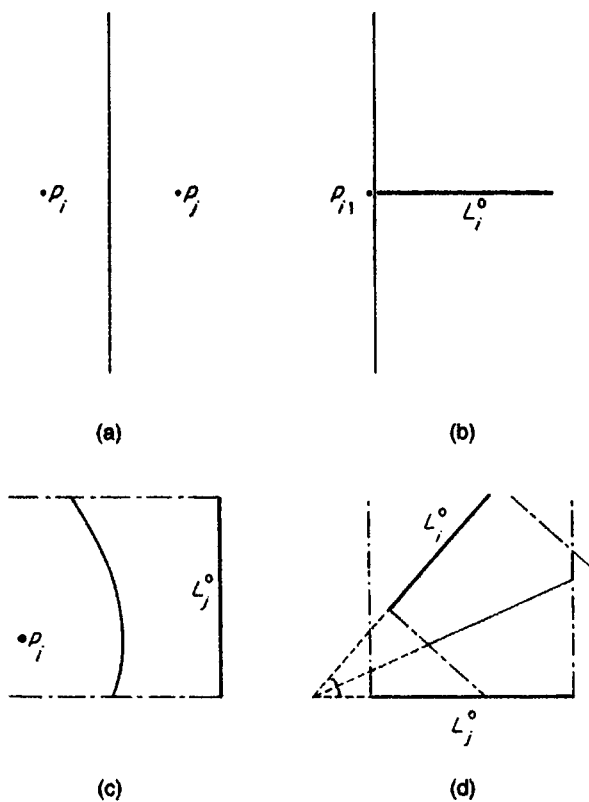


Figure 3.5.7 Four types of edges in a line Voronoi diagram: (a) type E1; (b) type E2; (c) type E3; (d) type E4.

Property L2 Edges in $\mathcal{V}(L^{(d)})$ are straight lines or parabolic arcs. These edges can be classified into the following four types according to the types of generators generating the edges.

Type E1. An edge generated by points p_i and p_j . The edge is the straight line perpendicularly bisecting $\overline{p_i p_j}$ (Figure 3.5.7(a)).

Type E2. An edge generated by a straight line segment L_i^o , and its end point $p_{i1} \in \partial L_i$. The edge is the straight line perpendicular to L_i^o passing through p_{i1} (Figure 3.5.7(b)).

Type E3. An edge generated by a point p_i and a straight line segment L_j^o ($p_i \notin \partial L_j$). The edge is the locus of a point p satisfying the condition that the distance from p to p_i is equal to the distance from p to the line L_j . This locus is known as a parabolic arc whose focus is p_i and whose directrix is L_j^o (Figure 3.5.7(c)).

Type E4. An edge generated by straight line segments L_i^o and L_j^o . The edge is the straight line dividing the angle made by L_i^o and L_j^o (Figure 3.5.7(d)).

The reader should not confuse Figures 3.5.7(c) and (d) with Figures 3.5.3(b) and (c). The bisectors in Figure 3.5.3 are generated by the generators that are not decomposed. Using Property L2, the reader should confirm that the bisectors in Figures 3.5.3(b) and (c) consist of edges of types E1, E3 and E4. In Figure 3.5.3 we indicate the type of each edge by E1–E4.

As a consequence of Property L2, we obtain the following property.

Property L3 A line Voronoi region $V(L_i)$ is not necessarily convex.

When exactly three edges are incident at every vertex in a line Voronoi diagram, we say that the line Voronoi diagram is *non-degenerate*. Regarding a non-degenerate line Voronoi diagram $\mathcal{V}(L^{(d)})$, we obtain the following property from Property L2.

Property L4 Vertices $\{q_i\}$ in a non-degenerate line Voronoi diagram can be classified into the following six types according to the types of three edges, e_{i1}, e_{i2} and e_{i3} , which are generated by three generators.

Type V1. A vertex q_i generated by points p_i, p_j and p_k . The edges e_{i1}, e_{i2} and e_{i3} are all type E1 (Figure 3.5.8(a)).

Type V2. A vertex q_i generated by a point p_i , a straight line segment L_i^o , and its end point $p_{j1} \in \partial L_j$. The edges are types E1, E2 and E3. The edge of type E1 and that of type E3 are tangent at the Voronoi vertex q_i (Figure 3.5.8(b)).

Type V3. A vertex q_i generated by a straight line segment L_i^o and two points p_j and p_k which are not the end points of L_i . The edges are types E1 and E3. The edges of type E3 have the common directrix L_i^o (Figure 3.5.8(c)).

Type V4. A vertex q_i generated by two straight line segments L_i^o and L_j^o , and its end point $p_{i1} \in L_i^o$. The edges are types E2, E3 and E4. The edges of type E3 and E4 are tangent at q_i (Figure 3.5.8(d)).

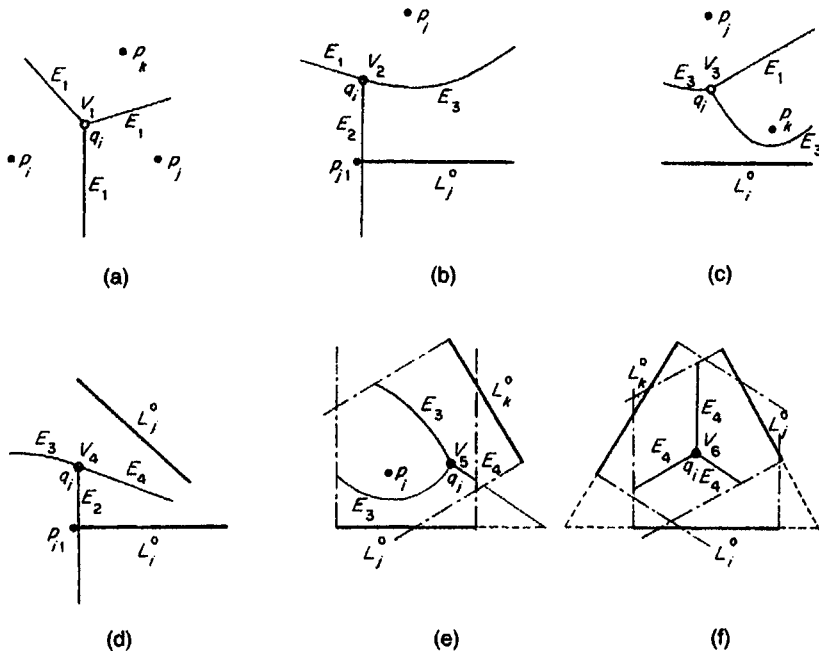


Figure 3.5.8 Types of vertices in a line Voronoi diagram: (a) type V1; (b) type V2; (c) type V3; (d) type V4; (e) type V5; (f) type V6.

Type V5. A vertex q_i generated by a point p_i and two straight line segments L_j^o and L_k^o ($p_i \notin \partial L_j, p_i \notin \partial L_k$). The edges are types E3 and E4 (Figure 3.5.8(e)).

Type V6. A vertex q_i generated by straight line segments L_j^o, L_k^o and L_l^o . The edges are type E4. The extended lines of L_j^o, L_k^o , and L_l^o form a triangle. If q_i is inside this triangle, q_i is its inscribed centre. If q_i is outside the triangle, q_i is one of its excentres (Figure 3.5.8(f)).

In Figure 3.5.8, types of vertices are indicated by V1–V6 with edge types. Finally, almost the same derivation used in Property V2 leads to the following property.

Property L5 A line Voronoi region $V(L_i^o)$ is unbounded if and only if L_i^o is on the boundary of the convex hull of $L^{(d)}$.

3.5.2 Voronoi diagrams for a set of points, straight line segments and circular arcs

We now add circular arcs to the generator set examined in the preceding subsection. For computational convenience we assume that a circular arc is less than or equal to a semicircle. We treat a circular arc greater than a semicircle as two circular arcs connected at a point, and a full circle as two

semicircles connected at two points. For a circular arc with radius r_i centred at x_{ci} , the shortest distance of equation (3.5.1) is explicitly written as

$$d_s(p, L_i) = \begin{cases} \|x - x_{ii}\| & \text{if } x \in R_{ii}, \\ \|x - x_{iz}\| & \text{if } x \in R_{iz}, \\ \|x - x_{ci}\| - r_i & \text{if } x \in R_{iz} = \mathbb{R}^2 \setminus [R_{ii} \cup R_{iz}], \end{cases} \quad (3.5.8)$$

where R_{ii} , R_{iz} and R_{iz} are the regions defined in Figure 3.5.2(b).

Since the dominance region is well-behaving, a generator set consisting of points, straight line segments and circular arcs gives a line Voronoi diagram. An example is depicted in Figure 3.5.1. We construct this Voronoi diagram in the same manner as we employed in the preceding subsection. First, we decompose a given generator set L and next construct the line Voronoi diagram for the decomposed generator set $L^{(d)}$. The line Voronoi diagram $\mathcal{V}(L)$ is obtained from the line Voronoi diagram $\mathcal{V}(L^{(d)})$ by deleting superfluous edges.

To observe the geometric property of the line Voronoi diagram, let $L_{pl}^{(d)}$ be the decomposed generator set consisting of points and straight lines, and $L_{plc}^{(d)}$ be the decomposed generator set consisting of points, straight lines and circular arcs (the subscript ‘plc’ indicates points, lines and circles). Since the line Voronoi diagram $\mathcal{V}(L_{pl}^{(d)})$ is a special case of the line Voronoi diagram $\mathcal{V}(L_{plc}^{(d)})$, some properties of $\mathcal{V}(L_{pl}^{(d)})$ mentioned in Section 3.5.1 hold in such a special case. In fact, Properties L1, L3 and L5 of $\mathcal{V}(L_{plc}^{(d)})$ hold for $\mathcal{V}(L_{pl}^{(d)})$. Also Property L2 of $\mathcal{V}(L_{pl}^{(d)})$ holds for $\mathcal{V}(L_{plc}^{(d)})$, but we should add the following six types.

Property L7 Edges in $\mathcal{V}(L_{plc}^{(d)})$ are straight line segments, parabolic arcs, elliptic arcs and hyperbolic arcs. Those edges can be classified into ten types according to the types of generators generating the edges. The first four types are given by E1–E4 in Property L2.

Type E5. An edge generated by a circular arc L_i^o and a point $p_j \notin \partial L_i$ which is inside the circle containing L_i^o centred at p_{ci} . The edge is the locus of a point p satisfying the condition that the total distance from p to two fixed points p and p_{ci} is constant, which is known as an elliptic arc whose foci are p_{ci} and p_j (Figure 3.5.9(a)).

Type E6. An edge generated by a circular arc L_i^o and a point $p_j \notin \partial L_i$ which is outside the circle containing L_i^o centred at p_{ci} . The edge is the locus of a point p satisfying the condition that the difference between the distances from p to p_{ci} and p_j is constant. This locus is known as a branch of a hyperbolic curve whose foci are p_{ci} and p_j (Figure 3.5.9(b)).

Type E7. An edge generated by a circular arc L_i^o and its end point $p_{i1} \notin \partial L_i$. The edge generated by these generators is a straight line radiating from the centre of the circle containing L_i^o to p_{i1} (Figure 3.5.9(c)).

Type E8. An edge generated by a circular arc L_i^o and a straight line containing L_i^o , which intersects the circle containing L_i^o centred at p_{ci} with radius r_i (note that $L_i^o \cup L_i^o = \emptyset$). The edge is the locus of a point p satisfying the

condition that the sum of the distances from p to the line L_i^o and to the fixed point p_{ci} is constant. This locus is known as a parabolic arc whose focus is p_{ci} and whose directrix is the line parallel to L_i at distance r_i (Figure 3.5.9(d)).

Type E9. An edge generated by two circular arcs L_i^o and L_j^o where the circle containing L_i^o centred at p_{ci} is contained in the circle containing L_j^o centred at p_{cj} . The edge is an elliptic arc whose foci are p_{ci} and p_{cj} (Figure 3.5.9(e)).

Type E10. An edge generated by two circular arcs L_i^o and L_j^o where the circle containing L_i^o centred at p_{ci} intersects the circle containing L_j^o centred at p_{cj} or the former circle is outside of the later circle. The edge is a branch of a hyperbolic curve whose foci are p_{ci} and p_{cj} (Figure 3.5.9(f)).

Note that the types of a bisector between a point and a parametric curve are classified by Farouki and Johnstone (1994), and those of a bisector between a point and a curve and that between a curve and a curve are classified by Kim *et al.* (1995) using rational quadratic Bézier curves. Also note that Haldar and Patnaik (1990) examine the bisector between monotone algebraic curve segments.

3.5.3 Voronoi diagrams for a set of circles

In the literature, special attention is paid to a line Voronoi diagram generated by a set L_c of full circles. To generate this special Voronoi diagram, we have to define a distance from a point to a circle. In the literature, several distances are proposed. Probably the most natural distance is given by the shortest distance of equation (3.5.1), which is explicitly written as

$$d_{cl}(p, L_i) = \left| \|x - x_{ci}\| - r_i \right|, \quad (3.5.9)$$

where L_i is the circle centred at p_{ci} with radius r_i . A line Voronoi diagram $\mathcal{V}(L_c)$ generated by a set of circles with this distance is a special case of the line Voronoi diagram $\mathcal{V}(L_{plc})$ defined in the above subsection (the generator set is a set of paired semicircles). Hence the line Voronoi diagram $\mathcal{V}(L_c)$ shares the properties of $\mathcal{V}(L_{plc})$ mentioned above. In Figure 3.5.10 we depict the line Voronoi diagram generated by two intersecting circles. The reader should confirm the types of edges using Property L7.

Lee and Drysdale (1981) and Sharir (1985) employ a similar but slightly different distance given by

$$d_{c2}(p, L_i) = \|x - x_{ci}\| - r_i. \quad (3.5.10)$$

This distance is not a metric because it may take a negative value. The difference between $d_{cl}(p, L_i)$ and $d_{c2}(p, L_i)$ appears when $d_{cl}(p, L_i)$ and $d_{c2}(p, L_i)$ have different signs. We can observe this difference in Figure 3.5.10 where panel (a) uses $d_{cl}(p, L_i)$ and panel (b) uses $d_{c2}(p, L_i)$. The elliptic curve does not appear if we employ $d_{c2}(p, L_i)$. The properties of this line Voronoi diagram are examined in detail by Sharir (1985). We also note that if the

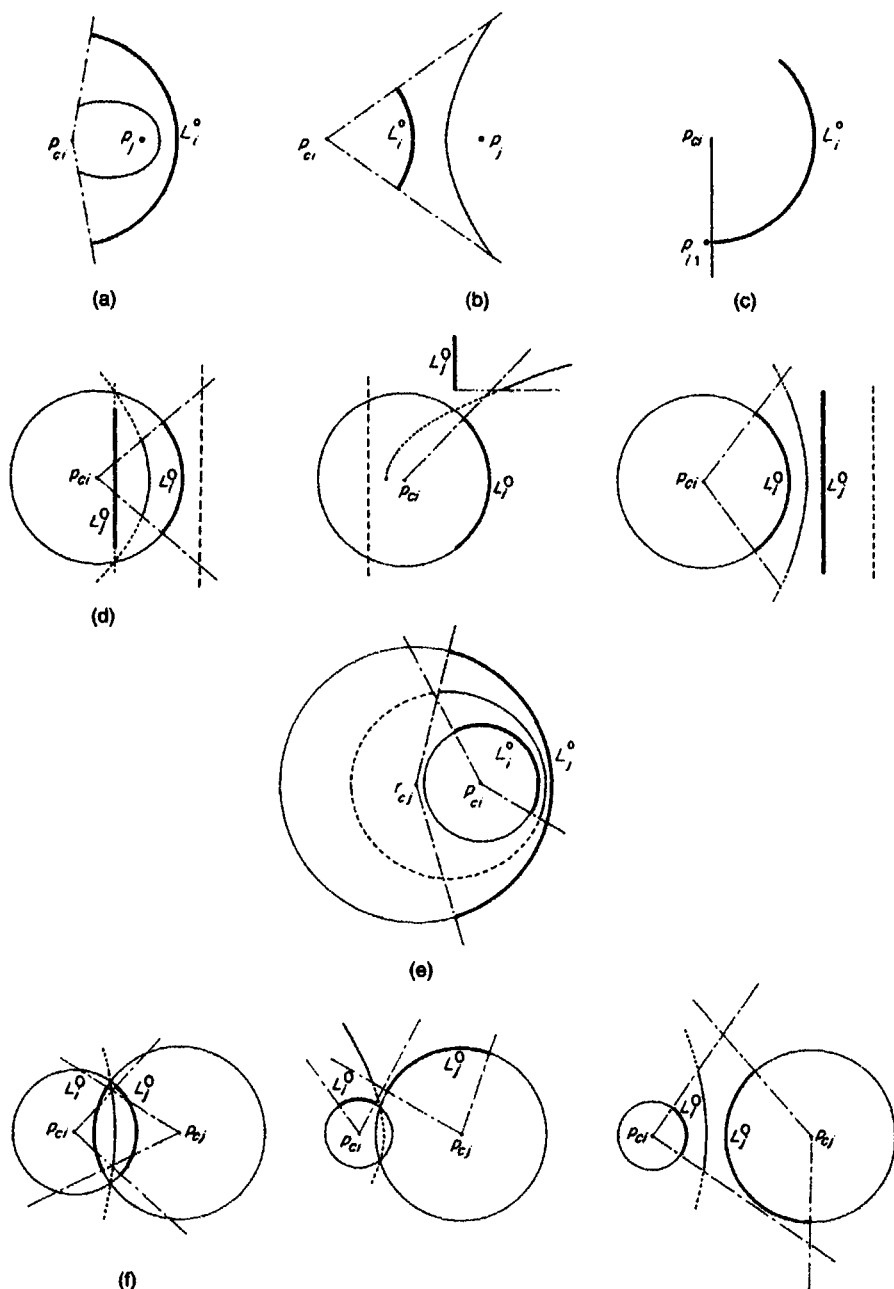


Figure 3.5.9 Types of edges generated by a circular arc and a point, a straight line or a circular arc: (a) type E5; (b) type E6; (c) type E7; (d) type E8; (e) type E9; (f) type E10.

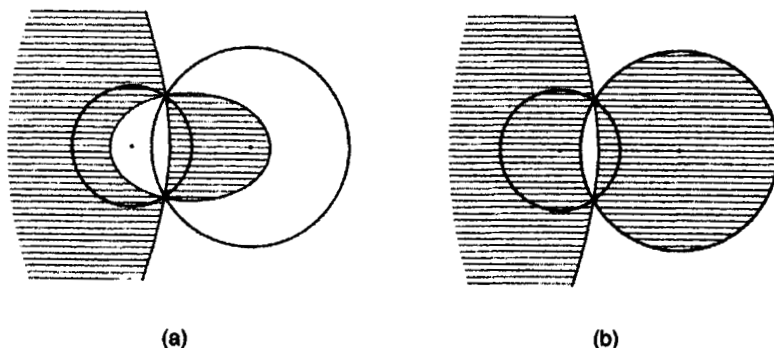


Figure 3.5.10 The line Voronoi diagrams generated by two intersecting circles with (a) the distance given by equation (3.5.9), and (b) the distance given by equation (3.5.10).

circles do not overlap, the distance $d_{c1}(p, L_i) = d_{c2}(p, L_i) = \|x - x_c\| - r_i$ is the additively weighted distance (equation (3.1.5) in Section 3.1); thus $\mathcal{V}(L_c)$ reduces to the AW-Voronoi diagram.

A fairly different distance is employed by Aurenhammer (1988a,b), Imai *et al.* (1985), Telly *et al.* (1992, 1996), which is given by

$$d_{c3}(p, L_i) = \|x - x_{ci}\|^2 - r_i^2. \quad (3.5.11)$$

If p is outside the circle, $\sqrt{d_{c3}(p, L_i)}$ indicates the distance from point p to the point p_i on L_i , where $\overline{pp_i}$ is tangential to L_i at p_i (the broken line in Figure 3.5.11). We call the line Voronoi diagram with this distance the *Laguerre Voronoi diagram* or *Laguerre diagram*. This term is named after Laguerre geometry in which a point $(x, y, z) \in \mathbb{R}^3$ corresponds to a directed

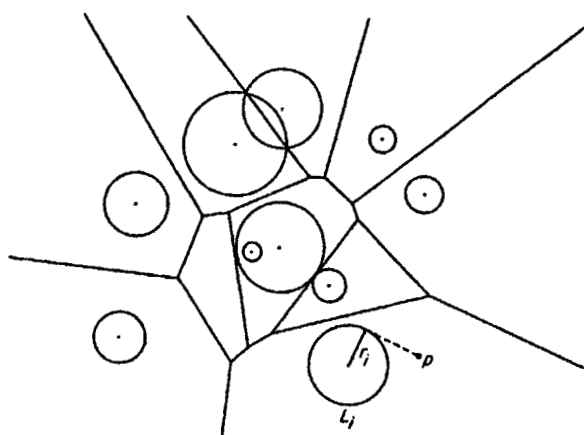


Figure 3.5.11 The Laguerre Voronoi diagram.

circle centred at (x, y) with radius $|z|$ on \mathbb{R}^3 . The bisector with this distance is given by a radical axis in \mathbb{R}^2 and a radical plane in \mathbb{R}^3 , and hence the Laguerre Voronoi diagram may be called the *radical axis Voronoi diagram* or *radical axis tessellation* (Gellatly and Finney, 1982c; Weaire and Rivier, 1984; Venema, 1991). Note that Venema (1991) also defines the *radical axis triangulation* as the dual of the radical axis Voronoi diagram. Also note that since the distance of equation (3.5.11) is the power distance, the Laguerre Voronoi diagram is exactly the same as the power Voronoi diagram (Section 3.1.4).

Extending the closest pair problem for a set of points (Problem V1 in Section 2.3), we may consider the closest problem for a set of circles. In fact, Sharir (1985) develops a computational method for this problem.

3.5.4 Medial axis

In conjunction with the line Voronoi diagram, we refer to a ‘medial axis’ which is often applied in shape analysis (Blum, 1967). The medial axis can be defined for a connected geometric figure C (disconnected regions can be treated separately; a polygon C may have holes, called the *multiply connected polygonal domain* (Srinivasan and Nackman, 1987; Meshkat and Sakkas, 1987; Srinivasan *et al.*, 1992; Mayya and Rajan, 1996)). The *medial axis* is defined as the locus of all points that have at least two closest points on the boundary of C . Alternatively, the *medial axis* can also be defined as the locus of the centres of all the interior maximal disks of C , where a *maximal disk* is a disk which is not contained by any other disks that are included in C (the disks in Figure 3.5.12(a)) (Pfaltz and Rosenfeld, 1967; Peleg and Rosenfeld, 1981; Held, 1993, calls it a *clearance disk*). The medial axis may be intuitively understood if we imagine a grassfire in a prairie. The set C represents a region covered with grass and the region C is surrounded by a wetland. Suppose that the border of the region C is set on fire. Then the subsequent internal quenching points of the fire represent the medial axis (Blum, 1973; Blum and Nagel, 1978; Leymarie and Levine, 1992; Dehne and Klein, 1997 (who generalize this idea)). Stated a little more precisely, the *medial axis* of C is

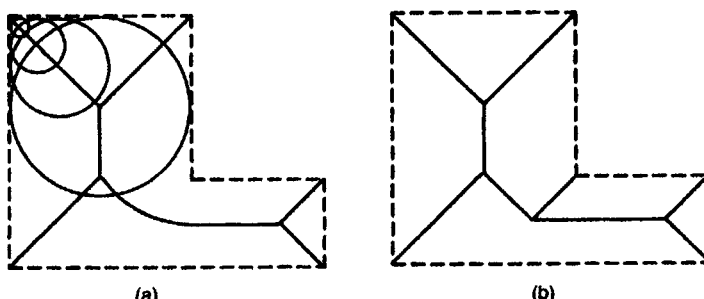


Figure 3.5.12 A medial axis with a maximal disk (a) and a straight skeleton (b).

the set $M(C)$ of points x in C for which there exist at least two distinct points, x_i and x_j , on the boundary of C such that the distance between x and x_i is the same as that between x and x_j , and these distances are both the minimum distance between x and a point on the boundary of C . Mathematically,

$$M(C) = \left\{ x \mid \|x - x_i\| = \|x - x_j\| = \min \{ \|x - y\| \mid y \in \partial C \}, \begin{array}{l} x_i \neq x_j, x_i, x_j \in \partial C, x \in C \end{array} \right\}. \quad (3.5.12)$$

A point $x \in M(C)$ is called a *skeletal point* (Mayya and Rajan, 1996). The medial axis of C is alternatively called the *symmetric axis* (Blum 1973), *(continuous) skeleton* (Montanari, 1968, 1969; Kirkpatrick, 1979) or *stick figure* (Blum, 1967) of C . An example is illustrated in Figure 3.5.12(a). The transform from C into $M(C)$ is called the *medial axis transform* (Blum, 1967), *symmetric axis transform* (Blum, 1973), *skeletonization* (Smith, 1987) or *Blum's transform* (Aurenhammer, 1991). Fukushima and Okumura (1991) and Fukushima (1997) propose a modified symmetric axis transform, called the *division-based analysis of symmetry*.

Let $R(x) = \min_u \{ \|x - u\| \mid u \in \partial C, x \in M(C)\}$, which is the radius of the maximal disk, $D_{\max}(x)$, centred at a point x on the medial axis $M(C)$. The function $R(x)$ is called the *radius function* of the maximal disk (in the analogy to the grassfire, the time of quenching for unity velocity propagation is the radius function). From the definitions of the medial axis and the radius function, we note the following property (Gürsoy and Patrikalakis, 1991, 1992).

Property L8 The medial axis is unique for a given figure C . The figure C can be exactly reconstructed by taking the union of all maximal disks with radius equal to the radius function $R(x)$ on the medial axis $M(C)$, i.e. $C = \bigcup_{x \in M(C)} D_{\max}(x)$.

Note that other theoretical properties of $M(C)$ are discussed in depth by Calabi and Hartnett (1968) and Chou (1995).

The definition of $M(C)$ by equation (3.5.12) is applicable to \mathbb{R}^3 . In this case, however, $M(C)$ is called the *medial (axis) surface* and $D_{\max}(x)$ is called the *maximal sphere*. An example is shown in Figure 3.5.13. Computational methods for constructing medial surfaces are developed by many: Nackman and Pizer (1985), Goldak *et al.* (1991), Sherbrooke *et al.* (1996), Reddy and

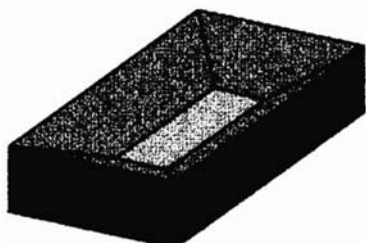


Figure 3.5.13 A medial surface of a rectangular parallelepiped.

Turkiyyah (1995), Sheehy *et al.* (1996), Turkiyyah *et al.* (1997), Näf *et al.* (1997), and others.

The medial axis method can treat a polygonal figure as well as a curved figure C . When a figure C is a polygon, we can obtain its medial axis by the use of the line Voronoi diagram (Kirkpatrick, 1979; Lee, 1982a). First, we decompose a set, L , of line segments forming the boundary of C (the dashed line in Figure 3.5.12(a)) into $L^{(d)}$ as we did in Section 3.5.1. Second, we generate the line Voronoi diagram $\mathcal{V}(L^{(d)})$ by the decomposed generator set $L^{(d)}$. Recalling the property that points on the edges of line Voronoi regions are equally distant from generator lines (the boundaries of the geometric figure), we notice that the medial axis is included in the edges in $\mathcal{V}(L^{(d)})$. Deleting unnecessary edges in $\mathcal{V}(L^{(d)})$, we obtain the medial axis of C (the solid line in Figure 3.5.12(a)). Because of this, the medial axis is sometimes called the *Voronoi skeleton* (Ogniewicz and Ilg, 1992; Näf *et al.* (1997)) or *Voronoi medial axis* (Ogniewicz and Kübler, 1995).

The detailed computational methods for vector data (i.e. C is represented by vectors) are shown in Preparata (1977), Kirkpatrick (1979), Lee (1982a), Yao and Rokne (1991), Devillers (1992), Klein and Lingas (1995) and Imai (1996). When C is represented by raster data as in image analysis, some special treatments are necessary, and alternative computational methods are developed by Rosenfeld and Pfaltz (1966), Pfaltz and Rosenfeld (1967), Montanari (1968), Peleg and Rosenfeld (1981), Smith (1987; a review), Xia (1989), Brandt and Algazi (1992), and Arcelli and Baja (1993).

When the boundary of C is curved, we usually approximate C by a polygon C' , and obtain the medial axis for C' by applying the line Voronoi diagram (Montanari, 1968; Lee, 1982a). This method, however, may suffer from computational burden because C' has many edges to approximate to C . To overcome this burden, a simple method was proposed by Blum and Nagel (1978), which has been developed by Boissonnat and Kofakis (1985), Yun (1989), Brandt and Algazi (1991, 1992), Goldak *et al.* (1991), Brandt (1994) and Sheehy *et al.* (1996). First, we approximate C by C' . Second, we construct the Delaunay triangulation spanning the vertices of C' . Third, we classify the resulting triangles into inside triangles and outside triangles (the triangles that are not included in C'). Last, we join the centres of any two Delaunay disks by line segments if they are adjacent. We call the resulting set of line segments the *discrete medial axis* of C (Goldak *et al.*, 1991; Yu *et al.*, 1991; Ogniewicz and Kübler, 1995). Obviously, the discrete medial axis of C is not exactly the same as the true medial axis. Schmit (1988), Goldak *et al.* (1991), Brandt and Algazi (1992), and Brandt (1994) examine the degree of this approximations theoretically. Roughly speaking, if the shape of C is ‘nice’ (r -nice in Brandt, 1994), increasingly dense vertices of the polygon C' give rise to increasingly accurate approximations of the true medial axis. Marston and Shih (1995) develop a multi-scale representation for the approximation levels of C' .

As is seen in Figure 3.5.12(a), the medial axis may include a curved line. Alternatively, Aichholzer and Aurenhammer (1996) propose the axis of a

polygonal figure C consisting of only straight line segments, called the *straight skeleton* (for more general figures, see Aichholzer and Aurenhammer, 1996). Intuitively the straight skeleton is given by the ridges of roofs that rise from the edges of the figure C at the same slant. An example is shown in Figure 3.5.12(b).

The Voronoi diagram may be alternatively defined in terms of the medial axis (Ó'Dúnlaing and Yap, 1985). If we replace ∂C by $P = \{p_1, \dots, p_n\}$, and C by \mathbb{R}^2 in equation (3.5.12), i.e.

$$\begin{aligned} M(P) = \{x \mid \|x - x_i\| = \|x - x_j\| = \min_y \{\|x - y\| \mid y \in P\}, \\ x_i \neq x_j, x_i, x_j \in P, x \in \mathbb{R}^2\}, \end{aligned} \quad (3.5.13)$$

then, $M(P)$ coincides with the Voronoi edges of the planar ordinary Voronoi diagram generated by P . Similarly, for a set L of line segments, we may modify $M(C)$ as

$$\begin{aligned} M(L) = \{x \mid \|x - x_i\| = \|x - x_j\| = \min_y \{\|x - y\| \mid y \in L_1 \cup \dots \cup L_n\}, \\ x_i \neq x_j, x_i, x_j \in L_1 \cup \dots \cup L_n, x \in \mathbb{R}^2\}. \end{aligned} \quad (3.5.14)$$

We might expect that $M(L)$ coincides with the Voronoi edges of the line Voronoi diagram generated by L (or $L^{(d)}$). This is true when L consists of separated line segments, but it is not always true in general. For example, when L is a set of connected line segments or a set of curved line segments, $M(L)$ does not always form a tessellation. An example of the former case is shown in Figure 3.5.14 (or Figure 4 in Lavender *et al.*, 1992), and the latter case by Alt and Schwarzkopf (1995, Figure 1).

3.5.5 Applications

Okabe and Fujii (1984) showed a possible application of the line Voronoi diagram for testing the effect of car emissions on withered trees along expressways. The same method was used by Okabe and Yoshikawa (1989) and Yoshikawa and Okabe (1991) to test the effect of arterial streets on the

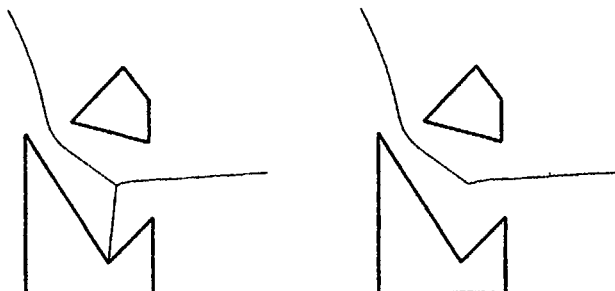


Figure 3.5.14 (a) The modified medial axis for a set L of lines defined by equation (3.5.14) and (b) the line Voronoi diagram generated by L .

distribution of apartment buildings in the Setagaya and Koito-Sumida districts in Tokyo (see Section 8.3.2).

In converting contour lines in a raster format to those in a vector format, we often have a problem of inconsistent contour lines, such as crossing contour lines and broken contour lines. To search for such errors, Mizutani *et al.* (1993) use the line Voronoi diagram. Using the topology of the line Voronoi diagram they suggest how to correct these errors. A closely related method is also proposed by Kawashima *et al.* (1994), Gold *et al.* (1996) and Gold (1997).

Zaninetti (1991b) uses the line Voronoi diagram in \mathbb{R}^3 to analyse the distribution of galaxies. Medvedev (1994) and Anishchik and Medvedev (1995) apply the Voronoi diagram for circles to a packing problem found in dense granular systems. This problem dates back to the *Appollonian packing problem*: find the circle inscribed among three given circles in a plane. Rounse *et al.* (1990) deal with particles on a two-dimensional section in terms of the Voronoi diagram for ellipsoids. The same diagram is also used for directional clustering (Reyes and Adjouadi, 1997).

Gellatly and Finney (1982c) use the radical axis Voronoi diagram for the characterization of crystalline structures when atoms have different sizes, and Venema (1991) uses the same diagram to examine muscle fibre patterns. Telly *et al.* (1992) use the Laguerre Voronoi diagram as geometric idealization of two dimensional polycrystals. Gerstein *et al.* (1995) propose a similar diagram with a slightly different distance which reflects the size of atoms. See also the related applications shown in Section 7.1.

The medial axis associated with the line Voronoi diagram in a simple polygon is applied to shape analysis (Blum, 1967, 1973; Philbrick, 1968; Blum and Nagel, 1978; Lee, 1982a; Brady, 1983; Rosenfeld, 1979), pattern recognition (Calabi and Hartnett, 1968; Fujii, 1976), character recognition or font generation (Hobby, 1993), object identification of overlapping objects (Kübler *et al.*, 1990; Ogniewicz and Ilg, 1992), image processing (Smith, 1987; Lantuejoul and Maisonneuve, 1984; Tam and Armstrong, 1991), mesh generation (Srinivasan *et al.*, 1992 (a review); Gürsoy and Patrikalakis, 1992, among others), pocket machining (Held, 1991, 1993; Lambregts *et al.*, 1996), design rule checking (Meshkat and Sakkas, 1987), documentation analysis (Ilg, 1990), segmentation (Chassery and Melkemi, 1990), motion planning (see the Voronoi diagram with convex distances in Section 3.7.2), and so forth.

Applications of the straight skeleton are found in architecture (Recuero and Gutiérrez, 1993), a data structure for finding pairwise interactions (Eppstein and Erickson, 1998), and origami constructions (Lang, 1996).

The line Voronoi diagram is closely related to the buffer zones of lines often used in geographical information systems. The boundaries of the buffer zone give parallel lines to generator lines, which may be used in spatial analysis (Okabe and Fujii, 1984). The problem of determining lines that are parallel to the edges of a polygon is called the *offset problem*, and is studied by Tiller and Hanson (1984), Sutherland (1990) and Hoschek (1985). The line Voronoi diagram can also be applied to the optimization of service lines (Takeda, 1985; see Chapter 9).

3.6 VORONOI DIAGRAMS FOR AREAS

Noticing that the preceding subsection has extended a generator from a point to a line, the reader might expect that the next extension would be from a line to an area. This extension is actually possible and useful in many applications.

3.6.1 The area Voronoi diagram

We consider a set of areas, $A = \{A_1, \dots, A_n\}$ ($2 \leq n < \infty$), in \mathbb{R}^2 . We assume that A_i is a connected closed set and areas do not overlap each other. An area A_i is not necessarily convex, and may have holes in which another area may exist. Under these assumptions, we define a distance from a point to an area A_i as the shortest Euclidean distance from p to A_i , i.e.

$$d_s(p, A_i) = \min_{x_i} \{ \|x - x_i\| \mid x_i \in A_i \}, \quad (3.6.1)$$

where x and x_i are the location vectors of p and p_i , respectively. With this distance, we define a set by

$$V(A_i) = \{p \mid d_s(p, A_i) \leq d_s(p, A_j), j \neq i, i, j \in I_n\}. \quad (3.6.2)$$

We call this set the *area Voronoi region* associated with A_i , and the set of area Voronoi regions, $\mathcal{V}(A) = \{V(A_1), \dots, V(A_n)\}$, the *area Voronoi diagram* generated by the generator set A . Mathematically, an area includes a line and a line includes a point. Thus the area Voronoi diagram includes the line Voronoi diagram, which includes the ordinary Voronoi diagram. Figure 3.6.1(a) shows an area Voronoi diagram. We may restrict the set A to a set of special figures. Rappaport (1992) deals with the area Voronoi diagram generated by a set of disks.

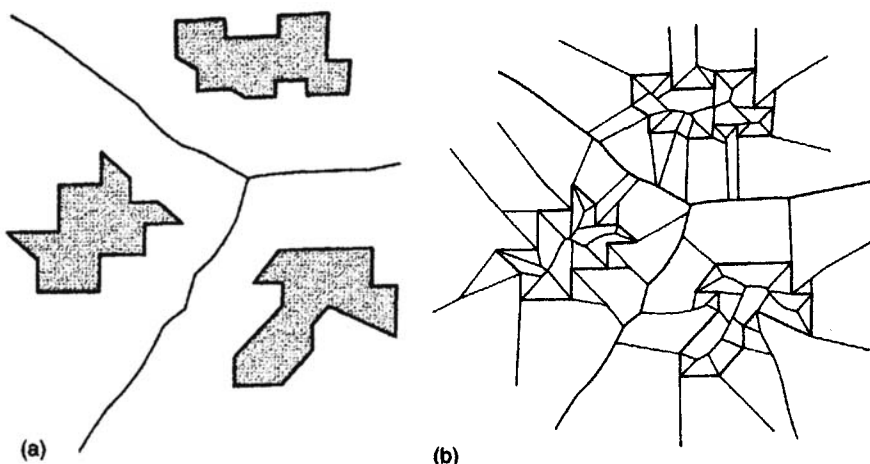


Figure 3.6.1 (a) An area Voronoi diagram and (b) its corresponding line Voronoi diagram.

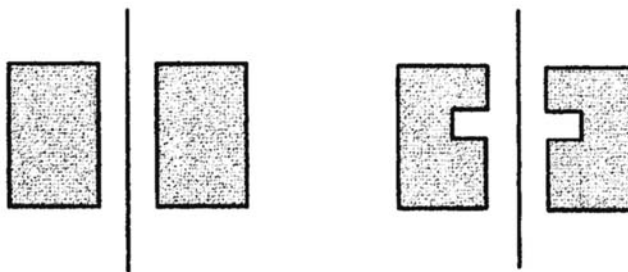


Figure 3.6.2 The same area Voronoi diagrams generated by two different sets of areas.

The area Voronoi diagram is unique for a given set of areas, but the converse is not true (Jones, 1991). Different sets of areas may give the same area Voronoi diagram. An example is shown in Figure 3.6.2.

An area (which does not degenerate into a line) appears different from a line, but computationally the area Voronoi diagram is quite similar to the line Voronoi diagram. As a matter of fact, we construct an area Voronoi diagram from its corresponding line Voronoi diagram. To be explicit, let $L(A)$ be the set of the boundaries of A , i.e. $L(A) = \{\partial A_1, \dots, \partial A_n\}$. We first construct the line Voronoi diagram with $L(A)$ (Figure 3.6.1(b)). We next delete the superfluous edges. Then the remaining edges form the area Voronoi diagram (Figure 3.6.1(a)). As is noticed from this procedure, some properties of the area Voronoi diagram are similar to those of the line Voronoi diagram. It should be noted, however, that the properties of the line Voronoi diagram that are related to the inside of a circuit chain or a circle are not applicable to those of the area Voronoi diagram. For instance, an elliptical curve does not appear in the area Voronoi diagram because the curve only appears inside a circle.

We may extend the order- k Voronoi diagram for points (Section 3.2) to that for areas. If we replace p_i with A_i and $d(p, p_i)$ with $d_s(p, A_i)$ in equation (3.2.3), we obtain a tessellation, which we call the *order- k area Voronoi diagram* (Roos, 1989). We present two properties similar to Property OK7 shown in Roos (1989).

Property OKA1 Let n , $n_a^{(k)}$, $n_v^{(k)}$, $n_e^{(k)}$, $n_u^{(k)}$, and $n_c^{(k)}$ be the number of generator polygons, Voronoi polygons, Voronoi vertices, Voronoi edges, unbounded Voronoi polygons, and connected components of Voronoi edges, respectively. For $1 \leq k \leq n - 1$, the following equations hold:

$$n_e^{(k)} = 3n_a^{(k)} - n_u^{(k)} - n_c^{(k)} - 2, \quad (3.6.3)$$

$$n_v^{(k)} = 2n_a^{(k)} - n_u^{(k)} - n_c^{(k)} - 1. \quad (3.6.3)$$

Property OKA2 For $2 \leq k \leq n - 1$, the following relation holds:

$$n_a^{(k)} \leq (2k - 1)n - (k^2 - k) - \sum_{i=1}^{k-1} (n_u^{(k)} + n_c^{(k)}). \quad (3.6.5)$$

An extension of the area Voronoi diagram in \mathbb{R}^3 is a Voronoi diagram generated by three-dimensional solid objects (which may be represented by polyhedra). We may call it a *solid object Voronoi diagram*.

3.6.2 Applications

Yoshikawa *et al.* (1987) and Okabe *et al.* (1988) examined the effect of large parks on the distribution of high-class apartment buildings in Tokyo using the area Voronoi diagram (see Section 8.3.3). Fujii (1983), Fujii and Oikawa (1986) and Oikawa (1986) determine the sphere of influence of parks with the weighted area Voronoi diagram, where the weights reflect the area of a park. Boggs (1951) and Ricketts (1986) dealt with the delimitation of seaward areas under national jurisdiction which implicitly uses the area Voronoi diagram, where areas correspond to national domains. Tagare *et al.* (1995) use the area Voronoi diagram to evaluate the similarity of tomographic sections. Edwards (1993) clarifies the linguistic structure of space (such as ‘inside’–‘outside’; ‘near’–‘far’) in terms of the area Voronoi diagram; similarly Gold (1992) interprets the meaning of neighbour. Edwards *et al.* (1996) apply the line and area Voronoi diagram to route descriptions expressed in natural language. Burge and Monagan (1995a,b) apply the area Voronoi diagram to grouping words and multi-part symbols in documents. Gold (1989a) shows that the area Voronoi diagram is useful to determine the spatial adjacency between objects in a map, e.g. the spatial adjacency between a house and a road. Lam and Ip (1994) and Ip and Lam (1995) examine the structural texture using the area and solid object Voronoi diagrams.

The area Voronoi diagram is often used in robot path planning (Lozano-Pérez, 1981). Consider a region in which obstacles are placed and a disk-shaped robot is supposed to move avoiding these obstacles (Ó'Dúnaing and Yap, 1985; Krozel and Andrisani II, 1989 (who approximate an area Voronoi diagram by a Voronoi diagram for a set of vertices of generator polygons); Rao *et al.*, 1991). The area in which the robot can move without collision is called the *free placements* (Kedem and Sharir, 1985) or *free configuration space* (Aronov and Sharir, 1994) or *free space* for short. The free space is readily obtained by the complement of the area enclosed by the parallel lines at distance r from the obstacles, where r is the radius of the disk robot.

Voronoi edges of an area Voronoi diagram included in the free space may be regarded as *collision-free paths* along which the robot can move without collision. Recalling the property of a Voronoi edge, we notice that a point on a Voronoi edge is equally distant from at least two polygons, A_i and A_j , and that the minimum distance in $\{d_s(q, A_i), d_s(q, A_j)\}$ for points q in a sufficiently small neighbourhood of p achieves maximum when $q = p$. In this sense, we may say that the collision-free paths given by Voronoi edges in the free space are the safest paths.

When we determine the size (radius) of a disk robot, the critical size is given by the minimum distance between the polygonal objects, which is called

the *bottleneck width*. We can find the bottleneck width by using the area Voronoi diagram, because the centre of the critical disk is found in a Voronoi vertex of the area Voronoi diagram generated by the polygonal objects.

The problem of robot motion planning occurs in a three-dimensional space where objects are solid objects. In this case, we may use the solid object Voronoi diagram. Such an application is discussed in Meng (1987), Latombe (1991) and Quin *et al.* (1995). The solid object Voronoi diagram is also used to analyse patterns of capillary blood vessels in the human liver (Saito and Toriwaki, 1992).

When the shape of a robot is not a disk, we have to use another area Voronoi diagram, which is discussed in depth in the next section.

3.7 VORONOI DIAGRAMS WITH V-DISTANCES

As we mentioned in the introduction of Chapter 3, we can define a generalized Voronoi diagram with any distance as long as the distance is a V-distance. The distance is not necessarily the Euclidean distance. In fact, we showed in the preceding sections that the multiplicatively weighted distance, the additively weighted distance, the compoundly weighted distance, the power distance and the shortest-path distance, which are not the Euclidean distance, produced generalized Voronoi diagrams. In this section we show other generalized Voronoi diagrams defined with various kinds of V-distances. First, we deal with V-distances defined in \mathbb{R}^m (in particular, $m = 2$) and next V-distances defined on surfaces in \mathbb{R}^3 .

3.7.1 Voronoi diagrams with the Minkowski metric L_p

We begin with a Voronoi diagram defined with the Minkowski metric in \mathbb{R}^m . The *Minkowski (power) metric* from a point p to a point p_i in \mathbb{R}^m is defined by

$$d_{L_p}(p, p_i) = \left[\sum_{j=1}^m |x_j - x_{ij}|^p \right]^{1/p}, \quad (3.7.1)$$

where (x_1, \dots, x_m) and (x_{i1}, \dots, x_{im}) are the Cartesian coordinates of p and p_i , respectively. Customarily, the symbol L_p is used for the Minkowski metric, where p refers to the degree of the power. The reader should not confuse the symbol p for a point with p of the degree of the power. The parameter p varies in the range of $1 \leq p < \infty$. If $p = 1$, equation (3.7.1) becomes

$$d_{L_1}(p, p_i) = \sum_{j=1}^m |x_j - x_{ij}|, \quad (3.7.2)$$

which is called the *Manhattan metric*, the *city-block distance* or the *taxis-cab distance*. If $p = 2$, the Minkowski metric is the Euclidean distance. If $p = \infty$, the Minkowski metric is called the *supremum metric* or *dominance metric*, which is alternatively written as

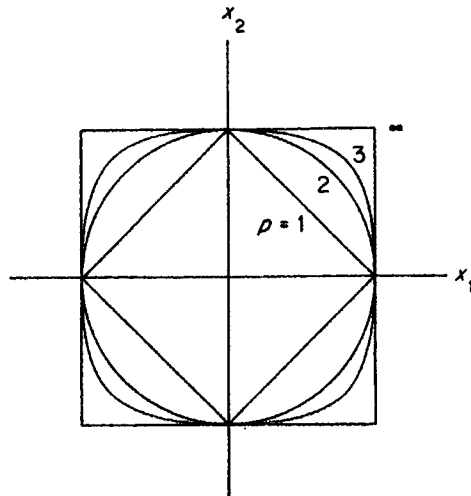


Figure 3.7.1 The contour lines of the Minkowski metric L_p for $p = 1, 2, 3, \infty$.

$$d_{L_\infty} = \max_j \{ |x_j - x_{ij}|, j \in I_m \}. \quad (3.7.3)$$

Figure 3.7.1 shows the contours of the Minkowski metric from the origin for $p = 1, 2, 3, \infty$.

The geometric properties of Voronoi diagrams with the Minkowski metrics L_p vary drastically according to the value of p ($1 \leq p \leq \infty$). We first consider a planar Voronoi diagram defined with the Manhattan metric. To see its geometric properties, let us observe the bisector defined with the Manhattan metric. From equation (3.7.2) ($p = 1$), we notice that the shape of the bisector varies according to the parameter value $\alpha = (x_{j2} - x_{i2})/(x_{j1} - x_{i1})$, where $x_{j1} \geq x_{i1}$ is assumed without loss of generality. We have eight possible types: (i) $-\infty < \alpha < -1$; (ii) $-1 < \alpha < 0$; (iii) $0 < \alpha < 1$; (iv) $1 < \alpha < \infty$; (v) $\alpha = \pm \infty$; (vi) $\alpha = 0$; (vii) $\alpha = -1$; and (viii) $\alpha = 1$. However, those types are essentially grouped into three types: I = (i)–(iv); II = (v) and (vi); and III = (vii) and (viii), which are shown in Figure 3.7.2. The bisector of type I consists of three straight lines as depicted in Figure 3.7.2(a). The diagonal line segment has angle $\pi/4$ or $3\pi/4$ with the x_1 -axis. This bisector is well-behaving. The bisector of type II is a straight line (Figure 3.7.2(b)), which is also well-behaving. The bisector of type III, however, is not well-behaving. In this case, as is indicated by the shaded area in Figure 3.7.2(c), the bisector consists of not only a straight line but also an area. To avoid this indeterminacy, we usually define the bisector as the straight perpendicular line bisecting $\overline{p_i p_j}$ (the solid and dashed lines in Figure 3.7.2(c)).

Once the above modification is made, the bisector becomes well-behaving, and hence the set $\mathcal{V}_M = \{V(p_1), \dots, V(p_n)\}$ defined in terms of $V(p_i) = \bigcap_{j \in I_M \setminus \{i\}} \text{Dom}(p_i, p_j)$ with equation (3.7.2) ($p = 1$) gives a generalized Voronoi diagram. We call the set \mathcal{V}_M the *Manhattan-metric Voronoi diagram* generated

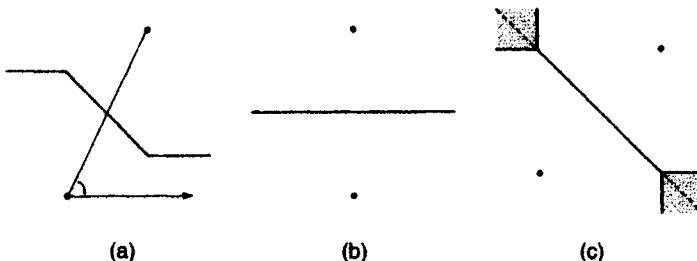


Figure 3.7.2 The bisector $b(p_i, p_j)$ defined with the Manhattan metric: (a) the bisector of type I ($\infty < \alpha < -1$, $-1 < \alpha < 0$, $0 < \alpha < 1$, $1 < \alpha < \infty$); (b) the bisector of type II ($\alpha = \pm\infty, 0$); (c) the bisector of type III ($\infty = \pm 1$); where $\alpha = (x_{j2} - x_{i2})/(x_{j1} - x_{i1})$ and where $x_{j1} \geq x_{i1}$ is assumed without loss of generality.

by P or the *Manhattan Voronoi diagram* in brief, and the set $V(p_i)$ the *Manhattan(-metric) Voronoi polygon* associated with p_i (Carter *et al.*, 1972; Hwang, 1979; Lee, 1980; Lee and Wong, 1980; Guha, 1993). An example is illustrated in Figure 3.7.3. Jeong (1991) and El Gindy and Wetherall (1995) develop computational methods with parallel computing, and Melter and Stojmenović (1995) develop a parallel computational method for the discrete Manhattan Voronoi diagram (see the discrete Voronoi diagram in Section 2.1).

From the properties of the bisector mentioned above with Figure 3.7.2, we note the following properties.

Property M1 The set $V(p_i)$ defined by $V(p_i) = \bigcap_{j \in I_n \setminus i} \text{Dom}(p_i, p_j)$ with the Manhattan metric (equation (3.7.2)) is not empty, and forms a (Manhattan Voronoi) polygon. The Manhattan Voronoi polygon $V(p_i)$ is not necessarily convex, but it is always star-shaped with respect to the generator p_i .

Property M2 Every edge of a Manhattan Voronoi polygon consists of at most three straight lines which are parallel to the x_1 -axis, x_2 -axis, or diagonal lines with angle $\pi/4$ or $3\pi/4$.

Property M3 The Manhattan Voronoi polygon $V(p_i)$ is unbounded if p_i is on the boundary of the convex hull of P , but not conversely.

Compared with Property V2 of the ordinary Voronoi diagram, the converse relation in Property M3 should be noted. An actual example is found in the Manhattan Voronoi polygon of p_1 in Figure 3.7.3. In addition to the above properties, Guha (1993) shows several properties that are utilized for parallel computing. Boissonnat *et al.* (1995) show the combinatorial complexity properties of \mathcal{V}_M in \mathbb{R}^3 .

A quite similar Voronoi diagram to the Manhattan Voronoi diagram is the Voronoi diagram defined with the supremum metric, which we call the

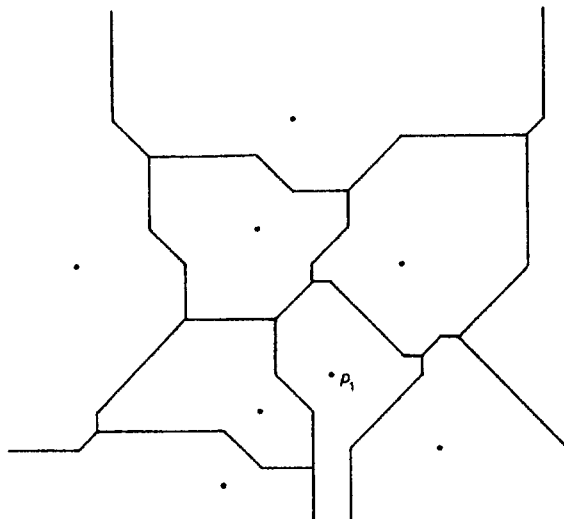


Figure 3.7.3 A Manhattan-metric Voronoi diagram.

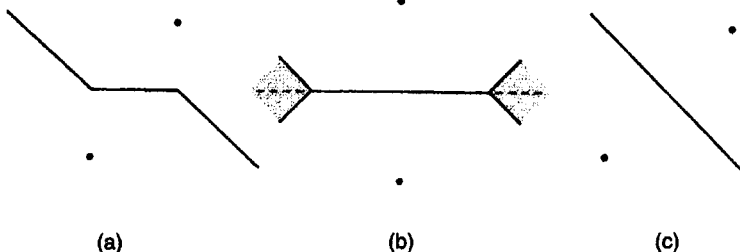


Figure 3.7.4 The bisector defined with the supremum metric: (a) the bisector of type I ($\infty < \alpha < -1$, $-1 < \alpha < 0$, $0 < \alpha < 1$, $1 < \alpha < \infty$); (b) the bisector of type II ($\alpha = \pm \infty$); (c) the bisector of type III ($\alpha = \pm 1$); where $\alpha = (x_{j2} - x_{i2})/(x_{j1} - x_{i1})$ and where $x_{ji} \geq x_{ii}$ is assumed without loss of generality.

supremum-metric Voronoi diagram. To see this similarity, we depict the bisector of the supremum metric in Figure 3.7.4 in which the locations of the generators are the same as those of the bisector of the Manhattan metric in Figure 3.7.2.

Comparing Figure 3.7.4(b) with Figure 3.7.2(c), we notice that if we rotate the x_1-x_2 plane in Figure 3.7.2(c) with generators counterclockwise by $\pi/4$, we obtain Figure 3.7.4(b). Generally, if we rotate the bisector defined with the Manhattan metric counterclockwise by $\pi/4$, we obtain the bisector defined with the supremum metric. From this property, we obtain the following property.

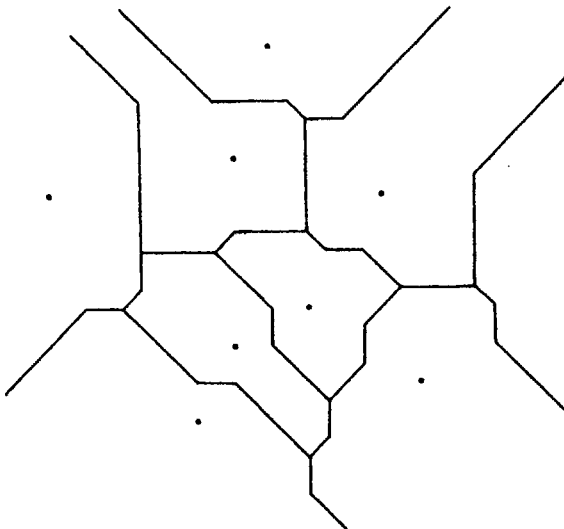


Figure 3.7.5 The supremum-metric Voronoi diagram generated by the generators whose locations are the same as those in Figure 3.7.3.

Property SUP1 The supremum-metric Voronoi diagram of P is obtained by first rotating P counterclockwise by $\pi/4$, next constructing the Manhattan Voronoi diagram for the rotated set of points, and finally rotating the resultant diagram clockwise by $\pi/4$.

We should note that Property SUP1 does not say that the supremum-metric Voronoi diagram of P is the same as the Manhattan Voronoi diagram of P . As we notice from Figures 3.7.3 and 3.7.5, these two Voronoi diagrams are different. The properties of the combinatorial complexity of the diagram in \mathbb{R}^m are shown in Boissonnat *et al.* (1995).

In the above, we focused on the Voronoi diagrams with L_1 and L_∞ in \mathbb{R}^2 , but we can define the Voronoi diagram with L_p , $1 \leq p \leq \infty$, in \mathbb{R}^m , which we call the *Minkowski (metric) Voronoi diagram*. Lê (1996) examines the Minkowski Voronoi diagram in \mathbb{R}^m , $m \geq 2$, from a combinatorial viewpoint.

We may construct a dual diagram of the Minkowski Voronoi diagram as we constructed the Delaunay triangulation from the ordinary Voronoi diagram. In fact, Shute *et al.* (1991) define a Delaunay triangulation as a dual diagram of the Minkowski Voronoi diagram for L_1 and L_∞ . We call it the *Minkowski Delaunay triangulation*. Note that their procedure is slightly different from the procedure employed in Section 2.2 (see Section 2 of Shute *et al.*, 1991).

In conjunction with the Manhattan Voronoi diagram, it may be worth noting a similar diagram, called the ‘rectangular Voronoi diagram’. For points $p_i, p_j \in P$, we define the half plane $H(p_i, p_j)$ by

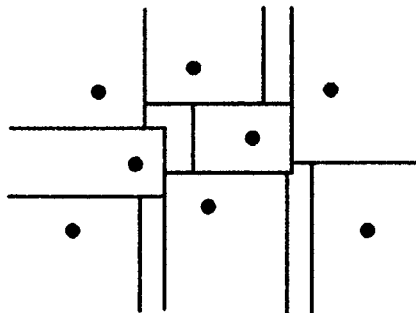


Figure 3.7.6 A rectangular Voronoi diagram.

$$H(p_i, p_j) = \begin{cases} \{(x_1, x_2) \mid x_2 \leq (x_{ii} + x_{jj})/2\} & \text{if } |x_{ii} - x_{jj}| \leq |x_{ii} - x_{jj}|, \\ \{(x_1, x_2) \mid x_1 \leq (x_{ii} + x_{jj})/2\} & \text{otherwise.} \end{cases} \quad (3.7.4)$$

Let $V(p_i) = \cap_{j \in I_n \setminus \{i\}} H(p_i, p_j)$, and $\mathcal{V}_{\text{rec}} = [V(p_1), \dots, V(p_n)]$. We call \mathcal{V}_{rec} the *rectangular Voronoi diagram* (Choi and Kyung, 1991). An example is shown in Figure 3.7.6. Note that, as is noticed in this figure, \mathcal{V}_{rec} is not a tessellation, because \mathcal{V}_{rec} does not cover the whole plane.

3.7.2 Voronoi diagrams with the convex distance

As is seen in Figure 3.7.1, the contour lines of the Minkowski metric are convex. This property is shared not only by the Minkowski metric but also by other distances, and those distances are subsumed under the ‘convex distance’. To be explicit, let us consider a closed convex figure, C , in \mathbb{R}^2 and choose an arbitrary interior point of C as the reference point of C (say, a triangle with its interior point in Figure 3.7.7). The figure C moves in \mathbb{R}^2 under a translational motion (without rotation). To indicate the position of C , we use the notation $C(p)$, implying that the reference point of C is placed at p (Figure 3.7.7). When p of $C(p)$ is placed at the origin o , we call $C(o)$ the *standard position* of $C(p)$. Mathematically, if p is represented by its location vector x , $C(p)$ is written as $C(p) = \{u + x \mid u \in C(o)\}$. The figure $C(p)$ may be scaled up (down) by $\lambda > 0$ fixing the similarity centre at p . The scaled up (down) figure is denoted by $C(p, \lambda)$ (Figure 3.7.7). Mathematically, $C(p, \lambda) = \{\lambda u + x \mid u \in C(o)\}$. Note that $C(p) = C(p, 1)$.

In terms of $C(p, \lambda)$, we define the *convex distance (function)* from a point p to a point p_i as the minimum value of λ that satisfies the condition that p_i is included in $C(p, \lambda)$ (the arrow from p to p_i in Figure 3.7.7). Mathematically, the *convex distance (function)*, $d_{\text{conv}}(p, p_i)$, from p to p_i is defined by

$$d_{\text{conv}}(p, p_i) = \min \{\lambda \mid p_i \in C(p, \lambda), \lambda > 0\}. \quad (3.7.5)$$

In terms of this distance, the convex distance from p to a polygon A_i is defined by

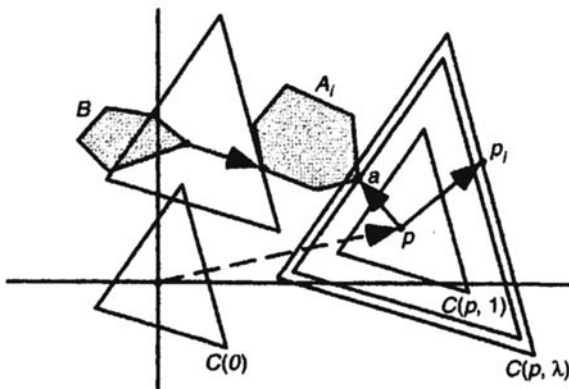


Figure 3.7.7 A convex distance from a point to a point, from a point to a polygon, and from a polygon to a polygon (points on the boundary of the triangle $C(o)$ are equally distant from o ; a is an attachment point).

$$d_{\text{conv}}(p, A_i) = \min_q \{ d_{\text{conv}}(p, q), q \in A_i \} \quad (3.7.6)$$

(the arrow from p to A_i in Figure 3.7.7). More generally, the convex distance from a polygon B to a polygon A_i is defined by

$$d_{\text{conv}}(B, A_i) = \min_{p, q} \{ d_{\text{conv}}(p, q), p \in B, q \in A_i \} \quad (3.7.7)$$

(the arrow from B to A_i in Figure 3.7.7).

Three remarks should be made. First, all points on the boundary of $C(p, \lambda)$ are at the same convex distance from p ; hence the boundary of $C(p, \lambda)$ indicates an equi-distant line (a contour line) from p (three equi-distant lines (triangles) from p in Figure 3.7.7). Second, when C is given by a disk, the convex distance becomes the Euclidean distance. Third, the convex distance does not satisfy $d_{\text{conv}}(p, q) = d_{\text{conv}}(q, p)$ when $C(p)$ is not symmetric with respect to p .

For ease of exposition, from now on we assume that A_i is convex and that the edges of C and those of A_i are not parallel (this assumption is relaxed, for example, in Leven and Sharir, 1987). Under these assumptions, there exists a unique point, a , for which the convex distance from p to A_i is equal to the convex distance from p to a , i.e. $d_{\text{conv}}(p, A_i) = d_{\text{conv}}(p, a)$ (Figure 3.7.7). We call the point a an *attachment point*, and the line segment \overline{pa} a (*finite*) *spoke* (McAllister *et al.*, 1996, p.77).

For two polygons A_i and A_j , we define the bisector $b(A_i, A_j)$ between A_i and A_j by $b(A_i, A_j) = \{p \mid d_{\text{conv}}(p, A_i) = d_{\text{conv}}(p, A_j)\}$. This bisector, however, may not be well-behaving, as is seen in Figure 3.7.8(a), where the convex distance from any point in the hatched area to A_1 is the same as that to A_2 . To avoid this indeterminacy, McAllister *et al.* (1996, p.78) propose the following rule. The boundary edges of the convex polygon $C(p, \lambda)$ are

directed, say counterclockwise, and each directed edge is supposed to include the end vertex but not the start vertex (Figure 3.7.8(a)). In terms of this directed polygon, we define the bisector $b(A_i, A_j)$ with the condition that the attachment point for A_i and that for A_j are not on the same edge. When this rule is adopted, the bisector becomes well-behaving. Note that this rule intuitively means that we rotate the convex polygon $C(p, \lambda)$ clockwise infinitesimally. In the hatched region in Figure 3.7.8(a), only the points on the heavy line form part of the bisector. Figure 3.7.8(b) shows the bisector between A_1 and A_2 obtained under the above rule. Since this bisector becomes well-behaving, it divides the plane into two half regions, and let $H(A_i, A_j)$ be the half region including A_i with $b(A_i, A_j)$. For a set $A = \{A_1, \dots, A_n\}$ of disjoint closed polygons, we define $V(A_i) = \bigcap_{j \in I_n \setminus i} H(A_i, A_j)$, and let $\mathcal{V}_{\text{conv}} = \{V(A_1), \dots, V(A_n)\}$. We call the diagram $\mathcal{V}_{\text{conv}}$ the *convex distance Voronoi diagram*. Chew and Drysdale (1985) call $\mathcal{V}_{\text{conv}}$ the *Voronoi diagram based on a convex distance function*, and Leven and Sharir (1987) call $\mathcal{V}_{\text{conv}}$ the *B-Voronoi diagram*. An example is shown in Figure 3.7.9. As we noted above, since the Euclidean distance is included in the convex distance, the ordinary Voronoi diagram is included in $\mathcal{V}_{\text{conv}}$. Also, the Manhattan-metric Voronoi diagram and the supremum metric Voronoi diagram are subsumed under $\mathcal{V}_{\text{conv}}$.

In addition to those diagrams, we refer to a specific $\mathcal{V}_{\text{conv}}$ where C is given by an ellipse. To be explicit, $C(o) = \{x \mid x^T G x \leq 1\}$ or the distance between x and x_i is given by

$$d_{\text{ellip}}(x, x_i) = \sqrt{(x - x_i)^T G (x - x_i)}, \quad (3.7.8)$$

where G is a positive definite symmetric matrix. We call the convex distance Voronoi diagram specified by d_{ellip} the *elliptic distance Voronoi diagram*, $\mathcal{V}_{\text{ellip}}$.

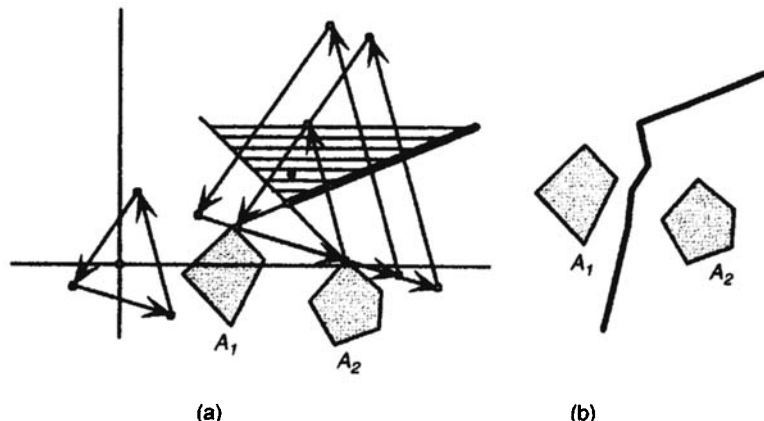


Figure 3.7.8 A bisector with a convex distance: (a) the indeterminant region in which the distances from any point in the hatched region to A_1 and A_2 are equal; (b) the well-behaving bisector between A_1 and A_2 defined in terms of the directed triangle C in panel (a).

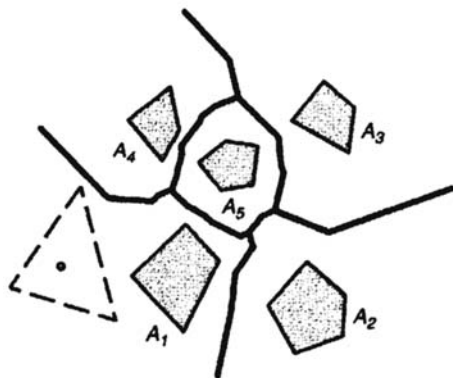


Figure 3.7.9 A convex distance Voronoi diagram (the heavy lines) generated by a set of polygons (the shaded polygons) with a convex distance specified by a triangle (the broken lines) $C(o)$.

(Scheike, 1994 calls it the *Voronoi-G tessellation*). Examples are shown in Figure 3.7.10.

It should be noted that $\mathcal{V}_{\text{ellip}}$ is easily obtained from the ordinary Voronoi diagram through an affine transformation. In Figure 3.7.10, $\mathcal{V}_{\text{ellip}}$ in panel (b) is obtained by shrinking $\mathcal{V}_{\text{ellip}}$ in panel (c) in the vertical direction; $\mathcal{V}_{\text{ellip}}$ in panel (a) is obtained by rotating $\mathcal{V}_{\text{ellip}}$ in panel (b). Thus the construction of $\mathcal{V}_{\text{ellip}}$ is straightforward once the corresponding ordinary Voronoi diagram is obtained (Scheike, 1994).

Recalling the nearest search problem (V3) solved by the ordinary Voronoi diagram, we notice that that problem can be generalized for polygons and readily solved by $\mathcal{V}_{\text{conv}}$.

Problem C1 (the nearest polygon search problem with the convex distance) Given a finite set $A = \{A_1, \dots, A_n\}$ of disjoint polygons, find the nearest polygon among A from a given point in terms of the convex distance.

Obviously, this problem reduces to Problem V3 when polygons degenerate into points and C is given by a disk.

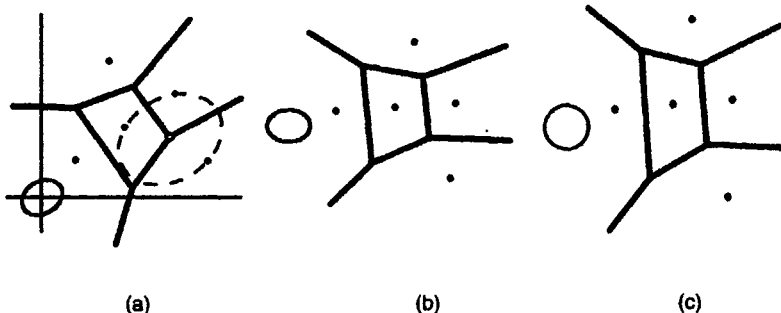


Figure 3.7.10 Elliptic distance Voronoi diagrams, $\mathcal{V}_{\text{conv}}$, with C : (a) $\mathcal{V}_{\text{conv}}$ with a tilted ellipse C (the broken ellipse is the largest ellipse whose centre is within the convex hull of the generator points); (b) $\mathcal{V}_{\text{conv}}$ with an upright ellipse C ; (c) $\mathcal{V}_{\text{conv}}$ with a disk C .

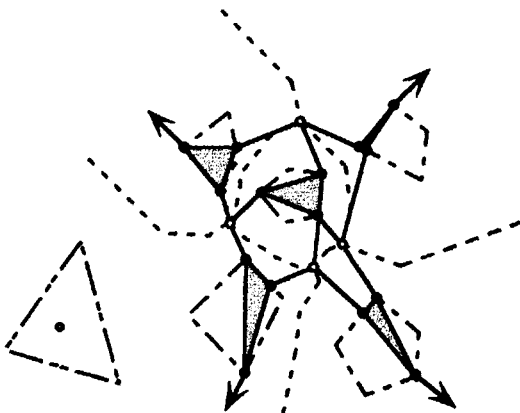


Figure 3.7.11 A core diagram (the continuous lines) and its corresponding convex distance Voronoi diagram (the broken lines) (the shaded regions are cores, the unfilled circles are Voronoi vertices, the filled circles are attachment points of the spokes from the Voronoi vertices, the dash-dot lines are generator polygons, the dash-dot-dot lines indicate a convex distance specified by a triangle, $C(o)$, at the standard position (the shaded circle)).

When our purpose is only to solve this problem, we may use a simplified $\mathcal{V}_{\text{conv}}$ to save memory space. Such a diagram is proposed by McAllister *et al.* (1996), which is constructed in the following manner. First, we obtain attachment points (the filled circles in Figure 3.7.11) of the spokes spanning from each Voronoi vertex of $\mathcal{V}_{\text{conv}}$. In addition to the ordinary Voronoi vertices (the unfilled circles in Figure 3.7.11), we suppose a fictitious Voronoi vertex placed at the farthest point at which all infinite Voronoi edges meet. From this fictitious Voronoi vertex, we span spokes and obtain attachment points (the filled circles connected to the arrows in Figure 3.7.11). As a result, each polygon A_i has a set of attachment points (the filled circles in Figure 3.7.11). For this set of attachment points, we construct a convex hull (the shaded triangle in Figure 3.7.11), which is called the *core* of A_i . The edges of cores and spokes from Voronoi vertices (the heavy continuous lines in Figure 3.7.11) partition \mathbb{R}^2 and form a tessellation. We call this tessellation the *compact piecewise-linear Voronoi diagram* (McAllister *et al.*, 1996) or the *compact Voronoi diagram* for short (McAllister and Snoeyink, 1994, call it the *spoke diagram*). The resulting polygons, except for cores, are called the *spoke regions*. If a probe point is included in a spoke region, the nearest polygon from the point is found in one of the polygons whose cores share the edges of the spoke region.

Each spoke region includes one Voronoi edge, and has at most six vertices regardless of the number of vertices of polygons in A and the number of line segments forming Voronoi edges (McAllister *et al.*, 1996). Thus the compact Voronoi diagram requires less memory space than the convex distance Voronoi diagram (regarding the search time, see McAllister *et al.*, 1996).

In a similar fashion to how we extended the nearest search problem (V3) to the nearest polygon search problem, we can extend the largest empty circle problem (V5) in Section 2.3 to the following problem.

Problem C2 (the largest empty polygon problem) Given a finite set P of distinct points, find the largest empty polygon, $C(p, \lambda)$, which is homothetic to a given polygon C and whose reference point p is included in the convex hull $\text{CH}(P)$ of P .

The position p^* of the largest $C(p^*, \lambda^*)$ is found in one of the Voronoi vertices of $\mathcal{V}_{\text{conv}}$, or cross points between the edges of $\mathcal{V}_{\text{conv}}$ and the boundary of $\text{CH}(P)$, or vertex of $\text{CH}(P)$. An example is shown in Figure 3.7.10 where the largest empty ellipse is indicated by the broken lines. A slightly more generalized probem is that given a convex polygon and an environment consisting of polygonal obstacles, we need to find the placement of the largest similar copy of the poygon that does not intesect any of the obstacles. This problem is solved by Chew and Kedem (1993).

In conjunction with the largest empty polygon problem, it may be worth noting the following problems (Chazelle, 1983; Fortune, 1985).

Problem C3 (the polygon containment problem) Find a position p , if it exists, of a polygon, $C(p, \lambda)$, contained in a simple polygon B (indicated by the light continuous lines in Figure 3.7.12) where $C(p, \lambda)$ is homothetic to a given polygon C .

Problem C4 (the largest convex polygon contained in a simple polygon) For a given simple polygon B , find the largest polygon $C(p, \lambda^*)$ contained in B , where $C(p, \lambda^*)$ is homothetic to a given polygon C .

To solve these problems, we construct $\mathcal{V}_{\text{conv}}$ for a set of line segments constituting the edges of B . Fortune (1985) calls $\mathcal{V}_{\text{conv}} \cap B$ the *C-diagram* (the heavy continuous lines in Figure 3.7.12). The position p^* of the largest $C(p^*, \lambda^*)$ contained in B can be found among one of the Voronoi vertices

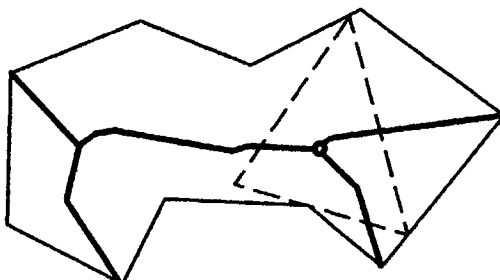


Figure 3.7.12 The largest triangle contained in a simple polygon where the triangle moves under translation and it may be scaled up or down.

(the broken line triangle in Figure 3.7.12), which is the solution to Problem C4. $C(p^*, \lambda^*)$ is called the *largest convex polygon contained in a simple polygon*.

If $C(p^*, \lambda^*)$ is not greater than $C(p^*, \bar{\lambda})$, i.e. $\lambda^* \leq \bar{\lambda}$, then there is no solution. If $C(p^*, \lambda^*)$ is smaller than $C(p^*, \bar{\lambda})$, i.e. $\lambda^* > \bar{\lambda}$, then p^* is a solution to Problem C3. This solution is optimal in the sense that the position p^* of $C(p^*, \bar{\lambda})$ is the farthest point from the edges of the polygon B in terms of the convex distance.

Note that Chazelle (1983), Aonuma *et al.* (1990) and Imai *et al.* (1998) deal with the case in which $C(p, \lambda)$ is allowed to rotate.

As in equation (3.7.5), the convex distance $d_{\text{conv}}(p, p_i)$ from a point p to a point p_i is defined by the minimum value of λ that satisfies the condition that p_i is included in $C(p, \lambda)$. Extending this definition, we may define an alternative convex distance, d_{conv^*} , from a point p to a polygon A_i by the minimum value of λ that satisfies the condition that A_i is included in $C(p, \lambda)$ (the arrow in the broken line triangle in Figure 3.7.13), i.e.

$$d_{\text{conv}^*}(p, A_i) = \min \{ \lambda \mid A_i \subset C(p, \lambda), \lambda > 0 \}. \quad (3.7.9)$$

Note that $d_{\text{conv}}(p, A_i) \neq d_{\text{conv}^*}(p, A_i)$ in general. With this distance, we can construct a Voronoi diagram for A . The resulting Voronoi diagram, $\mathcal{V}_{\text{conv}^*}$, is called the *closest covered set Voronoi diagram* (Abellanas *et al.*, 1995, 1997). An example is shown in Figure 3.7.13.

This diagram is used to prove the following interesting theorem: for a strictly compact convex set C and a family of disjoint compact convex sets, $A = \{A_1, \dots, A_n\}$, there exist two elements $A_i, A_j \in A$ such that any set homothetic to C containing A_i and A_j contains $[n/c]$ (the upper integer of n/c) elements of A , where c is a constant. The proof and the value of c are shown in Abellanas *et al.* (1995, 1997). Note that this problem is an extension of a similar problem defined for a set of points and a circle C (Neumann-Lara and Urrutia, 1988).

We may extend the convex distance Voronoi diagram in \mathbb{R}^2 to that in \mathbb{R}^3 . In fact, Icking *et al.* (1995) define such a diagram and show that the properties

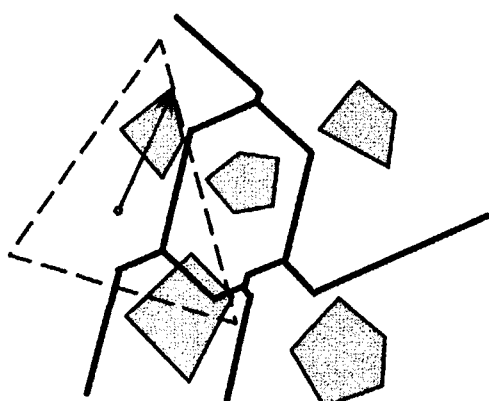


Figure 3.7.13 A closed covered set Voronoi diagram.

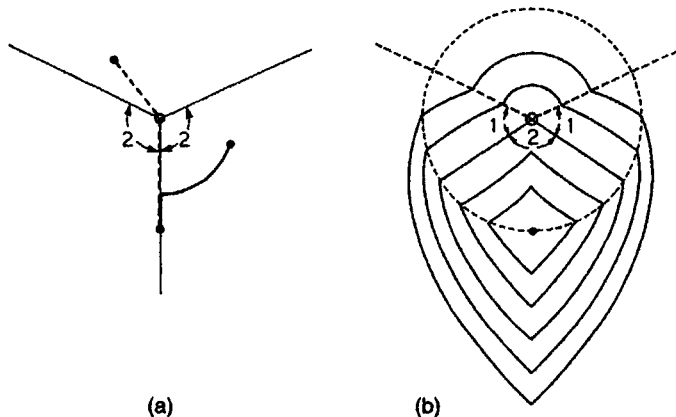


Figure 3.7.14 The contour lines of the Karlsruhe metric.

of that diagram are quite different from those in \mathbb{R}^2 . Chew *et al.* (1995) formulate the convex distance Voronoi diagram for lines in \mathbb{R}^3 .

3.7.3 Voronoi diagrams with the Karlsruhe metric

In Manhattan, we can move along either north–south avenues or east–west streets. In Karlsruhe, we can move along either radiating streets from the centre or circular avenues around the centre. We call the shortest distance in Karlsruhe the *Karlsruhe metric* (Klein, 1988). To be precise, let (r, θ) and (r_i, θ_i) be the polar coordinates of p and p_i , respectively, where $0 \leq \theta, \theta_i < 2\pi$, $r, r_i > 0$, and $\delta(\theta, \theta_i) = \min\{| \theta - \theta_i |, 2\pi - | \theta - \theta_i |\}$. Then, the *Karlsruhe metric* or *Moscow metric* from p to p_i is defined by

$$d_K(p, p_i) = \begin{cases} \min\{r, r_i\} \delta(\theta, \theta_i) + |r - r_i| & \text{for } 0 \leq \delta(\theta, \theta_i) < 2, \\ r + r_i & \text{for } 2 \leq \delta(\theta, \theta_i) < \pi \end{cases} \quad (3.7.10)$$

(Koshizuka and Kurita, 1986; Klein, 1988, 1989). In Figure 3.7.14(a) the shortest path for $0 \leq \delta(\theta, \theta_i) < 2$ is indicated by the heavy solid line and that for $2\delta(\theta, \theta_i) \leq \pi$ is indicated by the broken line. In Figure 3.7.14(b) the contour lines of the Karlsruhe metric from the point indicated by the filled circle (θ is measured from the line radiating from the unfilled circle (the origin) to the filled circle counterclockwise). In the fan-shaped region bounded by the lines radiating from the origin with 2 radians and $2\pi - 2$ radians, the contour lines are circular arcs centred at the origin, and the contour lines radiating from the origin with 1 radian and $2\pi - 1$ radians are straight lines in the dashed circle in Figure 3.7.14(b).

In most cases the bisector with the Karlsruhe metric is well-behaving, as is shown in Figure 3.7.15(a). In a special case (Figure 3.7.15(b)), however, the bisector is not well-behaving. The indeterminacy occurs when two

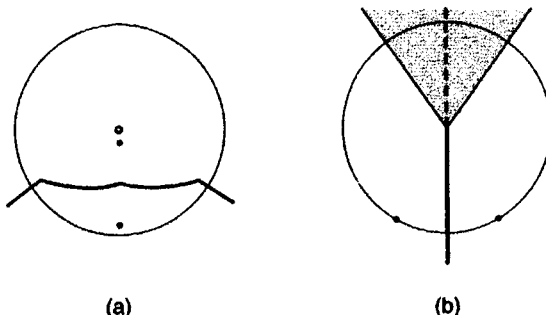


Figure 3.7.15 The bisectors defined with the Karlsruhe metric: (a) a well-behaving bisector; (b) not a well-behaving bisector and its modified bisector (the dashed line and heavy solid line).

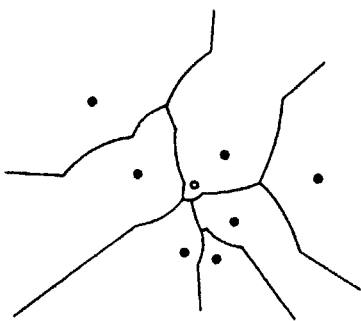


Figure 3.7.16 A Karlsruhe-metric Voronoi diagram (the unfilled circle is the centre). (Source: Klein, 1988, Figure 12.)

points p_i and p_j have the same distance from the origin ($r_i = r_j$) and $\delta(\theta_i, \theta_j) < 2\pi - 4$. In this case, as we did for the bisector of the Manhattan metric (Figure 3.7.2(c)), we define the bisector as the perpendicular line bisecting $\overline{p_i p_j}$ (the heavy solid and dashed lines in Figure 3.7.15(b)).

If we add the above modification to the bisector of the Karlsruhe metric, the set $V_K = \{V(p_1), \dots, V(p_n)\}$ gives a generalized Voronoi diagram. We call V_K the *Karlsruhe-metric Voronoi diagram*, or simply the *Karlsruhe Voronoi diagram*, and the regions constituting the Karlsruhe Voronoi diagram *Karlsruhe(-metric) Voronoi regions*. An example is shown in Figure 3.7.16.

3.7.4 Voronoi diagrams with the Hausdorff distance

The *Hausdorff distance* from a point p to a closed set A is defined by

$$d_H = \max_{x_i} \{ \|x - x_i\| \mid x_i \in A_i \}. \quad (3.7.11)$$

This distance is useful in applications when we are concerned with the farthest distance. For instance, if we are concerned with the location of a fire station in a rural region where A_i represents the area of a village, the crucial house is the farthest house in each village from the fire station.

Aurenhammer (1988a) employs the Hausdorff distance to define a line Voronoi diagram. This line Voronoi diagram is quite different from the ordinary line Voronoi diagram in Section 3.4. To see this difference, let $b(L_i, L_j)$ be the bisector generated by two straight line segments L_i and L_j ; p_{ik} and p_{jk} be the end points of L_k , $k = i, j$; and $H(p_i, p_j)$ be the half plane made by the perpendicular line bisecting $\overline{p_ip_j}$ that includes p_i . If a point p is in $H(p_{i2}, p_{i1}) \cap H(p_{j2}, p_{j1})$, then the farthest point in L_i from p is p_{i1} , and the farthest point in L_j from p is p_{j1} . Thus the bisector $b(L_i, L_j)$ in $H(p_{i2}, p_{i1}) \cap H(p_{j2}, p_{j1})$ is given by the line perpendicularly bisecting $\overline{p_{i1}p_{j1}}$. Generally, the bisector $b(L_i, L_j)$ in $H(p_{ik}, p_{ik}) \cap H(p_{jh}, p_{jh})$ is written as

$$\begin{aligned} & b(L_i, L_j) \cap [H(p_{ik}, p_{ik}) \cap H(p_{jh}, p_{jh})] \\ &= \{x \mid \|x - x_{ik}\| = \|x - x_{jh}\|\} \cap [H(p_{ik}, p_{ik}) \cap H(p_{jh}, p_{jh})] \quad k, h = 1, 2, \end{aligned} \quad (3.7.12)$$

where $k = 1$ if $k = 2$ and $k = 2$ if $k = 1$, and the same for h . An example is shown in Figure 3.7.17.

From Figure 3.7.17 we notice that the bisector consists of straight lines. A curved bisector observed in the ordinary line Voronoi diagram never appears here. The bisector is well-behaving and hence we can obtain a line Voronoi diagram with the Hausdorff distance. We call this diagram the *Hausdorff line Voronoi diagram*. An example is shown in Figure 3.7.18.

From equation (3.7.11) or (3.7.12) the reader may notice that the Hausdorff line Voronoi diagram can be constructed with the help of the farthest-point Voronoi diagram. The role of the farthest-point Voronoi diagram becomes more explicit when we construct a Hausdorff Voronoi diagram generated by a set of polygons, called a *Hausdorff area Voronoi diagram*. Consider a set of polygons $A = \{A_1, \dots, A_n\}$ and let $P_i = \{p_{il} \mid l \in I_{n,i}\}$ be the vertices of the polygon A_i , $i \in I_n$. To obtain the bisector $b(A_i, A_j)$ between polygons A_i and A_j , we first construct the farthest-point Voronoi diagrams for P_k , $k = i, j$ (the dashed lines in Figure 3.7.19). Let $V_{fp}(p_{kl} \mid P_k)$ be the farthest-point Voronoi polygon of p_{kl} in the farthest-point Voronoi diagram generated by P_k , $k = i, j$. Then part of the bisector is given by

$$\begin{aligned} & b(A_i, A_j) \cap \{V_{fp}(p_{il} \mid P_i) \cap V_{fp}(p_{jh} \mid P_j) \setminus [A_i \cup A_j]\} \\ &= \{x \mid \|x - x_{il}\| = \|x - x_{jh}\|\} \cap \{V_{fp}(p_{il} \mid P_i) \cap V_{fp}(p_{jh} \mid P_j) \setminus [A_i \cup A_j]\} \end{aligned} \quad (3.7.13)$$

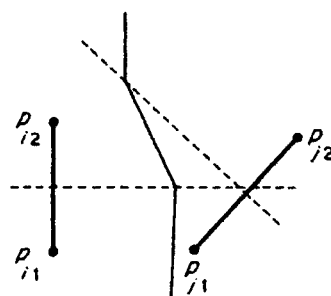


Figure 3.7.17 The bisector of two line segments defined with the Hausdorff distance.

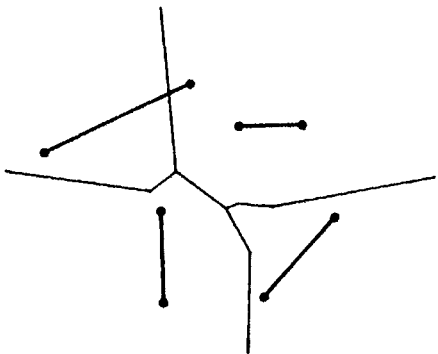


Figure 3.7.18 A Hausdorff line Voronoi diagram generated by a set of straight line segments.

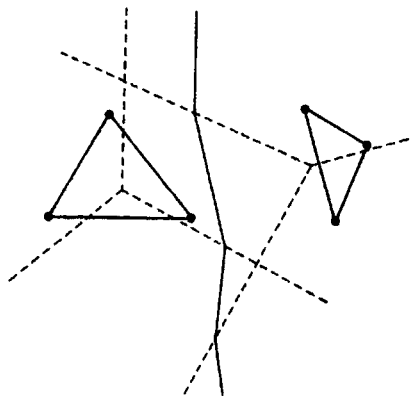


Figure 3.7.19 The bisector of two polygons with the Hausdorff distance, or a Hausdorff area Voronoi diagram generated by a set of two polygons (the dashed lines show the farthest-point Voronoi diagrams generated by the vertices of the polygons).

(the fine solid lines in Figure 3.7.19). Using this equation, we can construct a Hausdorff area Voronoi diagram.

3.7.5 Voronoi diagram with the boat-on-a-river distance

Imagine a wide river where lifeboats are moored at mooring posts and a lookout tower stands. When a watcher in the tower finds a boat driven on a rock, the watcher asks the lifeboat that can reach the boat in the shortest time to rescue the people in the boat. In this rescue system, the lifeboats have their own rescue regions covering the river, which may form a tessellation. We call this tessellation the *Voronoi diagram on a river* (Sugihara, 1992a).

To formulate this tessellation mathematically, let $P = \{p_1, \dots, p_n\}$ be a set of points (mooring posts) in the x - y plane; $w \geq 0$ be the flow velocity of a river running from west to east (which coincides with the x -axis); $v > 0$ be the velocity of a lifeboat; and $\alpha = w/v$, called the *relative flow velocity*. We measure the closeness from $p_i = (x_i, y_i)$ to a point $p = (x, y)$ by the shortest time, $t(p_i, p)$, spent in sailing from p_i to p . To be explicit, let θ be the angle

of the heading direction of a lifeboat measured from the x -axis. Then, $x - x_i = t(p_i, p) v \cos \theta + t(p_i, p) w$ and $y - y_i = t(p_i, p) v \sin \theta$ hold (Figure 3.7.20(a)). Eliminating θ from these equations, we obtain:

for $\alpha < 1$,

$$t(p_i, p) = \frac{-\alpha(x - x_i) + \sqrt{(x - x_i)^2 + (1 - \alpha^2)(y - y_i)^2}}{v(1 - \alpha^2)}; \quad (3.7.14)$$

for $\alpha = 1$,

$$t(p_i, p) = \begin{cases} \frac{(x - x_i)^2 + (y - y_i)^2}{2v(x - x_i)} & \text{for } x > x_i, \\ 0 & \text{for } x = x_i \text{ and } y = y_i, \\ \infty & \text{for } x \geq x_i \text{ and } y \neq y_i, \end{cases} \quad (3.7.15)$$

for $\alpha > 0$,

$$t(p_i, p) = \begin{cases} \frac{-\alpha(x - x_i) + \sqrt{(x - x_i)^2 + (1 - \alpha^2)(y - y_i)^2}}{v(1 - \alpha^2)} & \text{for } |x - x_i| \leq |y - y_i| \sqrt{\alpha^2 - 1}, \\ \infty & \text{otherwise.} \end{cases} \quad (3.7.16)$$

We call $t(p_i, p)$ the *boat-on-a-river distance*. The contour lines of the boat-on-a-river distance from the mooring pole p_i are shown in Figure 3.7.20, where the shaded regions (which correspond to $t(p_i, p) = \infty$ in equations (3.7.15) and (3.7.16)) indicate the regions which the lifeboat moored at p_i cannot reach (because the lifeboat cannot sail against the faster flow).

The dominance region of p_i over p_j is obtained from $\text{Dom}(p_i, p_j) = \{p \mid t(p_i, p) \leq t(p_j, p)\}, j \neq i$. When $0 < \alpha < 1$, this dominance region is well-behaving, and the boundary of $\text{Dom}(p_i, p_j)$ or the bisector between p_i and p_j is given by a hyperbolic curve. When $\alpha \geq 1$, the dominance region is not well-behaving, because there exists a region whose points are neither assigned to p_i nor p_j (recall Figure 3.7.20(b), (c)). The shape of the dominance region varies according to the value of α and the relative configuration of p_i and p_j (see Sugihara, 1992a).

When $0 \leq \alpha < 1$, the set $V(p_i) = \bigcap_{j \neq i, j=1}^n \text{Dom}(p_i, p_j)$ gives a region, and the set $\mathcal{V}_{\text{river}} = \{V(p_1), \dots, V(p_n)\}$ forms a tessellation (Figure 3.7.21(a)). Stated a little more formally, we have the following property.

Property RV1 The Voronoi regions $V(p_1), \dots, V(p_n)$ cover the whole plane \mathbb{R}^2 if and only if $0 \leq \alpha < 1$.

We call $\mathcal{V}_{\text{river}}$ the *Voronoi diagram on a river* generated by P . Note that in the specific case of $\alpha = 0$, $\mathcal{V}_{\text{river}}$ is reduced to the ordinary Voronoi diagram, because the boat-on-a-river distance becomes the Euclidean distance. When

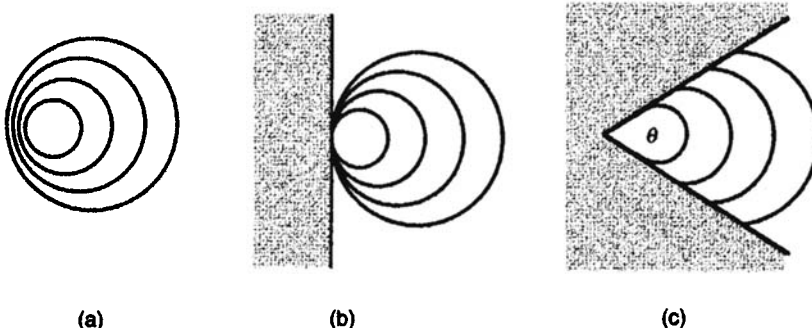


Figure 3.7.20 Contour lines of the boat-on-a-river distance from p_i ; (a) $0 < \alpha < 1$; (b) $\alpha = 1$; (c) $\alpha > 1$.

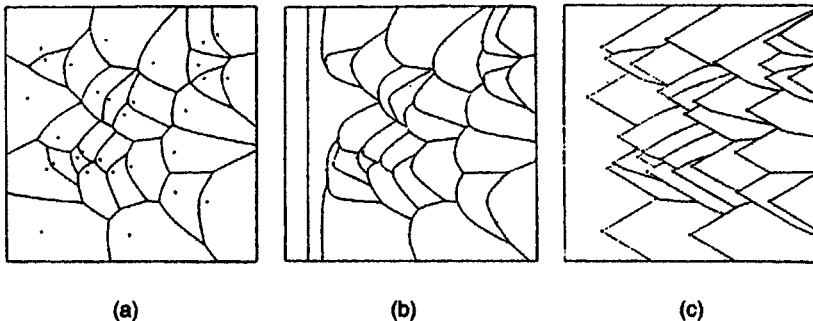


Figure 3.7.21 Voronoi diagrams on a river: (a) $\alpha = 0.5$; (b) $\alpha = 1$; (c) $\alpha = 2.0$.

$\alpha \geq 1$, $\mathcal{V}_{\text{river}}$ does not exhaust \mathbb{R}^2 , as shown in Figure 3.7.21(b), (c), but $\mathcal{V}_{\text{river}}$ may be regarded as a tessellation of $\bigcup_{i=1}^n V(p_i)$, which we also call the Voronoi diagram on a river.

We note one more important property.

Property RV2 For $0 \leq \alpha < 1$, the two generators of $\mathcal{V}_{\text{river}}$ are neighbours if and only if they are neighbours on the ordinary Voronoi diagram.

The proof is shown in Sugihara (1992a).

3.7.6 Voronoi diagrams on a sphere

In a military district problem, the dominance regions or coverage areas of air bases in the world is often discussed. We may treat this problem by a Voronoi diagram defined on a sphere.

Let $P = \{p_1, \dots, p_n\}$ ($2 \leq n < \infty$) be distinct points on a sphere S with the unit radius centred at the origin, and x and x_i be the location vectors of $p \in S$ and $p_i \in S$, respectively. The shortest distance from p to p_i on S is defined by the length of the lesser arc on the great circle (the circle whose centre is at the centre of S) passing through p and p_i . Mathematically, this distance is written as

$$d_{gc}(p, p_i) = \arccos(x^T x_i) \leq \pi. \quad (3.7.17)$$

We call this distance the *great circle distance*. The bisector defined with the great circle distance is given by the great circle that ‘perpendicularly’ passes through the mid-point of the great circular arc combining p_i and p (‘perpendicularly’ means that sufficiently small segments of the two great circles around the mid-point are orthogonal). This bisector divides the sphere S into two disjoint hemispheres. Thus the bisector defined with the great circle distance is well-behaving, and

$$V(p_i) = \{d_{gc}(p, p_i) \leq d_{gc}(p, p_j), j \in I_n \setminus \{i\}, p \in S\} \quad (3.7.18)$$

gives a non-empty set in S . We call this set the *spherical Voronoi polygon* associated with p_i . The set of resulting spherical Voronoi polygons gives a generalized Voronoi diagram, which we call the *spherical Voronoi diagram* generated by P on S (Miles, 1971; Brown, 1980; Paschinger, 1982; Ash and Bolker, 1985; Renka, 1984b; Augenbaum and Peskin, 1985; Sugihara, 1997). Figure 3.7.22 shows a spherical Voronoi diagram. Renka (1984b) provides software for constructing the spherical Voronoi diagram.

In a similar fashion to how we defined the Delaunay triangulation as the dual of the ordinary Voronoi diagram, we can define the *spherical Delaunay triangulation* as the dual of the spherical Voronoi diagram (Renka, 1984a,b).

The term ‘spherical polygon’ mentioned above is a ‘polygon’ on a sphere S . To be precise, let S_i be a hemisphere on S . Then, a spherical polygon is defined by the set of points on S which is obtained from the combination of intersections and/or unions of S_i , $i = 1, 2, \dots$. Like a convex polygon in \mathbb{R}^2 , we can define a *convex spherical polygon* by the spherical polygon in which the lesser arc of a great circle passing through any two points in the spherical polygon is embedded in the spherical polygon. From the definition of a spherical Voronoi polygon, we understand the following properties.

Property S1 The set $V(p_i)$ defined by equation (3.7.18) is a unique bounded non-empty convex spherical polygon.

Property S2 An edge of a spherical Voronoi polygon is an arc of a great circle.

These properties correspond to Properties V1–V3 of the ordinary Voronoi diagram. Properties V4–V7 of the ordinary Voronoi diagram also hold for the spherical Voronoi diagram by replacing relevant terms. Property V9,

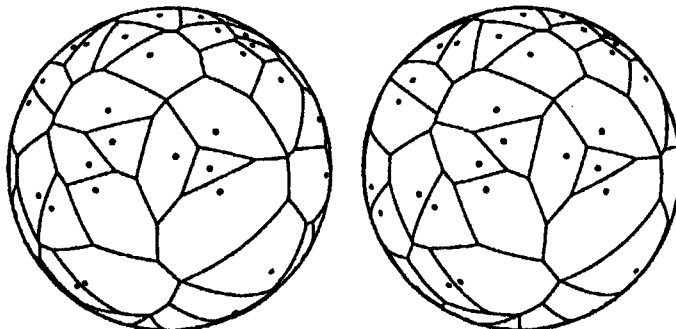


Figure 3.7.22 A stereographic view of a spherical Voronoi diagram.

however, becomes slightly different, because the ordinary Voronoi diagram is formulated in an unbounded space, whereas the spherical Voronoi diagram is formulated in a bounded space. From Euler's theorem, we obtain the following property.

Property S3 Let n_v and n_e be the number of vertices and edges in the spherical Voronoi diagram generated by $P = \{p_1, \dots, p_n\}$. Then the following equation holds:

$$n_v - n_e + n = 2. \quad (3.7.19)$$

Replacing equation (2.3.4) with equation (3.7.19) in the derivations used for Properties V11–V13, we can obtain the properties corresponding to Properties V11–V13 of the ordinary Voronoi diagram.

We may define a spherical Voronoi diagram by replacing the great circle distance with another distance. Sugihara (1997) shows the Voronoi diagram with the spherical Laguerre distance, called the *spherical Laguerre Voronoi diagram* or *spherical power (Voronoi) diagram*, following the power (Voronoi) diagram in Section 3.1. An example is shown in Figure 3.7.23.

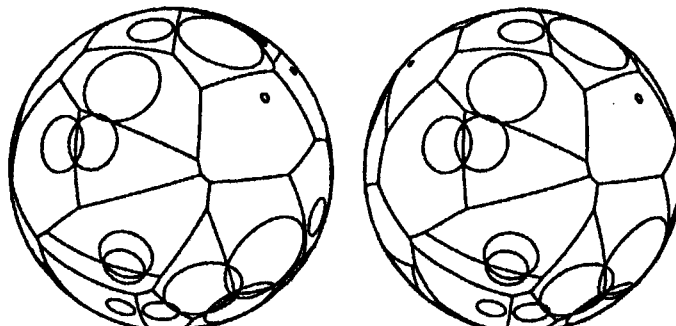


Figure 3.7.23 A spherical Laguerre Voronoi diagram.

3.7.7 Voronoi diagrams on a cylinder

When we meet phenomena in which the same configuration of generator points appears in cycles, we can analyse them with the aid of a Voronoi diagram on a cylinder.

Suppose that the axis of a cylinder S with unit radius is placed at an axis in \mathbb{R}^3 , and that a set $P = \{p_1, \dots, p_n\}$ of distinct points ($2 \leq n < \infty$) is placed on the cylinder S (Figure 3.7.24(a)). The location of p_i on S can be indicated by (x_i, y_i, z_i) , where $x_i^2 + y_i^2 = 1$, and the distance between p and p_i is defined by the length of the shortest path on S connecting p and p_i . At first glance this measurement appears difficult in practice, but if we notice that a cylinder can be developed on a plane, this measurement becomes quite easy. If we cut the cylinder S along the line parallel to the z -axis passing through $(1, 0, 0)$ (the dash-dotted line in Figure 3.7.24(a)), then S can be developed into S' on the plane, as is seen in Figure 3.7.24(b). The developed region S' is the region bounded by parallel lines at a distance 2π on \mathbb{R}^2 . To treat the location of a point p'_i on S' which corresponds to p_i on S , let θ_i be the counterclockwise angle (viewed from above the x - y plane, i.e. $z > 0$) from the x -axis to the half line radiating from the origin to the point $(x_i, y_i, 0)$, then we can indicate the point p'_i by (θ_i, z_i) (Figure 3.7.24(b)). Since the shortest path on S is represented by the straight line on S' , the distance between p and p_i on S is the same as the distance between $p' = (\theta, z)$ and $p'_i = (\theta_i, z_i)$ on S' (where $\theta \leq \theta_i$ is assumed without loss of generality), which is given by

$$d_{cy}(p, p_i) = \begin{cases} \sqrt{(\theta - \theta_i)^2 + (z - z_i)^2} & \text{for } \theta_i - \theta \leq \pi, \\ \sqrt{(\theta + 2\pi - \theta_i)^2 + (z - z_i)^2} & \text{for } \theta_i - \theta > \pi. \end{cases} \quad (3.7.20)$$

Since the bisector $b(p_i, p_j)$ defined with the distance of equation (3.7.20) splits S into two disjoint regions (Figure 3.7.25(a)), the dominance region is well-behaving. We can thus define a Voronoi diagram on S with this distance,

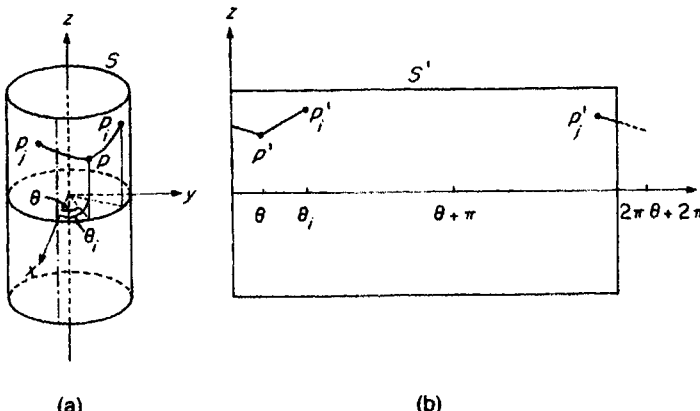


Figure 3.7.24 (a) A cylinder in \mathbb{R}^3 , and (b) its developed region in \mathbb{R}^2 .

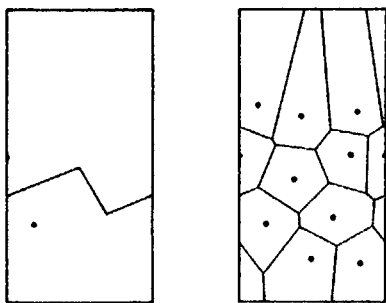


Figure 3.7.25 (a) A bisector on a cylinder, and (b) a cylindrical Voronoi diagram.

which we call the *cylindrical Voronoi diagram* on S generated by P (Figure 3.7.25(b)).

3.7.8 Voronoi diagrams on a cone

If a set $P = \{p_1, \dots, p_n\}$ of distinct points is placed on a cone, we may consider a Voronoi diagram on a cone. Suppose that a cone S is placed in \mathbb{R}^3 in such a way that the axis of the cone S is the z -axis of \mathbb{R}^3 , and the radius of the circle made by the intersection of the cone S with the x - y plane is unity (Figure 3.7.26(a)). Like a cylinder, a cone can be developed on a plane. If we cut the cone S along the line radiating from the top of the cone passing through $(1, 0, 0)$ and develop it on the plane, we get a fan-shaped region S' , as is shown in Figure 3.7.26(b). We can thus measure the distance between p and p_i on the cone S by the distance between p' and p'_i in the fan-shaped region S' . To write this distance mathematically, let (x_i, y_i, z_i) be the Cartesian coordinates of p_i in \mathbb{R}^3 ; θ_i be the counterclockwise angle (viewed from above the x - y plane, $z > 0$) from the x -axis to the half line radiating from the origin to the point $(x_i, y_i, 0)$; $\theta'_i = \theta_i \sin(\alpha/2)$, where α is the top angle of the cone (defined by the acute angle of the intersection lines made from the x - z plane and the cone); and

$$r_i = \sqrt{x_i^2 + y_i^2 + (z_i - \cot(\alpha/2))^2}, \quad (3.7.21)$$

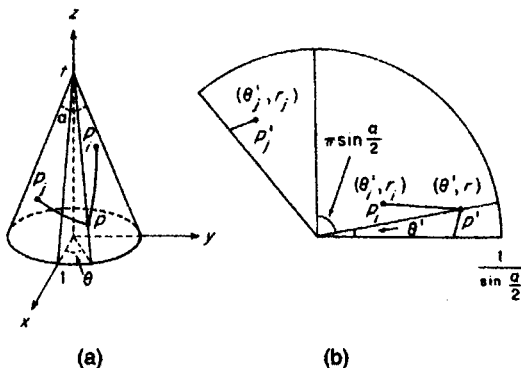


Figure 3.7.26 (a) A cone in \mathbb{R}^3 , and (b) its developed region in \mathbb{R}^2 .

which is the straight line distance from the top of the cone S to p_i . Then the point p_i on the cone S in \mathbb{R}^3 can be indicated by (θ_i, r_i) in the fan-shaped regions in \mathbb{R}^2 . Thus the distance between $p = (r, \theta)$ and p_i on the cone S is written as

$$d_{\text{cone}}(p, p_i) = \begin{cases} \sqrt{r^2 + r_i^2 - 2rr_i \cos(\theta'_i - \theta')} & \text{for } \theta'_i \leq \theta' + \pi \sin(\alpha/2), \\ \sqrt{r^2 + r_i^2 - 2rr_i \cos(\theta' + 2\pi \sin(\alpha/2) - \theta'_i)} & \text{for } \theta'_i > \theta' + \pi \sin(\alpha/2), \end{cases} \quad (3.7.22)$$

where $\theta' \leq \theta'_i$ is assumed without loss of generality (Figure 3.7.26(b)). The bisector defined with this distance consists of a chain of straight line segments which divides the fan-shaped region S' into two disjoint regions, as is shown in Figure 3.7.27(a). The chain of the bisector may form a circuit on S . The bisector is a circuit on S if and only if the top angle is less than $\pi/3$ (Dehne and Klein, 1987, Lemma 2). Since a circuit bisector as well as a non-circuit bisector is well-behaving, we can define a Voronoi diagram with this bisector. We call the resulting diagram the *conic Voronoi diagram* generated by P on S (Dehne and Klein, 1987; Klein, 1988; Klein and Wood, 1988). An example is depicted in Figure 3.7.27(b).

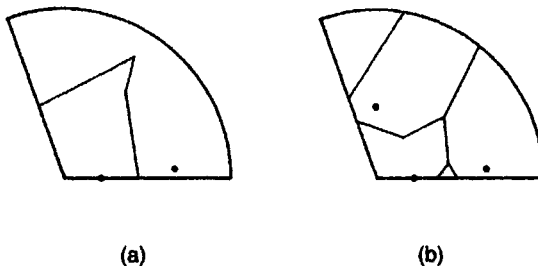


Figure 3.7.27 (a) A bisector in a cone, and (b) a conic Voronoi diagram.

3.7.9 Voronoi diagrams on a polyhedral surface

If the reader is interested in terrain navigation or a Voronoi diagram defined on uneven ground, a Voronoi diagram on an uneven surface in \mathbb{R}^3 may be useful. In most practical applications, a surface can be approximated by a polyhedral surface consisting of small polygonal faces. We can thus treat the above diagram as a Voronoi diagram on a polyhedral surface.

Let S be the surface of a polyhedron in \mathbb{R}^3 , and $P = \{p_1, \dots, p_n\}$ ($2 \leq n < \infty$) be a set of distinct points on S . A simple example is shown in Figure 3.7.28(a), where S is a tetrahedron. We measure the distance $d(p, p_i)$ from a point p on S to a point p_i by the length of the shortest path on S from p to p_i . A polyhedron can be developed into a region on a plane and

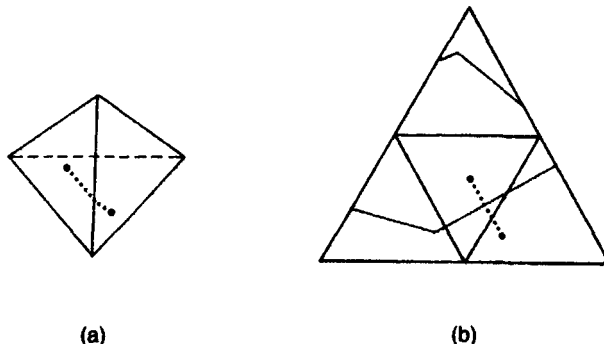


Figure 3.7.28 (a) A tetrahedron in \mathbb{R}^3 , and (b) its developed triangle in \mathbb{R}^2 where the heavy solid line shows a bisector.

we can measure this distance on the developed region. For instance, if we cut the tetrahedron in Figure 3.7.28(a) along three edges from the top, we obtain the triangle in Figure 3.7.28(b). The shortest path on the triangle is indicated by the dashed line in Figure 3.7.28. When the surface is given by a convex polyhedron, we may develop the surface on a plane without overlaps (Agarwal *et al.*, 1990a; Chen and Han, 1990; Aronov and O'Rourke, 1992). When the surface is given by a non-convex polyhedron, facets developed on a plane may overlap, and it is not straightforward to find the shortest path. In computational geometry, Mount (1985), Sharir and Schorr (1984), Sharir and Baltsan (1986) and Har-Peled *et al.* (1996) proposed several methods for finding the shortest path. Using these methods, we can define the bisector between p_i and p_j (the heavy solid line in the example of Figure 3.7.28(b)), and define a Voronoi diagram on the surface of a polyhedron. We call this diagram the *Polyhedral Voronoi diagram* generated by P (Figure 3.7.29).

3.7.10 Miscellany

In addition to the Voronoi diagrams with the above V-distances, we can find in the literature a few more Voronoi diagrams with other V-distances. We comment briefly on these diagrams.

A Voronoi diagram defined with the time-space distance is formulated by Seoung (1990), which will be shown in Chapter 8. A Voronoi diagram defined with the quadratic form distance is developed by Imai *et al.* (1985) (see also Section 18.2.2 in Boissonnat and Yvinec, 1995). A Voronoi diagram on a Riemannian manifold is investigated by Ehrlich and Im Hof (1979), Boissonnat and Yvinec (1995, Section 18.5.2) and Onishi and Takayama (1996). The geodesic distance, $d_{\text{Riemann}}(p_1, p_2)$, between $p_1 = (x_1, y_1)$ and $p_2 = (x_2, y_2)$ in the Riemannian manifold, called the upper half-plane, is given by

$$d_{\text{Riemann}}(p_1, p_2) = \left| \log \frac{A + \sqrt{A^2 - 4y_1^2 y_2^2}}{A - \sqrt{A^2 - 4y_1^2 y_2^2}} \right|, \quad (3.7.23)$$

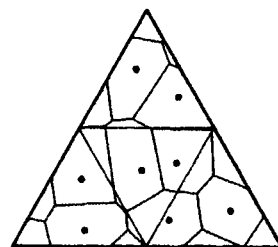


Figure 3.7.29 A polyhedral Voronoi diagram developed in \mathbb{R}^2 .

where $A = (x_1 - x_2)^2 + (y_1 + y_2)^2$. We call the Voronoi diagram defined with this distance the *Riemann Voronoi diagram*, which is alternatively called the (*hyperbolic*) *Voronoi diagram in the upper half-plane* by Onishi and Takayama (1996). An example is shown in Figure 3.7.30. In conjunction with the Riemann Voronoi diagram, we note that Onishi and Imai (1997) develop a Voronoi diagram for a set of points (each point correspond to a probability density function) in a statistical parametric space which is regarded as a Riemannian space.

A Voronoi diagram on a torus is referred to in conjunction with adjusting the boundary effect, which is discussed in Chapter 5 (or Upton and Fingleton, 1985, p. 72). It should be noted that this torus is a ‘quasi-torus’ in the sense that a distance between two points on the torus is not measured by the shortest path distance on the torus but by the Euclidean distance on the ‘developed’ rectangle from the torus. An example is shown in Figure 3.7.31(a), where generators are distributed over a unit square whose vertices are given by $(0,0)$, $(1,0)$, $(0,1)$ and $(1,1)$. Conceptually, we connect the edge \overline{ab} with the edge \overline{cd} and the edge \overline{ac} with the edge \overline{bd} in Figure 3.7.31 by deforming the square. Although we deform the square, we measure the distance between two points (x_i, y_i) and (x_j, y_j) by

$$\begin{aligned}
 d_{\text{torus}}(p, p_i) &= \min \left\{ \sqrt{(x_i - x_j)^2 + (y_i - y_j)^2}, \sqrt{(x_i - x_j + 1)^2 + (y_i - y_j)^2}, \right. \\
 &\quad \sqrt{(x_i - x_j)^2 + (y_i - y_j + 1)^2}, \sqrt{(x_i - x_j - 1)^2 + (y_i - y_j)^2}, \\
 &\quad \sqrt{(x_i - x_j)^2 + (y_i - y_j - 1)^2}, \sqrt{(x_i - x_j + 1)^2 + (y_i - y_j + 1)^2}, \\
 &\quad \sqrt{(x_i - x_j + 1)^2 + (y_i - y_j - 1)^2}, \sqrt{(x_i - x_j - 1)^2 + (y_i - y_j + 1)^2}, \\
 &\quad \left. \sqrt{(x_i - x_j - 1)^2 + (y_i - y_j - 1)^2} \right\}. \tag{3.7.24}
 \end{aligned}$$

This distance is readily obtained from the configuration which consists of nine squares with the same generators placed around the square, as shown in Figure 3.7.31(b). Then a Voronoi diagram on a quasi-torus is obtained as the solid lines in the central square in Figure 3.7.31(b).

When we can reach points only in a fan-shaped region, we may consider an ‘oriented Voronoi diagram’. To be explicit, let $C(p, \theta_1, \theta_2)$ be the fan-

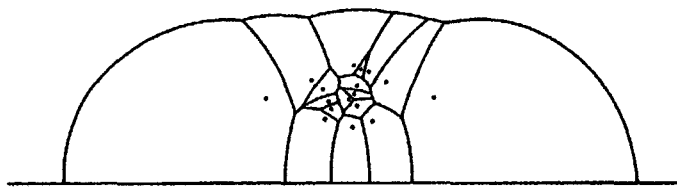


Figure 3.7.30 A Riemann Voronoi diagram. (Source: Onishi and Takayama, 1996).

shaped region with a vertex p and limiting angles θ_1 and θ_2 . Note that $C(p, \theta_1, \theta_2)$ includes its boundaries but excludes p , and $0 < \theta_2 - \theta_1 < \pi$ (the shaded area in Figure 3.7.32(a)). We define the *oriented distance* by

$$d_{\text{ori}}(p, p_i) = \begin{cases} \|x - x_i\| & \text{if } p \in C(p, \theta_1, \theta_2), \\ \infty & \text{if } p \notin C(p, \theta_1, \theta_2). \end{cases} \quad (3.7.25)$$

For example, in Figure 3.7.32(a), $d_{\text{ori}}(p, p_1)$ is the same as the Euclidean distance between p and p_1 but $d_{\text{ori}}(p, p_2)$ is infinity. This implies that the set of points from which the oriented distance to p_1 is finite is given by $C(p_1, \theta_1 + \pi, \theta_2 + \pi)$, the shaded area in Figure 3.7.32(b). For the two generator points p_1 and p_2 shown in Figure 3.7.32(c), the set of points satisfying $d_{\text{ori}}(p, p_1) \leq d_{\text{ori}}(p, p_2)$ is indicated by the shaded area (note that the broken line perpendicularly bisects the line segment $\overline{p_1 p_2}$).

With the oriented distance, we define

$$V(p_i) = \{p \mid d_{\text{ori}}(p, p_i) \leq d_{\text{ori}}(p, p_j), j \in I_n \setminus \{i\}\}. \quad (3.7.26)$$

We call $V(p_i)$ the *oriented Voronoi polygon* associated with p_i . The resulting set $\{V(p_1), \dots, V(p_n)\}$ is a tessellation of $\bigcup_{i=1}^n C(p_i, \theta_1 + \pi, \theta_2 + \pi)$. We call

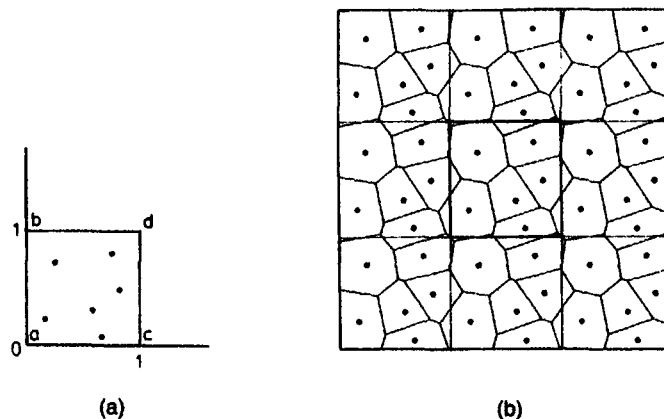


Figure 3.7.31 A Voronoi diagram on a quasi-torus.

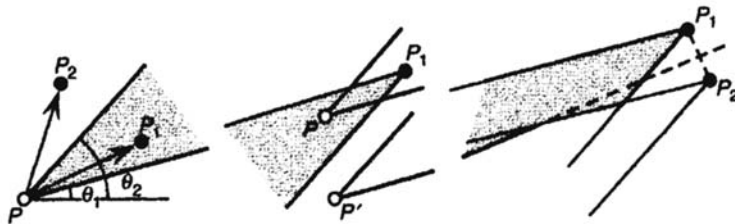


Figure 3.7.32 The oriented distance.

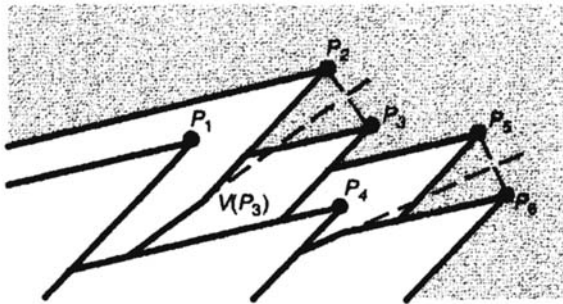


Figure 3.7.33 An oriented Voronoi diagram.

it the *oriented Voronoi diagram* generated by P (Chang *et al.*, 1990a; Georgakopoulos and Papadimitriou, 1987 (who call $V(p_i)$ the *oriented Dirichlet cell*)). An example of the oriented Voronoi diagram generated by six generator points is shown in Figure 3.7.33. In the special case where $\theta_1 = 0$ and $\theta_2 = \pi/2$, Chew and Fortune (1997) call the oriented Voronoi diagram the *right triangle distance Voronoi diagram*.

3.7.11 Applications

The Manhattan Voronoi diagram is used when movement is restricted to the north-south and the east-west directions. Applications are found in robot arm movements (Hwang, 1979; Lee and Wong, 1980), VLSI (Very Large Scale Integrated) circuit design (Li and Jabri, 1992; Guha, 1993; Tzionas *et al.* 1997), robot motion planning (Hague *et al.*, 1990; Tzionas *et al.*, 1997, for diamond-shaped robot) and market area analysis (Eaton and Lipsey, 1980). The rectangular Voronoi diagram is used for floor planning (Choi and Kyung, 1991).

The elliptic distance Voronoi diagram may represent a cell growth model, where the growth rate differs in directions, called *anisotropic growth* (Scheike, 1994). Suppose that the length of a line segment from o to a point on the boundary of an ellipse whose centre is placed on o indicates the growth rate in that direction in unit time, and that cells centred at p_1, \dots, p_n expand

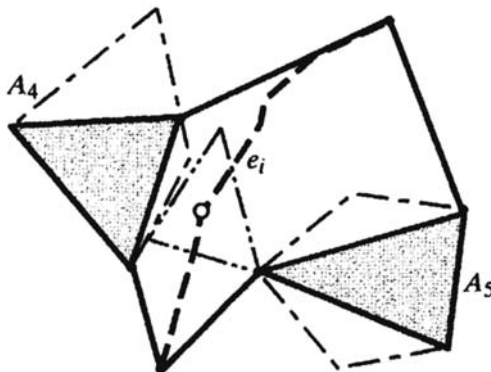


Figure 3.7.34 A bottleneck between two polygons in a spoke region in Figure 3.7.9.

simultaneously according to this growth rate (imagine that football shaped balloons (cells) are inflating with fixed centres). As the cells expand, they become tight and deformed; finally, the ‘packed’ cells form $\mathcal{V}_{\text{clip}}$ (a precise definition of the cell growth model is provided in Section 7.2). Figure 3.7.10(c) (the ordinary Voronoi diagram) shows the case in which the growth rate is the same in all directions; Figures 3.7.10(a) and (b) show the case in which the growth rate in the direction of the longer axis of the ellipse is twice as fast as that in the shorter axis. The elliptic distance Voronoi diagram is also used to analyse the growth of small fatigue cracks (Cox and Morris, 1988) and cluster analysis (Reyes and Adjouadi, 1995).

An application of the convex distance Voronoi diagram is found in robot motion planning, which is alternatively referred to as collision-free path planning (Lozano-Pérez and Wesley, 1979), the piano movers’ problem (Schwartz and Sharir, 1983a, b), the find path problem (Lozano-Pérez, 1983), the problem of moving a ladder (Ó'Dúnlaing *et al.*, 1986, 1987; Leven and Sharir, 1987), and the problem of moving a chair (Yap, 1987). *Robot motion planning* involves finding paths, called *collision-free paths*, on which a robot can move without colliding with obstacles A_1, \dots, A_n . If a robot moves under a translational motion and the robot can be represented by a convex polygon, $C(p, \bar{\lambda})$ (where $\bar{\lambda}$ is a fixed value), we can use $\mathcal{V}_{\text{conv}}$ to find collision-free paths.

To find the paths, consider a spoke region, and a point p on the Voronoi edge, e_i (the heavy broken line in Figure 3.7.34 in the spoke region). As p moves along e_i , the convex distance from p to the two polygons (A_4 and A_5 in Figure 3.7.34) changes, but the value has no plural local optimum (shown by McAllister *et al.*, 1996). The distance attains the minimum at a point on e_i (including the end points). Denote this point by p_i^* , and let a_{i1}^* and a_{i2}^* be attachment points of the spokes from p_i^* to the polygons whose Voronoi regions share e_i . We call the value $w_i^* = d_{\text{conv}}(p_i^*, a_{i1}^*)$ the *bottleneck width* of e_i . This implies that if the size $\bar{\lambda}$ of robot $C(p, \bar{\lambda})$ is less than the bottle-

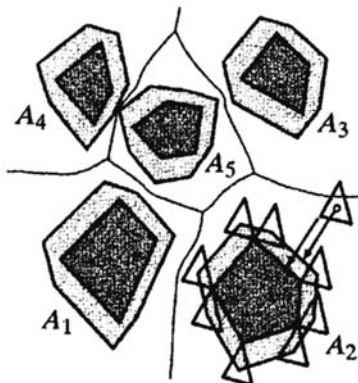


Figure 3.7.35 An area Voronoi diagram for expanded obstacles (the densely shaded polygons are obstacles A_1, \dots, A_5 , and the shaded polygons are expanded obstacles $A_1^{+C}, \dots, A_5^{+C}$; the distance $d_{\min E}(C(p, \bar{\lambda}), A_i)$ from robot $C(p, \bar{\lambda})$ to obstacle A_i is the same as the distance $d_{\min E}(p, A_i^{+C})$ from the shrunken robot p to the expanded obstacle A_i^{+C} indicated by the two arrow line segments.

neck width w_i^* of e_i , robot $C(p, \bar{\lambda})$ can move on the path (edge) e_i without collision. Let w^{**} be the minimum value among w_i^* for all Voronoi edges. If the size $\bar{\lambda}$ of robot $C(p, \bar{\lambda})$ is less than the minimum bottleneck width w^{**} , robot $C(p, \bar{\lambda})$ can move on the Voronoi edges of $\mathcal{V}_{\text{conv}}$ without collision. These paths are optimal in the sense that robot $C(p, \bar{\lambda})$ is as far from obstacles as possible in terms of the convex distance. When the size $\bar{\lambda}$ is greater than the minimum bottleneck width w^{**} , robot $C(p, \bar{\lambda})$ can move freely on the Voronoi edges whose bottleneck width w_i^* is greater than $\bar{\lambda}$.

The collision-free paths may be obtained by a slightly different method, called the *retraction method*, using a different Voronoi diagram (the original idea was proposed by Lozano-Pérez and Wesley, 1979; O'Dúnlaing *et al.*, 1983; O'Dúnlaing and Yap, 1985; and Kedem and Sharir, 1985). In place of the convex distance $d_{\text{conv}}(B, A_i)$, the diagram is defined in terms of the distance given by

$$d_{\min E}(B, A_i) = \min_{p, q} \{d_E(p, q), p \in B, q \in A_i\}, \quad (3.7.27)$$

where $d_E(p, q)$ is the Euclidean distance between two points p and q . Note that $d_{\text{conv}}(B, A_i) \neq d_{\min E}(B, A_i)$ in general. As a generator polygon (an obstacle), we consider an *expanded polygon (obstacle)* defined by $A_i^{+C} = \{p \mid A_i \cap C(p) \neq \emptyset\}$ (the heavy line polygon in Figure 3.7.35) (Kedem and Sharir, 1985). At the same time, we consider a 'shrunken robot', i.e. robot $C(p, \bar{\lambda})$ is shrunk to the point $p = C(p, 0)$. For $C(p, \bar{\lambda})$, $C(p, 0)$, A and A^{+C} , a nice relation holds: the distance $d_{\min E}(C(p), A_i)$ from robot $C(p, \bar{\lambda})$ to obstacle A_i is the same as the distance $d_{\min E}(p, A_i^{+C})$ from the shrunken robot $C(p, 0)$ to the expanded obstacle A_i^{+C} (observe in Figure 3.7.35 that the lengths of the two arrows are the same). Thus the region in which robot $C(p, \bar{\lambda})$ can move without colliding with obstacles A_1, \dots, A_n is the same as the region in which the shrunken robot $C(p, 0)$ is in the complement of the expanded obstacles $A_1^{+C}, \dots, A_n^{+C}$.

For a set $A^{+C} = \{A_1^{+C}, \dots, A_n^{+C}\}$, as shown in Section 3.6, we can construct the area Voronoi diagram, \mathcal{V}_{exp} , with the Euclidean distance (note that when A_i^{+C} and A_j^{+C} overlap, we use $A_i^{+C} \cup A_j^{+C}$ as a generator polygon). We call

\mathcal{V}_{exp} , the *area Voronoi diagram for expanded obstacles* (Figure 3.7.35). The paths consisting of Voronoi edges of \mathcal{V}_{exp} are collision-free paths, which are optimal in the sense that the robot is as far from the obstacles as possible in terms of the distance d_{mine} . It should be noted that $\mathcal{V}_{\text{conv}}$ is not the same as \mathcal{V}_{exp} . Both diagrams provide optimal collision-free paths, but the optimality is evaluated in terms of different distances. Also note that a fast algorithm is developed by Rajasekaran and Ramaswami (1995) using a mesh-connected computer.

Robot motion planning becomes difficult when a robot is allowed not only to translate but also to rotate. This problem is discussed in Lozano-Pérez and Wesley (1979), Schwartz and Sharir (1983a,b) and Canny and Donald (1988) who propose the ‘simplified’ Voronoi diagram, and Takahashi and Schilling (1989) (a rectangular robot).

The spherical Voronoi diagram and the spherical Delaunay tessellation are used for spatial data management of terrestrial objects (Lukatela and Russell, 1992; Gold, 1997), meteorological modelling, shallow water equations (Augenbaum, 1984, 1985), interpolation on the globe (Renka, 1984a,b), point pattern matching in astronautics (Weber *et al.*, 1994), and minimum spanning trees and Steiner minimum trees on a sphere (Dolan *et al.*, 1991).

An application of the cylindrical Voronoi diagram is found in the locational optimization of facilities that open periodically (see Chapter 9) Hyman and Mayhew (1983) use the cylindrical, conic and polyhedral Voronoi diagrams for emergency service medical provision in cities.

The oriented Voronoi diagram is utilized in finding the shortest paths among polygonal obstacles (Mitchell, 1992), and the right triangle distance Voronoi diagram is utilized for sorting (Chew and Fortune, 1997).

3.8 NETWORK VORONOI DIAGRAMS

In Section 3.7 we showed that the Manhattan Voronoi diagram or the Karlsruhe Voronoi diagram were useful to investigate dominance regions in a grid street system or a radial–circular street system. Many actual streets are, however, not so regular. Even in Manhattan the streets do not completely form a grid. To deal with a Voronoi diagram in a more realistic street system, it may be worth formulating a Voronoi diagram on a general network.

We consider a planar geometric graph $G(N, L)$ consisting of a set of nodes $N = \{p_1, \dots, p_n, p_{n+1}, \dots, p_l\}$ and a set of links $L = \{l_1, \dots, l_k\}$ which form a connected component. For simplicity, we assume that $G(N, L)$ is a non-directed graph (the extension to a directed graph is not difficult). On $G(N, L)$ we define the distance from a point p on a link in L to a node p_i in N by the length of the shortest path from p to p_i . We call this distance the *network distance*, and denote it by $d_{\text{net}}(p, p_i)$. We call a geometric graph $G(N, L)$ with the network distance a *network*, and denote it by $\mathcal{N}(N, L)$. We assume without loss of generality that the generators are the first n elements of N , i.e. $P = \{p_1, \dots, p_n\}$.

3.8.1 The network Voronoi node diagram

We first consider that a space S is given by the node set N , called a *node space* (the unfilled circles, triangles and squares in Figure 3.8.1) of a network $\mathcal{N}(N, L)$ (the dashed lines with the nodes in Figure 3.8.1). Let

$$\text{Dom}(p_i, p_j) = \{p_k \mid p_k \in N; d_{\text{net}}(p_k, p_i) \leq d_{\text{net}}(p_k, p_j)\}, \quad i \neq j, \quad (3.8.1)$$

$$b(p_i, p_j) = \{p_k \mid p_k \in N; d_{\text{net}}(p_k, p_i) = d_{\text{net}}(p_k, p_j)\}, \quad i \neq j. \quad (3.8.2)$$

We call $\text{Dom}(p_i, p_j)$ the *dominance node set* of p_i over p_j , and $b(p_i, p_j)$ the *bisector node set* between p_i and p_j . The bisector node set may be empty. In fact, if no nodes are equally distant from any two nodes in N , the bisector node set is empty. Note that the bisector node set has quite different features from bisectors defined on a continuous plane (such as a bisector producing the ordinary Voronoi diagram), because the bisector node set is a set of discrete points, and so the concept of a boundary is meaningless. We can, however, develop a parallel concept for the bisector node set. When the bisector node set is empty or the shortest path from $p_k \in b(p_i, p_j)$ to p_i and that from $p_l \in b(p_i, p_j)$ to p_j do not have common links for $p_k \neq p_l$, we say that the bisector node set is *well-behaving*, and $\text{Dom}(p_i, p_j)$ is a well-behaving dominance node set.

For well-behaving dominance node sets, we define

$$V_{\text{node}}(p_i) = \bigcap_{j \in I_n \setminus \{i\}} \text{Dom}(p_i, p_j), \quad (3.8.3)$$

and let $\mathcal{V}(P, d_{\text{net}}, N) = \mathcal{V}_{nn} = \{V_{\text{node}}(p_1), \dots, V_{\text{node}}(p_n)\}$. We call the set \mathcal{V}_{nn} the *network Voronoi node diagram* generated by the node set P in the node space N , and call the set $V_{\text{node}}(p_i)$ the *Voronoi node set* associated with the node p_i (Iri and Koshizuka, 1986, Chapter 4). In Figure 3.8.1, three Voronoi node sets generated by p_1, p_2 , and p_3 are indicated by the sets of the unfilled circles, triangles and squares. It should be noted that to avoid lengthy treatments, we assume in the following analysis that the bisector node is empty.

The geometric properties of \mathcal{V}_{nn} appear quite different from those of the generalized Voronoi diagrams defined on a continuous space, because the node space N is discrete. We find, however, a few common properties. First,

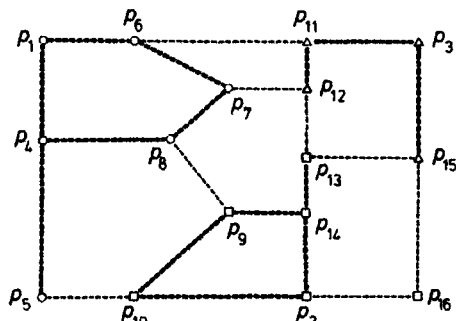


Figure 3.8.1 A network-node Voronoi diagram.

to discuss the ‘shape’ of the Voronoi node set, we consider the subgraph of the graph $G(N, L)$ in which the node set is given by $V_{\text{node}}(p_i)$ and the link set $L(p_i)$ is given by the links in L , both end points (nodes) of which are in $V_{\text{node}}(p_i)$. We denote this subgraph by $G(V_{\text{node}}(p_i), L(p_i))$. In Figure 3.8.1 the subgraphs $G(V_{\text{node}}(p_i), L(p_i)), i \in I_n$, are indicated by the heavy dashed lines. If the shortest path between any two nodes in $V_{\text{node}}(p_i)$ is embedded in $L(p_i)$ of $G(V_{\text{node}}(p_i), L(p_i))$, we say that the Voronoi node set $V_{\text{node}}(p_i)$ is *convex* (as an extension of convexity defined in Section 1.3). If the shortest path from any node in $V_{\text{node}}(p_i)$ to the generator node p_i is embedded in $L(p_i)$ of $G(V_{\text{node}}(p_i), L(p_i))$, we say that the Voronoi node set $V_{\text{node}}(p_i)$ is *star-shaped* (as an extension of star-shape defined in Section 1.3). In observing the shortest path between p_{12} and p_{15} in Figure 3.8.1, we notice that the shortest path is not embedded in $L(p_3)$ of $G(V(p_3), L(p_3))$. Thus, in general a Voronoi node set is not necessarily convex. We notice, however, that every Voronoi node set in \mathcal{V}_{nn} is star-shaped. To sum up, we obtain the following property.

Property NN1 No Voronoi node set $V_{\text{node}}(p_i)$ is empty. A Voronoi node set $V_{\text{node}}(p_i)$ is not necessarily convex, but it is star-shaped with respect to the generator node $p_i, i \in I_n$.

3.8.2 The network Voronoi link diagram

We next consider the space S given by points on links in L , i.e. $S = \bigcup_{i=1}^k l_i$, called a *link space*, and let

$$\text{Dom}(p_i, p_j) = \left\{ p \mid p \in \bigcup_{i=1}^k l_i, d_{\text{net}}(p, p_i) \leq d_{\text{net}}(p, p_j), j \in I_n \setminus \{i\} \right\}, \quad (3.8.4)$$

$$b(p_i, p_j) = \left\{ p \mid p \in \bigcup_{i=1}^k l_i, d_{\text{net}}(p, p_i) = d_{\text{net}}(p, p_j) \right\}, \quad i \neq j. \quad (3.8.5)$$

We call the set $\text{Dom}(p_i, p_j)$ the *dominance region* of p_i over p_j on links in L , and the set $b(p_i, p_j)$ the *bisector* between p_i and p_j on links in L . If the bisector consists of finite points, we say that the bisector $b(p_i, p_j)$ and the dominance region $\text{Dom}(p_i, p_j)$ are *well-behaving*. A well-behaving bisector implies that the shortest path from $p \in b(p_i, p_j)$ to p_i and that from $p \in b(p_i, p_j)$ to p_j does not share a positive length line segment. For well-behaving dominance regions, we define

$$V_{\text{link}}(p_i) = \bigcap_{j \in I_n \setminus \{i\}} \text{Dom}(p_i, p_j), \quad (3.8.6)$$

and let $\mathcal{V}(P, d_{\text{net}}, \bigcup_{i=1}^k l_i) = \mathcal{V}_{\text{nl}} = \{V_{\text{link}}(p_1), \dots, V_{\text{link}}(p_n)\}$. Since we define \mathcal{V}_{nl} for well-behaving dominance regions, elements in \mathcal{V}_{nl} are collectively exhaustive and mutually exclusive except for the finite number of points. We call this tessellation the *network Voronoi link diagram* generated by P on $N(N, L)$ and the set $V_{\text{link}}(p_i)$ the *Voronoi link set* associated with p_i . Hakimi *et al.* (1992) call \mathcal{V}_{nl} the *Voronoi partition*.

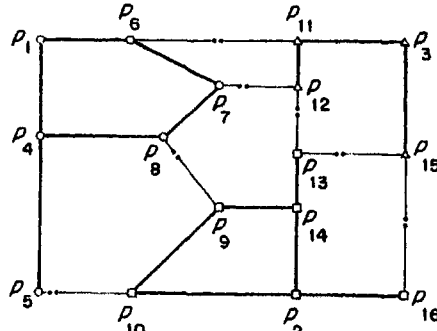


Figure 3.8.2 A network Voronoi link diagram.

Alternatively, we can define the set $V_{\text{link}}(p_i)$ with the subgraph $G(V_{\text{node}}(p_i), L(p_i))$ defined in Section 3.8.1. From the definition of the Voronoi node set, we note that if $p \in \cup_{l_j \in L(p_i)} l_j$, then $p \in V_{\text{link}}(p_i)$, i.e. a point on the heavy lines in Figure 3.8.2 is assigned to its generator. What is left to assign is a point on the links indicated by the light lines in Figure 3.8.2. We denote the k th link connecting a node in $V_{\text{node}}(p_i)$ and a node in $V_{\text{node}}(p_j)$ by l_{ijk} , $k \in I_{n_{ij}}$ (note that $I_{n_{ij}}$ may be empty for some pairs i and j). We divide the link l_{ijk} at the equally distant point from p_i and p_j and denote the resulting link connected to the node in $V_{\text{node}}(p_i)$ by l_{ijkl} , i.e.

$$l_{ijk\ell} = \{ p \in l_{ijk} \mid d_{\text{net}}(p, p_i) \leq d_{\text{net}}(p, p_j) \} \quad (3.8.7)$$

(Figure 3.8.2). Then the set $V_{\text{link}}(p_i)$ given by equation (3.8.6) is written as

$$V_{\text{link}}(p_i) = \left[\bigcup_{l_i \in L(p_i)} l_i \right] \bigcup \left[\bigcup_{j \in I_n \setminus \{i\}} \bigcup_{k \in I_{n_j}} l_{ijkl} \right]. \quad (3.8.8)$$

An actual network Voronoi link-diagram of roads is shown in Figure 3.8.3.

For the network Voronoi link diagram, almost the same property as in Property NN1 holds although a slight modification is necessary for the definition of convexity and star-shape. If the shortest path between any two points in $V_{\text{link}}(p_i)$ is embedded in $V_{\text{link}}(p_i)$, we say that the Voronoi link set is *convex*. If the shortest path from a point in $V_{\text{link}}(p_i)$ to the generator node p_i is embedded in $V_{\text{link}}(p_i)$, we say that the Voronoi link set $V_{\text{link}}(p_i)$ is *star-shaped*. Using these terms, we can state the following property.

Property NL1 No Voronoi node set $V_{\text{link}}(p_i)$ is empty. A Voronoi node set $V_{\text{link}}(p_i)$ is not necessarily convex, but it is star-shaped with respect to the generator node $p_i, i \in I_n$.

3.8.3 The network Voronoi area diagram

In the network Voronoi node diagram and link diagram, a point to be assigned to a generator is restricted to a point on a node or a link. In some



Figure 3.8.3 The network Voronoi link diagram of roads in the Nishinomiya district of Osaka (the large filled circles indicate generators and the small filled circles indicate the boundary points). (Source: Yomono, 1991, Figure 1.)

contexts, however, we find this restriction is too strong. For example, if we can access a network from any point in a region and take a path from the access point to a destination through links, every point (including a point on a node and a link) in a region should be assigned to a generator. To treat this assignment, we consider a Voronoi diagram formulated on \mathbb{R}^2 with a network $\mathcal{N}(N, L)$.

Let $P \subset N$ be a generator set on a network $\mathcal{N}(N, L)$ placed in \mathbb{R}^2 , and assume that the dominance region $\text{Dom}(p_i, p_j)$ defined by equation (3.8.4) is well-behaving for any $i, j \in I_l$, $i \neq j$. We first assign a point p in \mathbb{R}^2 to the nearest point, called the *access point*, on a link of L ; second, the access point is assigned to the nearest generator node p_i with respect to the network distance. To be precise, let $a(p)$ be the nearest point on $\bigcup_{i=1}^k l_i$ from p , i.e.

$$d_{\text{acc}}(p, a(p)) = \|x - x_a\| = \min_u \left\{ \|x - u\| \mid u \in \bigcup_{i=1}^k l_i \right\}, \quad (3.8.9)$$

where x , x_a , and u are the location vectors of points p , $a(p)$ and an arbitrary point on $\bigcup_{i=1}^k l_i$ (the dotted lines in Figure 3.8.4), respectively. We call the point $a(p)$ the *access point* of p to $N(N, L)$, and the distance $d_{\text{acc}}(p, a(p))$ the *access distance* from p . In terms of the access distance and the network distance, the distance from a point p in \mathbb{R}^2 to a node p_i in N is written as

$$d_{\text{acc-net}}(p, p_i) = d_{\text{acc}}(p, a(p)) + d_{\text{net}}(a(p), p_i) \quad (3.8.10)$$

(Okabe and Yomono, 1988). We should note that this distance is not always the shortest distance from a point p to a node p_i , because the access distance is determined locally by equation (3.8.9). With the distance of equation (3.8.10), we define

$$V_{\text{area}}(p_i) = \{p \mid d_{\text{acc-net}}(p, p_i) \leq d_{\text{acc-net}}(p, p_j), j \in I_n \setminus \{i\}\}. \quad (3.8.11)$$

This set is alternatively defined with the line Voronoi diagram defined in Section 3.5. First, recall that we can define $V_{\text{area}}(p_i)$ provided that the network Voronoi link diagram can be defined for $N(P, L)$. This means that $V_{\text{link}}(p_1), \dots, V_{\text{link}}(p_n)$ are mutually exclusive except at a finite number of points. If an access point $a(p)$ belongs to a link in $V_{\text{link}}(p_i)$, it follows from the definition of the network Voronoi link diagram that the point p is assigned to the generator p_i . Thus, a point p being assigned to p_i is equivalent to a point p being assigned to the nearest generator among the generators given by $\{V_{\text{link}}(p_1), \dots, V_{\text{link}}(p_n)\}$. This assignment is indeed the assignment of a point p in the line Voronoi diagram of $L = \{l_1, \dots, l_n\}$, where l_i is given by $V_{\text{link}}(p_i)$. The set $V_{\text{area}}(p_i)$ is hence written as $V_{\text{area}}(p_i) = V_L(V_{\text{link}}(p_i))$, where $V_L(V_{\text{link}}(p_i))$ is the line Voronoi region associated with the generator consisting of lines in $V_{\text{link}}(p_i)$. When we refer to this line Voronoi diagram in a network study, we call the set $\mathcal{V}(P, d_{\text{acc-net}}, \mathbb{R}^2) = \mathcal{V}_{\text{na}} = \{V_{\text{area}}(p_1), \dots, V_{\text{area}}(p_n)\}$ the *network Voronoi area diagram*.

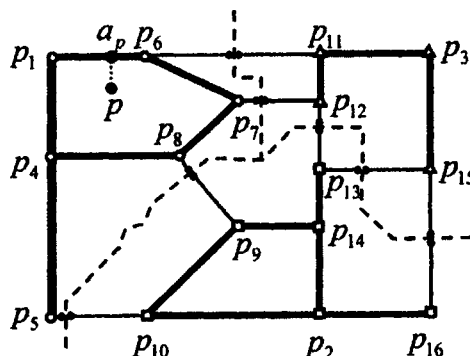


Figure 3.8.4 A network Voronoi area-diagram.

Since \mathcal{V}_{na} is exactly the same as the Voronoi line diagram, the properties of the network Voronoi area diagram are shared with those of the Voronoi link diagram.

3.8.4 Applications

As mentioned in Section 1.2, the earliest application of the network Voronoi diagram is found in Snow (1855) who studied spatial epidemiology on a street network around a water pump.

The network Voronoi diagram is implicitly used in multi-median problem (Hakimi, 1964, 1965), which is one of the central subjects in locational optimization on a network (Handler and Mirchandani, 1979). Yomono (1991) showed the network Voronoi line diagram with respect to stations in the Nishinomiya district of Osaka (Figure 3.8.3). Hakimi *et al.* (1992) consider the Voronoi p -centre problem (Section 9.2.8). Okabe and Okunuki (2000) use the network Voronoi area diagram to estimate market areas.

3.9 VORONOI DIAGRAMS FOR MOVING POINTS

In the preceding sections we assumed that the locations of generators are fixed over time. In this section we relax this assumption and consider a Voronoi diagram generated by a set of moving points over time or, more generally, a set of points whose locations are determined by one parameter.

3.9.1 Dynamic Voronoi diagrams

Let $\mathbf{x}_i(t)$ and $\mathbf{x}(t)$ be the location vectors of the i th generator point and an arbitrary point in \mathbb{R}^m at time t , respectively, and $P(t) = \{\mathbf{x}_1(t), \dots, \mathbf{x}_n(t)\}$. We assume that $\mathbf{x}_i(t)$ is continuous with respect to t in \mathbb{R}^m and no points collide. For a point (\mathbf{x}_i, t) in \mathbb{R}^{m+1} , we define a set $V(\mathbf{x}_i, t)$ of points (\mathbf{x}, t) in \mathbb{R}^{m+1} by

$$V(\mathbf{x}_i, t) = \{(\mathbf{x}, t) \mid \|\mathbf{x}(t) - \mathbf{x}_i(t)\| \leq \|\mathbf{x}(t) - \mathbf{x}_j(t)\|, j \in I_n \setminus \{i\}\}, \quad (3.9.1)$$

and let $\mathcal{V}(t) = \{V(\mathbf{x}_1, t), \dots, V(\mathbf{x}_n, t)\}$. We call the set $\mathcal{V}(t)$ the *dynamic (ordinary) Voronoi diagram* generated by $P(t)$ (Gowda *et al.*, 1983). Gold *et al.* (1997) call it the *kinematic Voronoi diagram*. Obviously, $\mathcal{V}(t)$ for a fixed point in time $t = t^*$, i.e. $\mathcal{V}(t^*)$, is the ordinary Voronoi diagram. In contrast to $\mathcal{V}(t)$, we call $\mathcal{V}(t^*)$ the *static (ordinary) Voronoi diagram*. An example of the dynamic Voronoi diagram in a two-dimensional space ($m = 2$) is shown in Figure 3.9.1 where four points move linearly with respect to t (the broken lines). Note that the dynamic Voronoi diagram defined here should be distinguished from that defined in the incremental method (Chapter 4) (Gowda *et al.*, 1983), that of Voronoi growth models (Section 5.6.2), that defined in astronomy (Zaninetti, 1989, 1990, 1995) and that defined in the dynamic maintenance of temporal maps (Gold *et al.*, 1996).

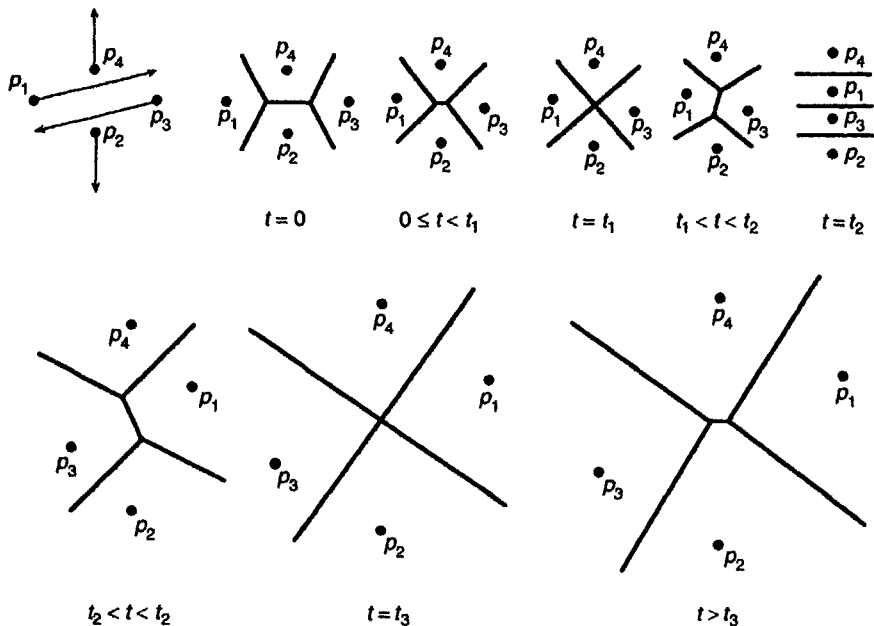


Figure 3.9.1 A dynamic Voronoi diagram in a two-dimensional space.

In Chapter 2 we defined a Delaunay triangulation as the dual of a Voronoi diagram. Similarly we can define a Delaunay triangulation as the dual of the dynamic Voronoi diagram. We call this triangulation the *dynamic Delaunay triangulation* (Devillers *et al.*, 1992). Rodin *et al.* (1992) call it the *flexible Delaunay triangulation*. Note that the dynamic Delaunay triangulation defined here should be distinguished from the Delaunay triangulation constructed by the incremental method (Devillers *et al.*, 1992), and cell growth models in crystallography (Section 7.2) or astrophysics (Zaninetti, 1990, 1995).

As is seen in Figure 3.9.1 (where four generator points move according to the arrows shown in the upper-left panel), the shape of $V(x_i)$ changes over time; in particular, a drastic change occurs when the topological configuration changes, i.e. at times t_1 , t_2 and t_3 in Figure 3.9.1. We call these topological changes *topological events* (Fu and Lee, 1991; Albers and Roos, 1992). In Figure 3.9.1 three topological events occur. The number of topological events depends on the manner of motion of $P(t)$. A typical motion is given by $x_i(t) = \sum_{j=0}^k c_{ij}t_j$, where c_{ij} is an m -dimensional constant vector. This motion is called *k-motion* (Atallah, 1983), and 1-motion is called *linear motion*. The motion in Figure 3.9.1 is the linear motion, i.e. $x_i(t) = c_{i1}t + c_{i0} \in \mathbb{R}^2$. The number of topological events varies according to the values of the constants c_{i1} and c_{i0} . For instance, if c_{11}, c_{21}, c_{31} and c_{41} are all different, as in the above example, the number of topological events is three; if they are all the same, the number of topological events becomes zero, because all points move

rigidly and no topological events occur over time. In the study of dynamic Voronoi diagrams, one of the major concerns is with the possible maximum number of topological events for a given manner of motion, say the k -motion. This number is called the *topological complexity* (Huttenlocher *et al.*, 1992a) or *combinatorial complexity* (Imai and Imai, 1993a,b).

The topological complexity of a dynamic Voronoi diagram may be written in terms of a sequence, called the 'Davenport-Schinzel sequence'. To state it explicitly, consider a set $B = \{b_1, \dots, b_n\}$ of n different alphabet letters (or integers), and let S_B be a set of all possible sequences consisting of letters chosen from B (the length of a sequence is between 1 and n). For a sequence in S_B , say $(b_1 b_2 b_4 b_3 b_5 b_1 b_3 b_2)$, we consider a subsequence of the sequence containing two different letters, for example b_1, b_2, b_1, b_2 of the sequence $(b_1 b_2 b_4 b_3 b_5 b_1 b_3 b_2)$, and denote it by $[b_1 b_2 b_1 b_2]$. Let $\xi_{ij}^1 = [b_i b_j b_i]$; $\xi_{ij}^{2q} = [\xi_{ij}^{2q-1} b_j]$; $\xi_{ij}^{2q+1} = [\xi_{ij}^{2q} b_i]$, $q = 1, 2, \dots$. For example, $\xi_{25}^2 = [b_2 b_5 b_2 b_5]$, $\xi_{25}^3 = [b_2 b_5 b_2 b_5 b_2]$, $\xi_{25}^4 = [b_2 b_5 b_2 b_5 b_2 b_5]$, and so forth. Then we call an element of S_B an (n, s) *Davenport-Schinzel sequence*, denoted by $DS(n, s)$, if it satisfies the condition that: (i) sequences in $DS(n, s)$ do not contain a subsequence $(b_i b_i)$ (not $[b_i b_i]$), i.e. letters change every time; (ii) sequences in $DS(n, s)$ do not contain any ξ_{ij}^s as a subsequence, $i, j \in I_n$ (Davenport and Schinzel, 1965). An example of a sequence in $DS(6, 2)$ is $(b_1 b_6 b_2 b_4 b_5 b_1 b_3)$ (confirm that letters change every time in the sequence and the sequence does not contain any $[b_i b_i b_i b_i]$).

The length of a sequence in $DS(n, s)$ is not constant, for example $(b_1 b_6 b_2 b_4 b_5 b_1 b_3)$, $(b_1 b_6 b_2 b_4 b_1)$ and $(b_1 b_2 b_3 b_5 b_6 b_5 b_4 b_2 b_1)$ are all in $DS(6, 2)$. We now ask: What is the maximum length, $\lambda(n, s)$, among the sequences in $DS(n, s)$? First, consider $\lambda(n, 1)$. Since a sequence in $DS(n, 1)$ does not contain $\xi_{ij}^1 = [b_i b_j b_i]$, the same letter does not appear in a sequence of $DS(n, 1)$. Thus the maximum length is achieved when a sequence is given by, for example, $(b_1 b_2 \dots b_n)$. Hence $\lambda(n, 1) = n$. Second, consider $\lambda(n, 2)$. Since a sequence in $DS(n, 2)$ does not contain any $\xi_{ij}^2 = [b_i b_j b_i b_j]$, a letter b_j between the same letters b_i does not appear after the second b_i in a sequence of $DS(n, 2)$. Thus the maximum length is achieved when a sequence is given by, for example, $(b_1 \dots b_{n-1} b_n b_{n-1} \dots b_1)$. Hence $\lambda(n, 2) = 2n - 1$. When $s \geq 3$, an explicit function of $\lambda(n, s)$ is difficult to derive. Here we only note that $\lambda(n, s)$ is of order $n \log^* n$ ($s \geq 3$), where $\log^* n$ means the number of taking logs that gives the first negative value, for example $\log 100 = 2$, $\log(\log 100) = 0.301 \dots$, $\log(\log(\log 100)) = -0.521 \dots$, and so $\log^* 100 = 3$. We also note that sharp upper and lower bounds of $\lambda(n, s)$ are shown by Agarwal *et al.* (1989b). In terms of $\lambda(n, s)$ we can state the following properties.

Property DV1 When generator points in $P(t) = \{x_1(t), \dots, x_n(t)\}$ move along continuous trajectories in \mathbb{R}^m , the topological complexity of the dynamic Voronoi diagram generated by $P(t)$ is of order $n^m \lambda(n, s)$, where s is a constant determined by the characteristic of the trajectories.

The proof is shown by Albers and Roos (1992). A slightly different theorem is proved by Roos (1993, Theorem 4.2).

The value of s in Property DV1 becomes explicit when the motion is explicitly stated. As a corollary to Property DV1, we have the following property.

Property DV2 When generator points in $P(t) = \{x_1(t), \dots, x_n(t)\}$ move in the linear motion in \mathbb{R}^2 , the topological complexity of the dynamic Voronoi diagram generated by $P(t)$ is of order $n^2 \lambda(n, 4)$.

The proof is shown by Guibas *et al.* (1991) and Imai and Imai (1990).

Huttenlocher *et al.* (1992a) show the topological complexity of $\mathcal{V}(t)$ in which subsets $P_1(t), \dots, P_q(t)$ of $P(t)$ move rigidly ($\bigcup_{i=1}^q P_i(t) = P(t)$, $P_i(t) \cap P_j(t) = \emptyset, i \neq j$). Guibas *et al.* (1991) and Roos (1994, 1997) show the topological complexity of $\mathcal{V}(t)$ in which only k points move while the other $n-k$ points are fixed.

In theory, all static generalized Voronoi diagrams shown in Sections 3.2–3.8 can be developed into *dynamic generalized Voronoi diagrams* by assuming that generators move over time. Actually Imai and Imai (1993a,b, 1998) formulate the *dynamic weighted Voronoi diagram* and the *dynamic kth order Voronoi diagram*.

3.9.2 Applications

A natural application of the dynamic Voronoi diagram is found in the dynamic configuration of service areas of mobile facilities. Consider a region in which mobile radio stations are moving under a certain time schedule. Receivers in the region want to catch the strongest wave among the waves transmitted from the mobile stations over time. Then a receiver at a location x at time t should use the mobile station whose Voronoi polygon $V(x_i, t)$ includes (x_i, t) , where $\mathcal{V}(t) = \{V(x_i, t), i \in I_n\}$ is the dynamic Voronoi diagram generated by the mobile stations. A similar application is shown by Devillers and Golin (1993) who extend the post-office problem (Section 2.3, Problem V3) of postmen (and a dog) moving with constant velocities. Blatov and Serezhkin (1997) investigate the connection between the topology of systems with many particles with the presence or absence of short-range or long-range order using the dynamic Voronoi diagram.

Another application is found in motion planning discussed in Section 3.7.11. The problem is to find a collision-free path or the safest path along which a robot moves among moving obstacles. Roos and Noltemeier (1991, 1992) solve this problem where a robot is represented by a disk. Rodin *et al.* (1992) apply the dynamic Voronoi diagram to implement a navigation system for an autonomous vehicle in an environment cluttered with both stationary and moving obstacles.

As noted in Section 3.9.1, t in $\mathcal{V}(t)$ does not necessarily represent time but a parameter. An application of $\mathcal{V}(t)$ with a non-time parameter is found in Problem FP3 discussed in Section 3.3.3 (the farthest-point Voronoi diagram).

The problem is to fit the configuration of points $P = \{p_{ij}, i \in I_{n_1}, j \in I_{n_2}\}$ placed at a square grid, i.e. $p_{ij} = (a(i-1), a(j-1))$, to a given configuration of points $Q = \{q_{ij}, i \in I_{n_1}, j \in I_{n_2}\}$ (see Figure 3.3.3) by translation and rotation in such a way that the distance between a point in P and a point in Q is minimized. In Section 3.3 we assumed that the configuration P moved through translation. Here we assume that the configuration P moves not only through translation but also rotation.

To solve the problem, let $p_{ij}(x_1, x_2, \theta)$ be the point p_{ij} that is translated by (x_1, x_2) and rotated by θ , i.e. $p_{ij}(x_1, x_2, \theta) = (x_1 + a(i-1) \cos \theta - a(j-1) \sin \theta, x_2 + a(i-1) \sin \theta + a(j-1) \cos \theta)$. Then the distance between $p_{ij}(x_1, x_2, \theta)$ and q_{ij} is given by

$$\begin{aligned} d(p_{ij}(x_1, x_2, \theta)) &= [(x_1 + a(i-1) \cos \theta - a(j-1) \sin \theta - u_{ij})^2 \\ &\quad + ((x_2 + a(i-1) \sin \theta + a(j-1) \cos \theta) - v_{ij})^2]^{1/2} \\ &= [(x_1 - (u_{ij} - a(i-1) \cos \theta + a(j-1) \sin \theta))^2 \\ &\quad + (x_2 - (v_{ij} - a(i-1) \sin \theta - a(j-1) \cos \theta))^2]^{1/2}. \end{aligned} \tag{3.9.2}$$

Thus $d(p_{ij}(x_1, x_2, \theta))$ may be regarded as the distance between (x_1, x_2) and $o_{ij}(\theta) = (u_{ij} - a(i-1) \cos \theta + a(j-1) \sin \theta, v_{ij} - a(i-1) \sin \theta - a(j-1) \cos \theta)$. Let $O(\theta) = \{o_{ij}(\theta), i \in I_{n_1}, j \in I_{n_2}\}$. Then the problem is restated as: find the point (x_1, x_2) from which the distance to the farthest point in $O(\theta)$ is the shortest. This problem can be solved through the dynamic farthest-point Voronoi diagram generated by $O(\theta)$ where points move linearly with respect to θ (Imai *et al.*, 1989, 1998; Imai and Imai, 1998 (an extension using the dynamic weighted Voronoi diagram)).

The dynamic Voronoi diagram may be used to construct the line Voronoi diagram. Gold (1990) and Gold *et al.* (1995, 1997) show an incremental method in which a line segment is generated by a trajectory of a point moving from one end point to the other end point of the line segment. Huttenlocher *et al.* (1992b) apply the dynamic Voronoi diagram to the problem of finding the minimum Hausdorff distance between two sets in the plane under Euclidean motion.